NPS69-81-006

NAVAL POSTGRADUATE SCHOOL

Monterey, California

THESIS

ENTRAINMENT MODELLING OF BUOYANT MOMENTUM JETS IN WATER

by

David Stuart Hilder

December 1981

Co-Advisors:
B. Gebhart
M. Kelleher

Approved for public release; distribution unlimited.

Prepared for:
Naval Sea Systems Command
Washington, D.C.

NAVAL POSTGRADUATE SCHOOL
Monterey, California

Rear Admiral J. J. Ekelund
Superintendent

David A. Schrady
Acting Provost

This thesis is prepared in conjunction with research supported in part by Naval Sea Systems Command under work request N0002481WR10497.

Released as a
Technical Report by:

REPORT DOCUMENTATION PAGE

READ INSTRUCTIONS BEFORE COMPLETING FORM

1. REPORT NUMBER NPS69-81-006	2. GOVT ACCESSION NO.	3. RECIPIENT'S CATALOG NUMBER
4. TITLE (and Subtitle) Entrainment Modelling of Buoyant Momentum Jets in Water		5. TYPE OF REPORT & PERIOD COVERED Engineer's Thesis; December 1981
		6. PERFORMING ORG. REPORT NUMBER
7. AUTHOR(s) David Stuart Hilder In conjunction with B. Gebhart and M. Kelleher		8. CONTRACT OR GRANT NUMBER(s) N0002481WR10497
9. PERFORMING ORGANIZATION NAME AND ADDRESS Naval Postgraduate School Monterey, California 93940		10. PROGRAM ELEMENT, PROJECT, TASK AREA & WORK UNIT NUMBERS
11. CONTROLLING OFFICE NAME AND ADDRESS Naval Postgraduate School Monterey, California 93940		12. REPORT DATE December 1981
		13. NUMBER OF PAGES 131
14. MONITORING AGENCY NAME & ADDRESS(if different from Controlling Office)		15. SECURITY CLASS. (of this report) Unclassified
		15a. DECLASSIFICATION/DOWNGRADING SCHEDULE

16. DISTRIBUTION STATEMENT (of this Report)

Approved for Public Release; distribution unlimited.

17. DISTRIBUTION STATEMENT (of the abstract entered in Block 20, if different from Report)

18. SUPPLEMENTARY NOTES

19. KEY WORDS (Continue on reverse side if necessary and identify by block number)

Buoyant Momentum Jets
Entrainment
Plumes
Jet Modelling
Thermal Discharge

20. ABSTRACT (Continue on reverse side if necessary and identify by block number)

The general characteristics of buoyant momentum jets in water are described. Previous analytical modelling techniques utilizing the entrainment concept for prediction of trajectory and residual physical properties are discussed, and an overview of the existing experimental data base is given. The limitations of previous analytical modelling techniques are enumerated, generally resulting from incomplete or inadequate equations of state. An existing comprehensive equation of state for pure and saline water is proposed

#20 - ABSTRACT - (CONTINUED)

for use in entrainment modelling. An original computerized procedure, based on appropriate conservation equations, is used to predict trajectory and physical properties of various buoyant momentum jets. Comparison is made with previous analytical and experimental results for the cases of quiescent, flowing, and stratified ambients. Finally, the comprehensive equation of state, coupled with the present computational procedure, is used to describe a complexly stratified ambient and the behavior of a buoyant momentum jet discharged into it.

ENTRAINMENT MODELLING
OF
BUOYANT MOMENTUM JETS IN WATER

by

David Stuart Hilder
Lieutenant, United States Navy
B.S., University of New Mexico, 1975

Submitted in Partial Fulfillment of the
Requirements for the Degrees of

MASTER OF SCIENCE IN MECHANICAL ENGINEERING

and

MECHANICAL ENGINEER

from the

NAVAL POSTGRADUATE SCHOOL
December 1981

ABSTRACT

The general characteristics of buoyant momentum jets in water are described. Previous analytical modelling techniques utilizing the entrainment concept for prediction of trajectory and residual physical properties are discussed, and an overview of the existing experimental data base is given. The limitations of previous analytical modelling techniques are enumerated, generally resulting from incomplete or inadequate equations of state. An existing comprehensive equation of state for pure and saline water is proposed for use in entrainment modelling. An original computerized procedure, based on appropriate conservation equations, is used to predict trajectory and physical properties of various buoyant momentum jets. Comparison is made with previous analytical and experimental results for the cases of quiescent, flowing, and stratified ambients. Finally, the comprehensive equation of state, coupled with the present computational procedure, is used to describe a complexly stratified ambient and the behavior of a buoyant momentum jet discharged into it.

TABLE OF CONTENTS

NOMENCLATURE

B - Characteristic jet width

b - Dimensionless jet width, B/D

c - Concentration

D - Jet discharge diameter

E - Volumetric entrainment

F - Densimetric Froude number, $U_0/(gD(\frac{\rho_a-\rho_0}{\rho_0}))^{1/2}$

F_L - Local densimetric Froude number, $U_m^2/gB(\frac{\rho_a-\rho_m}{\rho_0})$

g - gravity

Q - jet mass flow rate

R - Ambient flow ratio, U_a/U_0

r - Radial jet coordinate

S - Streamwise coordinate of jet velocity

s - Dimensionless streamwise jet coordinate, S/D; salinity

t - Temperature

U - Streamwise jet velocity

U^* - $U - U_a \cos \theta$, relative local velocity

u - Dimensionless streamwise jet velocity, U/U_0

X - Horizontal Cartesian coordinate

Z - Vertical Cartesian coordinate

GREEK SYMBOLS

α - Entrainment constant

β - Volumetric coefficient of thermal expansion

γ - Volumetric coefficient of concentration expansion

$\Delta(\ )$ - $(\ )_i - (\ )_j$

θ - Local angle of inclination from horizontal

λ - Relative spreading ratio

ρ - Density

ϕ - Azimuthal jet angle

SUBSCRIPTS

a - ambient

e - at beginning of zone of established flow

m - at jet centerline

0 - at jet discharge

I. INTRODUCTION

The cooling water discharge from a power plant into a large body of water, the thermally loaded condenser discharge from the condenser of a moving ship or submarine, and the high temperature gas issuing from a stack or gas turbine exhaust are all examples of buoyant momentum jets. The trajectory and behavior of such jets after discharge is influenced by factors such as initial jet velocity and buoyancy, ambient motion and stratification, and mixing rate. However, questions such as whether or not the jet will rise to a certain level, what the jet velocity and temperature will be at any point along its trajectory, or what effect ambient stratification will have on behavior, all require an involved quantitative analysis. Significant effort has been expended in the past few decades in attempting to understand the mechanics of buoyant jet mixing and trajectory, with the ultimate objective of developing accurate models to predict trajectory and decay.

Certainly the need for such predictive models has grown. Contemporary nuclear and fossil fueled power plants have thermal efficiencies on the order of 30-40%. The significant waste heat from these facilities takes the form of a thermally loaded discharge into either the atmosphere or a body of water. Sewage is often discharged as treated effluent into rivers, lakes, and oceans. The proper evaluation of the ecological impact of such discharges requires that their physical behavior be predictable. More stringent environmental regulations and heightened public awareness place a premium on the accuracy of such prediction.

The need to predict momentum jet behavior is not limited to environmental issues. Rapid advancement of the ability to detect small

temperature variations, concentration differentials, and turbulence anomalies may make it increasingly easy to detect various military craft and vehicles by virtue of propulsion system thermal discharges, wake turbulence, and wake concentration variations. The implications for weapons systems and platforms which rely on stealth for effectiveness are enormous.

Given the wide range of applications in which an analysis of fluid jet behavior might be used, it becomes obvious that the range of possible jet or ambient characteristics that may be of interest is equally wide. Initial jet geometry, discharge parameters, degree of thermal loading, and turbulence characteristics, as well as ambient flow conditions, turbulence, and stratification, can be combined into an almost infinite number of scenarios.

This investigation will be restricted to the case of a single, fully turbulent, circular water jet discharged into a surrounding water ambient. The case will be further restricted by limiting jet trajectory to two dimensions--in other words, ambient flow, if present, will be parallel to the horizontal component of jet velocity. Since jet encounter with an abrupt ambient discontinuity, such as a water-air interface, will not be addressed, the ambient will be considered to be infinite.

Among the variables which will be considered are:

(1) buoyancy effects, arising from density differentials between the jet and the surrounding ambient. These density differentials may arise from temperature and/or concentration variations.

(2) ambient density stratification, arising from vertical non-uniformity of temperature and/or concentration in the ambient.

(3) ambient flow conditions, in which the magnitude and orientation of the ambient flow velocity relative to the jet are varied.

(4) initial jet discharge characteristics, such as momentum orientation.

II. BASIC CHARACTERISTICS OF ROUND DISCHARGE SYSTEMS

The terms "jet", "momentum jet", "forced plume" and "plume" are often used to qualitatively describe certain characteristics of a discharge system as it progresses through an ambient medium. It is generally understood that "jet", "momentum jet", and "forced plume" refer to that region where the momentum of the initial discharge is still sufficient to influence jet behavior. "Plume" refers to a discharge in which the discharge momentum is either negligible to begin with, or small relative to the eventual total momentum produced by buoyancy. It is with this understanding that these terms will be used.

The jet/ambient system may be classified according to a number of characteristics:

(1) Jet buoyancy
    (a) buoyant (positively or negatively)
    (b) neutrally buoyant
(2) Initial jet orientation
    (a) horizontal (perpendicular to gravity field)
    (b) inclined
(3) Ambient stratification
    (a) unstratified
    (b) linearly stratified
    (c) non-linearly stratified
(4) Ambient motion
    (a) quiescent
    (b) flowing

Regardless of the classification of the jet or ambient, a jet passes through several flow regimes as it progresses along its trajectory. They are shown in Figure (2-1), and are:

1. (1) The zone of flow establishment. In this region, flow characteristics are dominated by discharge conditions. Velocity and scalar quantity profiles (temperature, salinity, etc.) undergo transition from their initial discharge shapes through the action of a turbulent shear layer formed on the jet periphery. As mixing with the ambient progresses, the turbulent shear layer grows inward and the extent of the core of undisturbed profiles becomes smaller. The zone of flow establishment ends at the point where turbulent mixing reaches the jet centerline. The jet behavior in this region is strongly influenced by initial momentum and discharge conditions, and is only slightly influenced by the ambient.

(2) The zone of established flow. This region begins when turbulent mixing reaches the jet centerline. The motion of the jet and its physical characteristics are governed by its momentum (initial and acquired), buoyancy, as well as ambient stratification and flow conditions. Initial discharge conditions play a progressively smaller role, and and the transition progresses from jet-like to plume-like behavior.

(3) The far field. In this region the jet's initial momentum has negligible effect, and the jet may be convected by ambient flow. The jet fluid may be further diffused by ambient turbulence, and the distinction of the jet as a separate entity gradually disappears.

The first two flow regimes constitute the near field, and will be the concern of this investigation.

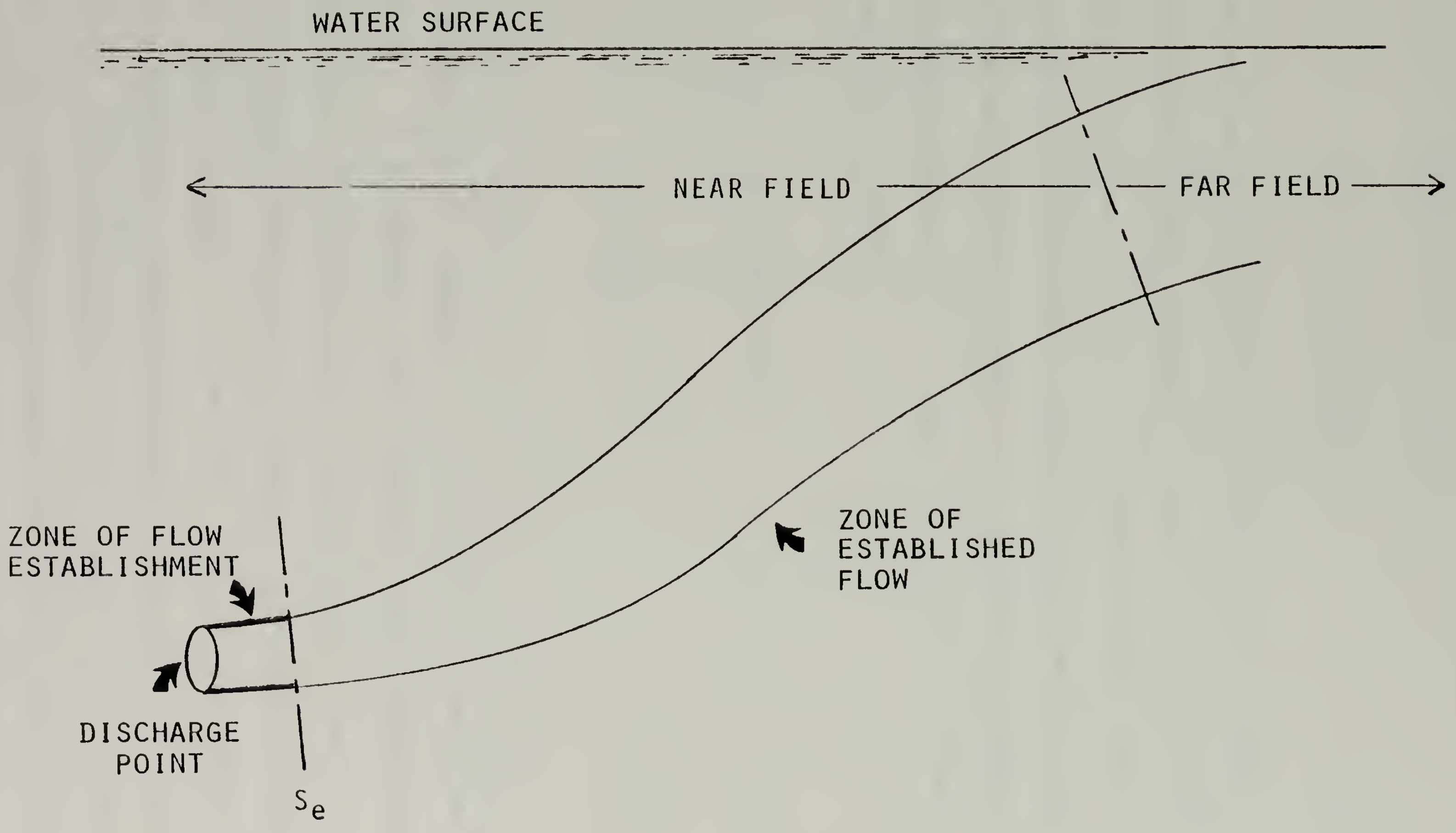

Figure 2-1. Flow regimes and typical progression of a buoyant momentum jet

Experimental work, begun by Albertson et al. [3] and continued and expanded by many others, has shown that within the zone of established flow, mean velocity profiles are nearly Gaussian:

$$U = U_m \exp\left[-r^2/B^2\right] \tag{2-1}$$

where U_m is the mean centerline velocity, r is the radial jet coordinate, and B is a characteristic measure of jet width, or that radial distance at which U is equal to (1/e) of its mean centerline value.

Profiles of jet scalar quantities, such as temperature and concentration, have also been found to be Gaussian in the zone of established flow by investigators such as Fan [7], Hoult et al. [16], and others. The profiles may be expressed as:

$$\Delta t = \Delta t_m \exp\left[-r^2/\lambda^2 B^2\right] \tag{2-2}$$

$$\Delta c = \Delta c_m \exp\left[-r^2/\lambda^2 B^2\right] \tag{2-3}$$

where $\Delta t = (t-t_a)$, $\Delta t_m = (t_m-t_a)$, $\Delta c = (c-c_a)$, $\Delta c_m = (c_m-c_a)$, and λ is the relative spreading ratio between velocity and density constituent scalar properties. λ^2 is defined as the inverse of the turbulent Schmidt Number. Figure (2-2) illustrates these profiles within the jet.

A coordinate system to describe the trajectory and physical dimensions of a jet system is shown in Figure (2-3). The X coordinate is perpendicular to the gravity field and parallel to the flow (if any) of the ambient fluid. The Z coordinate is vertical and opposite to the gravity vector. The streamwise coordinate S defines the direction of mean centerline jet velocity at any point along its trajectory. The

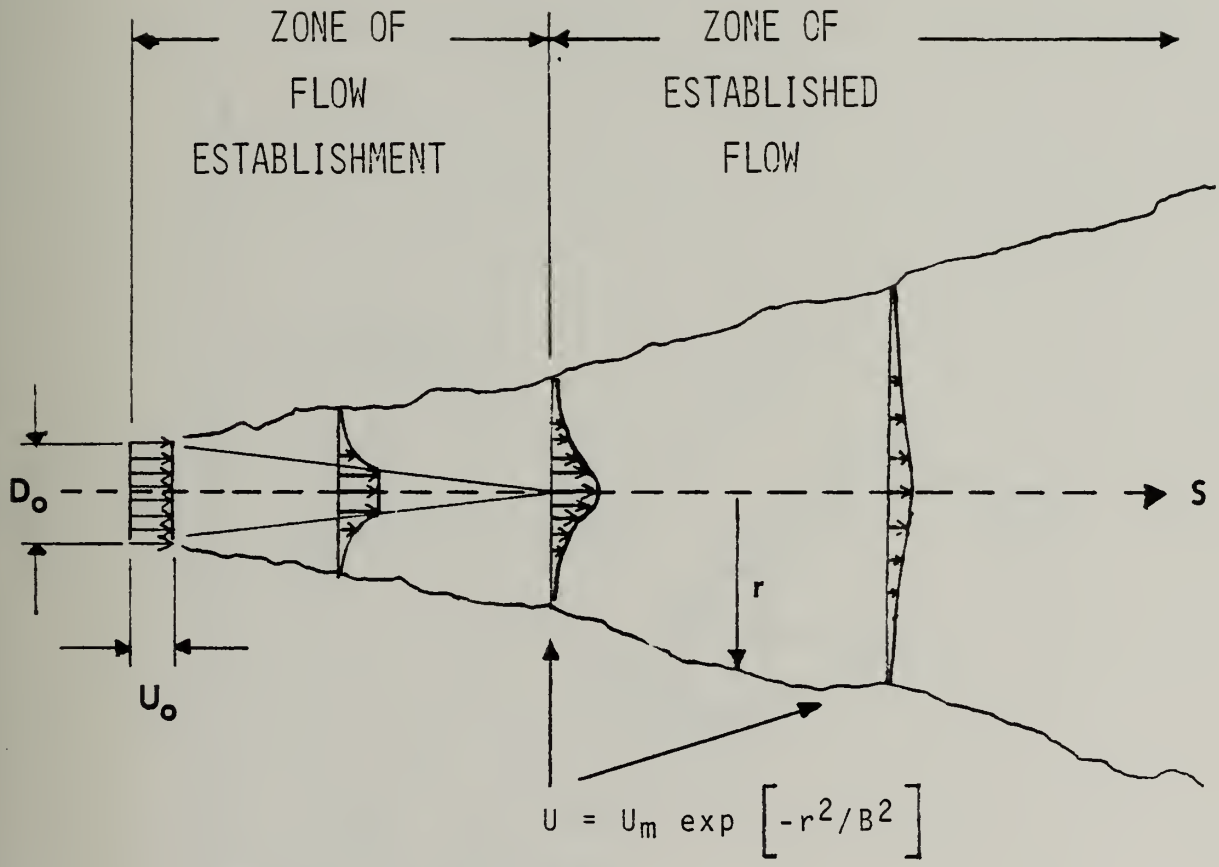

Figure 2-2. Development of Gaussian velocity profiles in a momentum jet after discharge

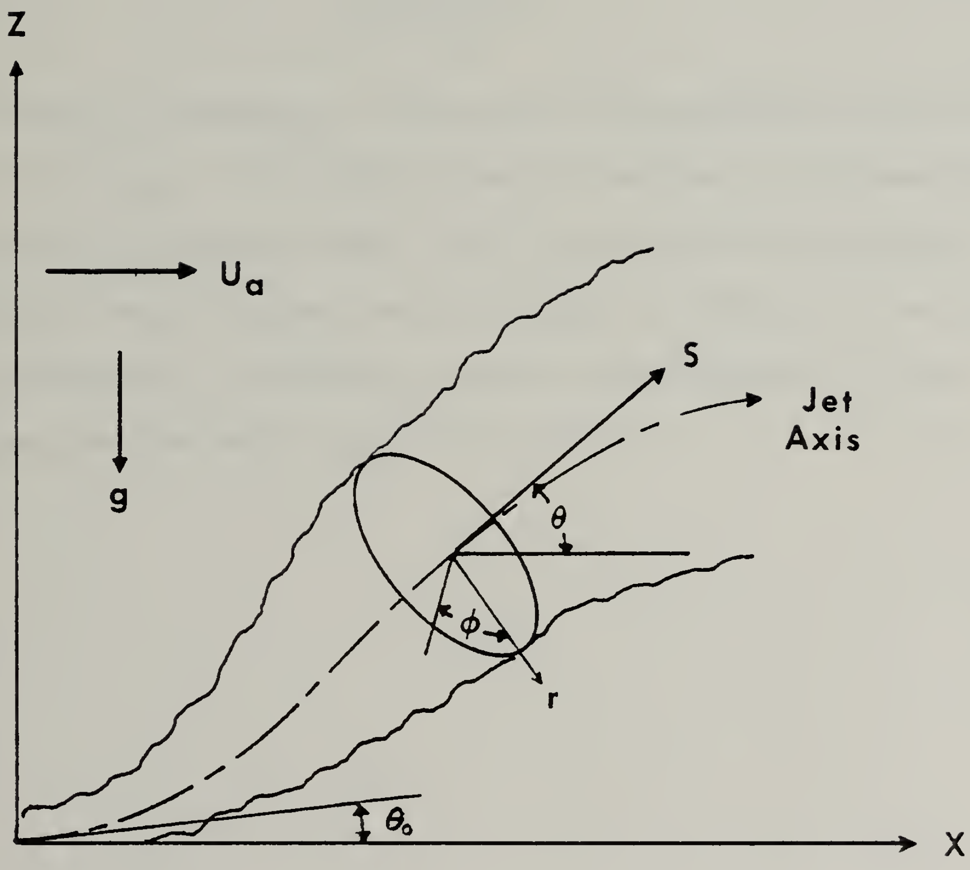

Figure 2-3. Coordinate system for physical dimensions and trajectory of a jet system

local angle between S and X, or the inclination of the jet from the horizontal, is θ. ϕ and r are polar coordinates defining the jet cross section, normal to S. Herein, any ambient medium motion is assumed to be horizontal.

An important quantitative measure of relative momentum and buoyancy is the densimetric Froude number, F, given by

$$F = \frac{U_0}{\left(gD \frac{\rho_a - \rho_0}{\rho_0}\right)^{1/2}} \tag{2-4}$$

The contribution of momentum is reflected in the numerator by the discharge velocity, U_0. The buoyancy effect is included in the denominator by the density differential term. Thus, the value of the densimetric Froude number ranges from near zero for plumes to infinity for pure, non-buoyant momentum jets. Hereafter, the term "Froude number" will be used to mean the densimetric form of Eqn. (2-4).

III. LITERATURE REVIEW

A. REVIEW OF PAST MODELLING

Several kinds of predictive models have been developed for the circular buoyant momentum jet. Although specific calculations consider different circumstances in origin of buoyancy, stratified/uniform ambients, quiescent/coflowing ambients, etc., they all may be classified by basic method:

(1) Algebraic models, based on either empirical data or simplification of differential model. These most typically predict only trajectory and jet width. Some, such as the model of Shirazi, McQuivey and Keefer [26], also predict velocity, concentration, and temperature residuals. Data-based algebraic models tend to become unreliable when the basic conditions upon which they were based, such as general temperature and salinity range of the jet and ambient, are significantly changed.

(2) Differential models, based on the relevant conservation equations (mass, momentum, energy, and scalar species). This modelling technique allows prediction of jet trajectory and width, as well as velocity, temperature, and concentration decay downstream in the jet. Stratification and motion of the ambient may also be accommodated.

Because of their limited scope, algebraic models will not be treated here. Certainly such models have a place in predictive use when the jet/ambient system involved is simple, and only information such as trajectory is required. However, the vast majority of effort in recent

years has involved the differential approach to jet modelling. In a majority of these differential models the entrainment mixing concept is invoked, rather than approaches utilizing mixing length hypotheses, k-ε models, or eddy diffusivity.

Morton et al. [20] were the first to use the entrainment concept to develop a buoyant jet model, as previously suggested by Taylor [27]. The concept supposes that the downstream induction of ambient fluid into the jet is proportional to the local jet centerline velocity, U_m, and a characteristic jet width, B. Thus,

$$E \propto 2\pi U_m B$$

where E represents volumetric rate of entrainment, or ambient inflow, into the jet, and is defined by

$$\frac{dQ}{dS} = \rho E$$

where Q is the total mass flow in the jet at any downstream location, s. Defining the constant of proportionality, the entrainment constant or coefficient as α, the rate of entrainment can be written as:

$$E = 2\pi\alpha U_m B$$

Solutions of the governing equations for differential modelling have been based on the following assumptions for round jets.

(1) The jet flow is steady.

(2) The jet flow is fully turbulent. Molecular diffusion can be neglected in comparison with turbulent transport.

(3) Streamwise turbulent transport is a negligible downstream transport mode, compared with streamwise convective transport.

(4) Variation of fluid density throughout the flow field is small compared to a chosen reference density. Density variations are included only in buoyancy terms, the Boussinesq approximation.

(5) Other fluid properties, such as viscosity, are constant over the range of interest.

(6) Pressure is hydrostatic throughtout the flow field.

(7) The jet remains axisymmetric throughout the near field. Velocity, temperature, density, and salinity profiles have no circumferential dependence.

The governing equations in the forms used in differential modelling are presented in Table (T3-1).

With the exception of Hoult et al. [16], all studies cited in the following discussion have assumed velocity, temperature, salinity, and density profiles are Gaussian. This assumption, therefore, limits the applicability of such models to the zone of established flow.

Hoult et al. circumvented the problem of having the model applicable only to the zone of established flow by assuming uniform ("top hat") profiles rather than a Gaussian distribution. This assumption was applied in the entire near field. As a result, the reduced form of the conservation equations for this model differ from the reduced form used by others. Since Hoult's modelling technique is valid for both the zone of flow establishment as well as the zone of established flow, initial conditions

Table (T3-1). Governing Equations for Entrainment Modelling of Buoyant Momentum Jets

EQUATION	NO.	
Continuity	3-1	$\frac{d}{dS}\{\int_0^{2\pi}\int_0^{\infty} Urdrd\phi\} = 2\pi\alpha U_m B$
Horizontal Momentum	3-2	$\frac{d}{dS}\{\int_0^{2\pi}\int_0^{\infty} U^2\cos\theta rdrd\phi\} = U_a E_v$
Vertical Momentum	3-3	$\frac{d}{dS}\{\int_0^{2\pi}\int_0^{\infty} \rho U^2\sin\theta rdrd\phi\} = \int_0^{2\pi}\int_0^{\infty} (\rho_a-\rho)grdrd\phi$
Energy	3-4	$\frac{d}{dS}\{\int_0^{2\pi}\int_0^{\infty} U(t-t_a)rdrd\phi\} = -\frac{dt_a}{dS}\int_0^{2\pi}\int_0^{\infty} Urdrd\phi$
Concentration (or scalar species)	3-5	$\frac{d}{dS}\{\int_0^{2\pi}\int_0^{\infty} U(c-c_a)rdrd\phi\} = -\frac{dc_a}{dS}\int_0^{2\pi}\int_0^{\infty} Urdrd\phi$
Horizontal Trajectory	3-6	$dX = dS\cos\theta$
Vertical Trajectory	3-7	$dZ = dS\sin\theta$

also differ. The end result of this approach is that values of ρ, t, c, and U ascribed to the jet at various points along the path are mean values for the entire jet cross section. This is a more limiting case than models using Gaussian profiles, where maximum values of jet properties result, and the entire cross section profile may be deduced from the appropriate Gaussian distribution.

Abraham [2] initially used the vertical and horizontal momentum equations, as well as the energy equation, to model jets discharged to a quiescent ambient. The continuity equation was not included. The solution required a pre-specification of the variation of B as a function of S. Most other models have included the continuity equation in lieu of pre-specifying the B variation.

The solution to the seven equations in Table (T3-1) yields values of jet centerline velocity, U_m, and temperature and concentration differences Δt_m and Δc_m, as well as jet width D(s) and trajectory as functions of S. The solution of the equations, of course, also requires that the entrainment function E be specified. Herein lie the principal differences between entrainment models. The models fall into two general categories: those for a quiescent ambient, and those for a flowing ambient.

1. Quiescent Ambient Media

Albertson et al. [3] and others have verified through measurements that for non-buoyant momentum jets, $F = \infty$, the appropriate value of within the zone of established flow is 0.057. There seems to be little disagreement with this value, based on numerous comparisons of differential modelling and experimental data.

Abraham [2] suggested, also on the basis of experimental evidence, that for relatively buoyant flows (small F), $\alpha = 0.085$. This is in good

agreement with the suggestion of List and Imberger [18] of $\alpha = 0.082$ for pure buoyant plumes ($F = 0$). Fan [9] also suggested $\alpha = 0.082$ for all flows except pure momentum jets. Fan also recommended, on the basis of his experiments, $\alpha = 0.057$ for the pure momentum jet.

In application, however, discharges are seldom either pure jets or plumes. Typically they are in some stage of transition away from jet behavior toward plume behavior. Morton et al. [20] proposed to model this transition by:

$$\alpha = 0.057 + \frac{a_2}{F_L}$$

where a_2 is an empirically determined coefficient, and F_L is a local Froude number, based on the local density difference. The same general form was derived by Fox [10] for a vertically discharged buoyant jet.

Hirst [14] maintained that for a discharge into a quiescent ambient, the entrainment function should depend on:

(1) local mean flow conditions in the jet, i.e., U_m and B.

(2) local buoyancy within the jet, as indicated by local Froude number, and

(3) jet orientation, θ_0.

The following form was proposed:

$$\alpha = 0.057 + \frac{0.97}{F_L} \sin(\theta)$$

This is the general form suggested by Morton and Fox, with the constants defined by fitting the function to known discharge and endpoint conditions of jet flow.

Another entrainment function for initially horizontal buoyant momentum jets is the jet-plume extrema fit proposed by Riester et al. [23]:

$$\alpha = \left[(0.057 \cos \theta)^2 + (0.082 \sin \theta)^2\right]^{1/2}$$

From data on a buoyant jet discharged vertically downward into a quiescent ambient, Davis et al. [6] proposed:

$$\alpha = 0.057 + \frac{0.083}{F^{.3}}$$

A tabular summary of entrainment functions for discharges into quiescent ambient media is given in Table (T3-2).

2. Flowing Ambient Media

Hirst [15] proposed an entrainment function applicable to 3-dimensional buoyant jet flow, in which the horizontal component of initial jet velocity was not necessarily parallel to ambient flow. Eliminating such terms, the form for two dimensional buoyant jets becomes:

$$E = (a_1 + \frac{a_2}{F_L} \sin \theta) b [|U_m - U_a \cos \theta| + a_3 U_a \sin \theta]$$

where the term

$$|U_m - U_a \cos \theta|$$

represents the relative velocity of the jet with respect to the ambient, in the direction of jet flow. It is a pure "coflow" term. The term

Table (T3-2). Entrainment Functions for Use with Quiescent Ambients

FORM: $E = 2\pi\alpha U_m B$

#	α	$\theta = 0$	$\theta = \pi/2$	F or $F_L \to 0$	F or $F_L \to \infty$	SOURCE
1	0.057	0.057	0.057		0.057	Albertson (1950) and others (1) [1]
2	0.082	0.082	0.082	0.082		List and Imberger (1973) and others (2) [18]
3	$0.057 + (0.97/F_L)\sin(\theta)$	0.057	$f(F_L)$	∞ $(\theta \neq 0)$	0.057	Hirst (1971) (3) [14]
4	$0.057 + 0.083/F^{0.3}$	$f(F)$	$f(F)$	∞	0.057	Davis, Shirazi, Slegel (1978) (4) [6]
5	$(0.057 \cos\theta)^2 +$ $(0.082 \sin\theta)^{2\ 1/2}$	0.057	0.082	$f(\theta)$	$f(\theta)$	Riester et al. (1980) (5) [23]
6	0.085	0.085	0.085	0.085		Abraham (1963) and others (6) [3]
7	$0.057 + (a_2/F_L)$	$f(F_L)$	$f(F_L)$		0.057	General Form of Morton et al. (1956) (7) [20]

(1) Applicable to simple momentum jet; (2) Applicable to simply buoyant plume;
(3) Applicable to buoyant jet discharged at varying angles to a quiescent ambient;
(4) Empirical fit for a buoyant jet discharged vertically downward to a quiescent ambient;
(5) Applicable to buoyant jet discharged horizontally to a quiescent ambient;
(6) Applicable to simple buoyant plume; (7)*Empirically determined coefficient, vertically discharged.

$$a_3 \, U_a \sin\theta$$

represents the contribution to the total value of entrainment of pure cross flow, or ambient motion normal to the jet axis, as the jet turns due to buoyancy.

Hirst specified values of a_1 and a_2 so that the flowing ambient entrainment function reduced to the quiescent ambient function if $U_a = 0$. He specified a value of 9.0 for a_3, based on a best fit to available data. This entrainment function thus became:

$$E = (0.057 + \frac{0.97}{F_L}\sin\theta)b[|U_m - U_a \cos\theta| + 9.0U_a \sin\theta]$$

Ginsberg and Ades [12] performed a least squares analysis on a large set of laboratory trajectory data. Using Hirst's entrainment model with a_1 and a_2 as specified, they found that a large variation in the value of a_3 was necessary to fit predicted results with the data. They constructed a correlation for a_3 as a function of F and the coflow ratio:

$$a_3 = 25.810[F^{0.19464} R^{0.35155}] - 10.825$$

where the coflow ratio, R, is defined as:

$$R = \frac{U_a}{U_0}$$

Other entrainment functions for coflowing ambients have appeared using variations of the governing differential equations. Schatzmann [25] proposed an entrainment function similar in form to that of Hirst, but

for use in a set of governing equations in which the Boussinesq approximation was not invoked. Fan [9] proposed an entrainment function for coflowing ambients which included a drag term as well as the standard proportionality of entrainment with centerline velocity and jet width. He found that the value of the drag coefficient used, as well as the entrainment constant ($\alpha = 0.082$ in this case) had to be readjusted to make the prediction conform with data with each change in discharge or ambient conditions. The entrainment functions of Hirst, Ginsberg and Ades, and Schatzmann are collected in Table (T3-3).

The progression of differential modelling, once the entrainment function is specified, is similar in most cases. First, the governing equations are integrated over the jet cross section so that they appear in differential form. They are then non-dimensionalized with respect to chosen reference variables. Initial conditions are specified. The resulting equations are then numerically integrated over the desired range of the streamwise pathlength, S. However, different downstream trajectory and decay may be calculated for a given jet due to differences in any of the following:

1. Entrainment function chosen;
2. Initial conditions specified for the beginning of the zone of established flow;
3. Equation of state specified for the density of the fluid;
4. Computational technique.

Examples of predicted jet trajectories and phsyical properties are presented in Figures (6-1) to (6-53). Comparison between models for identical or closely similar discharge and ambient conditions are presented in Figures (6-11) to (6-15). Discussion of these predictions and comparisons will be made later.

Table (T3-3). Entrainment Functions for Use with Flowing Ambients

With Coflowing Ambients:
Complete Volumetric Entrainment $(\lvert U^*\rvert = \lvert U-U_a \cos\theta\rvert)$

8	$E = [0.057 + (0.97/F_L) \sin\theta]b(\lvert U^*\rvert + 9.0U_a \sin \theta$	Hirst (1971) (8) [15]
9	$E = [0.057 + (0.97)/F_L) \sin\theta]b(\lvert U^*\rvert +$ $\{25.81[F^{0.195}(\frac{U_a}{U})^{0.352}] - 10.83\}U_a \sin\theta)$	Ginsberg & Ades (1975) (9) [12]
10	$E = [0.057 + (0.97/F_L \sin\theta]b(\lvert U^*\rvert$ $+ a_4U_a \sin\theta)/[1 + \frac{(a_3U_a\cos \theta)}{2\lvert U-U_a\rvert}]$	Schatzmann (1977) (10) [25]

(8) Applicable to buoyant jet discharged at varying angles to a flowing ambient. Cross flow terms omitted.
(9) Applicable to buoyant jet discharged at varying angles to a flowing ambient.
(10) Same as [9], empirically determined coefficients

B. REVIEW OF EXPERIMENTAL STUDIES

By far the most comprehensive and often cited set of data for buoyant water jets resulted from the work of Fan [7]. The experiments concerned two classed of buoyant jets:

(1) inclined jets discharged into a stagnant environment with linear density stratification.

(2) buoyant jets discharged into a uniform cross stream, $\theta_0 = 90°$, with no ambient stratification.

The experiments for the flows of group (1) above were conducted in a 2.26m × 1.07m tank with a depth of 0.61m. The tank was stratified with successive 3 cm to 5 cm layers of aqueous salt solutions. Tank temperature remained constant within a 2°C range over the duration of the experiments.

Nozzle diameters varied between 0.223 and 0.762 cm. Flow into the nozzle was provided from an unregulated head tank, which provided a discharge rate estimated by Fan to be constant within 3%. Measurements in each experimental run were limited to jet trajectory and half width, observed photographically by use of a tracer dye premixed into the discharged fluid.

Fan described one of the dilemmas of conducting experiments on jets of small physical scale:

> For complete experimental check on theory, it is necessary to determine values of the jet velocity and density. Practically however, laboratory experiments on density stratified flows are usually limited in scale and do not allow the time required in measuring time fluctuating quantities. On the other hand, the jet trajectories and half widths can be determined conveniently by photographic means. These two quantities are interrelated with other jet characteristics. Thus the comparison of the observed and calculated values of these two quantities is believed to be indicative of the applicability of the theoretical solutions. [8]

The experimental discharge Froude number ranged from 10 to 60, with the exception of 3 runs with a non-buoyant momentum jet ($F = \infty$).

In Fan's second group of experiments, with a flowing, unstratified pure water ambient, the saline jets were actually negatively buoyant. Conductivity measurements were taken by variable position probes at a number of downstream stations. The locus of stations of maximum concentration was defined as the jet centerline. The jet width was defined from concentration readings taken radially outward from the centerline.

These experiments were conducted in a 40m flume, 1.1m wide, with a water depth of .51m. Flow was induced by inclining the flume. A region in the core of the flume flow with the least shear effects from wall boundaries was selected to introduce the jet via a nozzle. Variation of ambient flow in this region was estimated at +6% to -9%.

Experimental runs were made for a Froude number range of 10 to 80, ambient flow of $R = 0.0625$ to 0.25, and a discharge diameter of 0.5 cm to 0.762 cm.

In an attempt to ascertain the effect of ambient turbulence and shear introduced by the restricted cross-sectional dimensions of the flume, a limited set of concentration measurements were made in which the fluid in the flume was stagnant and the jet discharge towed through the ambient by a carriage mounted over the flume. In this case, conductivity probes were fixed to the carriage and moved to different relative positions in successive runs.

The experiments of Fan have been used by numerous modellers, including Fan himself, as a basis for analytical/experimental comparison. The experiments also served to validate earlier hypotheses and observations regarding the Gaussian distribution of concentration in the zone of established flow.

Riester, Bajura, and Schwartz [23] studied horizontally discharged buoyant fresh and salt water jets. The ambient was quiescent and unstratified. A 6.2 × 1.1 × 0.8 m tank was used in conjunction with a 0.87 cm diameter discharge nozzle. Jet trajectory and width were recorded photographically by a tracer dye in the jet fluid. Temperature distributions were measured by a rake of thermocouples. Jet centerline was determined through the measured temperature distributions.

A novel aspect of these experiments was the wide range of ambient temperatures utilied (4.5°C-43.0°C), and the use of both salt and fresh water jets. Some possible implications of the results will be discussed in a later section.

Davis, Shirazi, and Slegel [6] measured the behavior of single and multiple port salt water discharges directed vertically downward into a fresh water ambient. A flowing ambient was simulated by mounting the discharge nozzle on a moving carriage mounted over a 17.1m tank. Water depth in the tank was 0.91m. Concentration profiles were measured by conductivity probes, and velocity measurements were made by hot film anemometry. Several runs of these experiments made with the carriage stationary led to the proposal of the entrainment function:

$$\alpha = 0.057 + \frac{0.083}{F^{.3}}$$

These same experiments verified the Gaussian nature of velocity profiles in the zone of established flow.

Shirazi, McQuivey, and Keefer [26] studied buoyant jets in flowing turbulent ambients. An inclined 120 ft. flume was used to produce

ambient flow. Turbulence was introduced by imposing a layer of varying sized rock in the flume bed. Temperature and salinity concentration were measured using conductivity probes. Turbulence was monitored by hot film anemometers.

As a result of these experiments, a set of algebraic correlations were made, expressing temperature and concentration residuals, jet width, and trajectory as functions of downstream distance, F, and R. It was determined that as the level of turbulence increases, the rate of decay of centerline temperature and concentration with respect to the streamwise coordinate increases. Not surprisingly, it was also found that correlation of the data became more difficult as turbulence level increased.

Pryputniewicz and Bowley [22] conducted measurements of a buoyant jet discharged vertically upward into a uniform quiescent ambient. Temperature profiles were measured by a rake of thermistors in the flow field. Of interest in these experiments was the presentation of data which showed temperature residuals as measured near the terminal point of rise at the surface. Froude numbers of 1 to 50 and nozzle diameters of 0.425 and 0.55 inches were used.

A summary of the range of parameters studied in various experiments is presented in Table (T3-4).

Table (T3-4). Summary of Experimental Parameters

Experimenter	Initial Jet Diameter	F	Ambient			Measured Quantities					Max. Vertical Range of Rise	R
			Unstrat.	Strat.	Flowing	Traj.	Width	Velocity	Conc.	Temp.		
Fan	0.223 - 0.762 cm	10-60		X		X	X				0.61 m	-
Fan	0.5 - 0.762 cm	10-80	X		X	X	X		X		0.61 m	0.625 -0.25
Riester et al	0.87 cm	3.16 - 20		X		X	X			X	0.8 m	-
Davis et al	1.12 - 3.81 cm	1.5 - 36	X		X	X	X	X	X		0.91 m	0.17 - 1.0
Shirazi et al	0.468 - 1.882 cm	6.3 - 210	X		X	X	X	X	X	X	2 ft	0.11 - 3.7
Pryputniewicz and Bowley	0.425 - 0.55 in	1-50	X			X	X			X	5 ft	-

IV. EQUATIONS OF STATE AND AMBIENT STRATIFICATION MODELLING

The determination of the discharge Froude number and the buoyancy force requires the evaluation of the temperature, t, and concentration, c, effects on density. Often the density, $\rho(t,c,p)$ is a sufficiently linear function of both t and c over the range of temperature and concentration difference between the jet and the ambient. Then density differences may be accurately estimated in terms of the two volumetric coefficients of expansion,

$$\beta = -\frac{1}{\rho_r}\left(\frac{\partial\rho}{\partial t}\right)_{c,p} \quad \text{and} \quad \gamma = -\frac{1}{\rho_r}\left(\frac{\partial\rho}{\partial c}\right)_{t,p}$$

where ρ_r is some reference value of ρ, say $\rho_0 = \rho(t_0,c_0,p_0)$. Then

$$\Delta\rho = -\beta\rho_r\Delta t \quad \text{and} \quad \Delta\rho = -\gamma\rho_r\Delta c$$

for the separate t and c effects on density. The density at some t and c, in terms of the initial jet density ρ_0, is written as

$$\rho(t,c,p_0) - \rho(t_0,c_0,p_0) = -\rho(t_0,c_0,p_0)[\beta(t-t_0)-\gamma(c-c_0)]$$

or

$$\rho = \rho_0[1 - \beta(t-t_0) - \gamma(c-c_0)]$$

In particular, the initial density difference between the local ambient and the initial jet, which appears in the Froude number, is

$$\frac{\rho_{a0} - \rho_0}{\rho_0} = \beta(t_0 - t_a) + \gamma(c_0 - c_a)$$

In an unstratified ambient medium, the reduced, non-dimensional forms of equations (3-3,4 and 5) will contain the following three non-dimensional terms:

$$\left(\frac{\rho_a - \rho_m}{\rho_{a0} - \rho_0}\right), \qquad \left(\frac{t_m - t_a}{t_0 - t_{a0}}\right), \qquad \left(\frac{c_m - c_a}{c_0 - c_{a0}}\right).$$

With the values of λ in Equations (2-2 and 3) the same, profiles of t and c are the same and

$$\left(\frac{t_m - t_a}{t_0 - t_{a0}}\right) = \left(\frac{c_m - c_a}{c_0 - c_{a0}}\right)$$

at all points along a trajectory at which $(t_0 - t_{a0}) \neq 0$ and $(c_0 - c_{a0}) \neq 0$.

Thus, for constant values of β and γ in an unstratified ambient,

$$\left(\frac{\rho_a - \rho_m}{\rho_{a0} - \rho_0}\right) = \left(\frac{t_m - t_a}{t_0 - t_{a0}}\right) = \left(\frac{c_m - c_a}{c_0 - c_{a0}}\right)$$

and defined values of β and γ are not required for integration, computation, and solution, beyond initial definition of discharge Froude number.

A similar situation exists for some special cases of linearly stratified ambients. If $\rho = \rho(t)$, and density stratification is defined solely by a temperature stratification parameter

$$\frac{\left(\frac{\partial t_a}{\partial z}\right) D}{(t_{a0} - t_0)}$$

Then the definition of β beyond the initial computation of discharge Froude number is not required. For such flows,

$$\left(\frac{\rho_a-\rho_m}{\rho_{a0}-\rho_0}\right) = \left(\frac{t_m-t_a}{t_0-t_{a0}}\right)$$

pertains throughout. In addition, if $\rho \neq \rho(c)$, an assumption that might be made in a jet with a tracer dye, the concentration and vertical momentum equations are not coupled. Concentration computations can proceed independently, even to the point of specifying a concentration stratification if desired.

Parallel reasoning holds true for the case of $\rho = \rho(c)$, in which case a density dependence on concentration stratification parameter would couple the concentration and vertical momentum equation. Presumably temperature would be uniform throughout the system in such a case.

These simple, degenerate cases of the overall modelling problem are important because they represent conditions under which measurements are often taken. Modellers then specify these conditions to compare data with their analytical models.

The underlying assumptions and limitations of such formulation are:

(1) With no equation of state incorporated in the computational process, only unstratified ambients may be acommodated if $\rho = \rho(t,c)$, and then only if β and γ are assumed constant.

(2) If no equation of state is included in the model, density stratification in the ambient may be specified as either

$$\frac{\left(\frac{\partial t_a}{\partial z}\right)D}{(t_{a0}-t_0)}, \quad \rho = \rho(t)$$

or

$$\frac{(\frac{\partial c_a}{\partial z})D}{(c_{a0}-c_0)}, \qquad \rho = \rho(c)$$

or

$$\frac{(\frac{\partial \rho_a}{\partial z})D}{(\rho_{a0}-\rho_0)}, \qquad \text{(directly).}$$

Ambients with more than one density-constituent gradient cannot be accommodated, since temperature, concentration, and density residuals would be independent of each other and profiles could be dissimilar.

The more general case of an ambient medium with temperature and concentration stratification requires an equation of state for solution of the governing equations. Such a temperature/concentration/density relation may be used in one of two ways:

(1) Internally in the calculational scheme, with ambient temperature and concentration gradients specified. The local density differences are computed downstream from jet temperature and concentration decays calculated from the energy and concentration equations.

(2) External to the actual integration calculations, by using specified ambient stratification to calculate the ambient density variation a priori. The resulting ambient density gradient is then used in an equation of density excess or deficiency of the form:

$$\frac{d}{dS}\{\int_0^{2\pi}\int_0^{\infty} U(\rho_a-\rho_m)rdrd\phi\} = -\frac{d\rho_a}{dS}\{\int_0^{2\pi}\int_0^{\infty} Urdrd\phi\}$$

assuming the same Gaussian profile for density as for two of its constituent properties, temperature and concentration. This extra equation effectively uncouples the temperature and concentration equations from the vertical momentum equation.

Method (1) above was used by Hirst [15]. The second method above was used by Fan [9]. Other models specify the method of use of an equation of state, only as noted below.

Hirst specified values of β and γ, assumed constant throughout the downstream integration of the governing equations. The equation of state was:

$$\frac{\rho_a - \rho}{\rho_0} = \beta(t - t_a) + \gamma(c - c_{a0})$$

In reality, of course, density of water is a complex and, under some conditions, highly non-linear, function of three variables--temperature, species concentration, and pressure. Many modelling situations might arise in which the range of these variables clearly argue against the use of constant values of γ and β, as well as the omission of the pressure dependence of density. Table (T4-1) shows some of the variation of β encountered over small temperature ranges, for both saline water at 35 ‰ (typical of sea water) and fresh water. The pressure in both cases is one atmosphere.

In their model, Riester, Bajura, and Schwartz [23] attempted to account for the effect of variable β by representing it in the form

$$\beta_a = a_1 + a_2 t + a_3 t^2 \qquad (4\text{-}1)$$

Table T4-1. Variation of β over limited temperature range, for pure and saline water

$-\frac{1}{\rho}\left(\frac{\partial \rho}{\partial t}\right)_P \times 10^5 \left(\frac{1}{^{\circ}C}\right)$ FOR PRESSURE = 1 ATM.

SALINITY, ‰	TEMPERATURE ($^{\circ}$C)									
	-1	0	1	2	3	4	5	6	7	8
35	3.70	5.01	6.27	7.49	8.67	9.83	10.97	12.09	13.19	14.29
0				-3.31	-1.77	0.05	1.68	3.22	4.66	6.05

where the coefficients a_1, a_2, and a_3 were evaluated for the temperature range pertinent to a given calculation. The discharge Froude number was then "adjusted" using the relation

$$F_a = \frac{U_0}{(gD\beta_a(t_0-t_a))^{1/2}}$$

They summarized the need for an effective equation of state as follows:

> ...if the initial temperature difference between the jet and the ambient is greater than 3°C, the effect of the temperature-density relationship of water on the trajectory must be considered. This result is of particular significance when laboratory models are operated at high temperature differences to simulate prototype flow characterized by low temperature differences....the effects of temperature on the trajectory can be minimized by using the (adjusted) Froude number ... to define flow conditions....Additional work is required to determine the correlation application to jet flows which experience reversing buoyancy for cases near 4°C.
>
> Salt water jets cannot simulate the characteristics of fresh water jets operating over large temperature differences since the salt models do not duplicate the temperature-density characteristics of the fresh water system. [24]

In view of this last observation, it is noted that, although the proposed model attempted to compensate for the variable temperature effects on density, no dependence on salinity was included except for that which may have been implicit in the choice of the three coefficients in Equation (4-1).

The ideal equation of state for buoyant jet modelling would comprehensively represent density as a function of temperature, species concentration, and pressure. Such an equation should be applicable in all temperature, concentration, and pressure ranges of interest. Also, for most modelling of fresh/salt water systems, the concentration variable should be salinity. An equation of state which seems to fulfill these requirements will be suggested in the following section.

V. PRESENT METHOD

The foregoing modelling system assumptions regarding the flow field also apply to all the calculations done in this work. Generally, they assume a steady, axisymmetric jet with negligible molecular transport, negligible streamwise turbulent transport, and small curvature effects, operating in a hydrostatic pressure field under the Boussinesq approximation.

The governing equations in the zone of established flow follow.

Continuity of mass equates the downstream change in total mass of the jet to the mass of fluid entrained. The entrainment concept results in the following:

$$\frac{d}{dS}\{\int_0^{2\pi} \int_0^{\infty} \rho U r dr d\phi\} = \rho(2\pi a U_m B)$$

The first Boussinesq approximation, concerning density level, yields:

$$\frac{d}{dS}\{\int_0^{2\pi} \int_0^{\infty} U r dr d\phi\} = 2\pi\alpha U_m B \qquad (5\text{-}1)$$

Horizontal momentum is conserved in a hydrostatic pressure field. Thus, the change in horizontal momentum within the jet is equal to the horizontal momentum of the fluid entrained:

$$\frac{d}{dS}\{\int_0^{2\pi} \int_0^{\infty} \rho U^2 \cos\theta r dr d\phi\} = \rho U_a E_v$$

Again, invoking the Boussinesq approximation:

$$\frac{d}{dS}\{\int_0^{2\pi}\int_0^{\infty} U^2 \cos\theta rdrd\phi\} = U_a E_v \tag{5-2}$$

The change in the vertical momentum of the jet system is the result of the action of the buoyancy force over the extent of the jet:

$$\frac{d}{dS}\{\int_0^{2\pi}\int_0^{\infty} \rho U^2 \sin\theta rdr\} = \int_0^{2\pi}\int_0^{\infty} (\rho_a-\rho)grdrd\phi \tag{5-3}$$

In a stratified ambient, the ambient temperature, as well as the temperature of the jet, may be variable along the trajectory. The energy equation relates the change in energy of the system, as expressed by a temperature excess or deficiency relative to the ambient, to the rate at which the ambient temperature is changing.

$$\frac{d}{dS}\{\int_0^{2\pi} C_p\rho U(t-t_a)rdrd\phi\} = -\frac{dt_a}{dS}\int_0^{2\pi}\int_0^{\infty} \rho C_p Urdrd\phi$$

Assuming constant specific heat and the Boussinesq approximation,

$$\frac{d}{dS}\{\int_0^{2\pi}\int_0^{\infty} U(t-t_a)rdrd\phi\} = -\frac{dt_a}{dS}\int_0^{2\pi}\int_0^{\infty} Urdrd\phi \tag{5-4}$$

Similarly, the change in concentration excess relative to the ambient is related to the rate at which the ambient reference concentration is changing:

$$\frac{d}{dS}\{\int_0^{2\pi}\int_0^{\infty} \rho U(c-c_a)rdrd\phi\} = -\frac{dc_a}{dS}\int_0^{2\pi}\int_0^{\infty} \rho Urdrd\phi$$

Again, invoking the Boussinesq approximation:

$$\frac{d}{dS}\left\{\int_0^{2\pi}\int_0^{\infty} U(c-c_a)rdrd\phi\right\} = -\frac{dc_a}{dS}\int_0^{2\pi}\int_0^{\infty} Urdrd\phi \qquad (5\text{-}5)$$

Geometrically, the incremental trajectory of the jet may be described by:

$$dX = dS\cos\theta, \qquad (5\text{-}6)$$

$$dZ = dS\sin\theta \qquad (5\text{-}7)$$

It will be assumed that the Gaussian velocity, temperature, and concentration profiles cited previously are valid for the zone of flow establishment.

Appendix A contains the development of the governing equations from their stated form above to their reduced form. In Appendix B the equations are non-dimensionalized. The dimensionless equations appear in Table (T5-1). The forms of the equations for degenerate cases are presented as follows:

(1) Flowing unstratified ambient--Table (T5-2);

(2) Quiescent, stratified ambient--Table (T5-3);

(3) Quiescent, unstratified ambient--Table (T5-4).

The above equations apply only in the zone of established flow, which begins at S_e, see Figures F-2-1 and F-2-2. Estimates of the end of the region of flow establishment have been made. The procedures followed here in calculations are based on the experimental work of Abraham [2] and the analytical development by Hirst [13]. They are also consistent with assumptions made in references [14], [15], and [12]. The initial conditions are:

Table (T5-1). Non-dimensional Differential Form of the Governing Equations for a Flowing, Stratified Ambient

EQUATION

CONTINUITY	$\frac{d}{ds}(u_m b^2) = 2\alpha b[\lvert u_m - R\cos\theta\rvert + a_3 R\sin\theta]$
HORIZONTAL MOMENTUM	$\frac{d}{ds}(u_m^2 b^2 \cos\theta) = 4R\alpha b[\lvert u_m - R\cos\theta\rvert + a_3 R\sin\theta]$
VERTICAL MOMENTUM	$\frac{d}{ds}(u_m^2 b^2 \sin\theta) = (\frac{\rho_a - \rho_m}{\rho_{a0} - \rho_{m0}}) \cdot \frac{2\lambda^2 b^2}{F^2}$
ENERGY	$\frac{d}{ds}(u_m \Delta t \frac{\lambda^2 b^2}{(\lambda^2+1)}) = - \frac{\Delta t_a}{ds}\{u_m b^2\}$
CONCENTRATION	$\frac{d}{ds}(u_m \Delta c \frac{\lambda^2 b^2}{(\lambda^2+1)}) = - \frac{\Delta c_a}{ds}\{u_m b^2\}$
HORIZONTAL TRAJECTORY	$\frac{d}{ds}(x) = \cos\theta$
VERTICAL TRAJECTORY	$\frac{d}{ds}(z) = \sin\theta$

Table (T5-2). Non-dimensional Differential Form of the Governing Equations for a Flowing, Unstratified Ambient

EQUATION	
CONTINUITY	$\frac{d}{ds}(u_m b^2) = 2\alpha b[\lvert u_m - R\cos\theta\rvert + a_3 R\sin\theta]$
HORIZONTAL MOMENTUM	$\frac{d}{ds}(u_m^2 b^2 \cos\theta) = 4R\alpha b[\lvert u_m - R\cos\theta + a_3 R\sin\theta]$
VERTICAL MOMENTUM	$\frac{d}{ds}(u_m^2 b^2 \sin\theta) = (\frac{\rho_a - \rho_m}{\rho_{a0} - \rho_{m0}}) \cdot \frac{2\lambda^2 b^2}{F^2}$
ENERGY	$\frac{d}{ds}(u_m \Delta t \frac{\lambda^2 b^2}{(\lambda^2+1)}) = 0$
CONCENTRATION	$\frac{d}{ds}(u_m \Delta c \frac{\lambda^2 b^2}{(\lambda^2+1)}) = 0$
HORIZONTAL TRAJECTORY	$\frac{d}{ds}(x) = \cos\theta$
VERTICAL TRAJECTORY	$\frac{d}{ds}(z) = \sin\theta$

Table (T5-3). Non-dimensional Differential Form of the Governing Equations for a Quiescent, Stratified Ambient

EQUATION	
CONTINUITY	$\frac{d}{ds}(u_m b^2) = 2\alpha u_m b$
HORIZONTAL MOMENTUM	$\frac{d}{ds}(u_m^2 b^2 \cos\theta) = 0$
VERTICAL MOMENTUM	$\frac{d}{ds}(u_m^2 b^2 \sin\theta) = (\frac{\rho_a - \rho_m}{\rho_{a0} - \rho_{m0}}) . \frac{2\lambda^2 b^2}{F^2}$
ENERGY	$\frac{d}{ds}(u_m \Delta t \frac{\lambda^2 b^2}{(\lambda^2+1)}) = - \frac{\Delta t_a}{ds}\{u_m b^2\}$
CONCENTRATION	$\frac{d}{ds}(u_m \Delta c \frac{\lambda^2 b^2}{(\lambda^2+1)}) = - \frac{\Delta c_a}{s}\{u_m b^2\}$
HORIZONTAL TRAJECTORY	$\frac{d}{ds}(x) = \cos\theta$
VERTICAL TRAJECTORY	$\frac{d}{ds}(z) = \sin\theta$

Table (T5-4). Non-dimensional Differential Form of the Governing Equations for a Quiescent, Unstratified Ambient

EQUATION	
CONTINUITY	$\frac{d}{ds}(u_m b^2) = 2\alpha u_m b$
HORIZONTAL MOMENTUM	$\frac{d}{ds}(u_m^2 b^2 \cos\theta) = 0$
VERTICAL MOMENTUM	$\frac{d}{ds}(u_m^2 b^2 \sin\theta) = (\frac{\rho_a - \rho_m}{\rho_{a0} - \rho_{m0}}) \cdot \frac{2\lambda^2 b^2}{F^2}$
ENERGY	$\frac{d}{ds}(u_m \Delta t \frac{\lambda^2 b^2}{(\lambda^2+1)}) = 0$
CONCENTRATION	$\frac{d}{ds}(u_m \Delta c \frac{\lambda^2 b^2}{(\lambda^2+1)}) = 0$
HORIZONTAL TRAJECTORY	$\frac{d}{ds}(x) = \cos\theta$
VERTICAL TRAJECTORY	$\frac{d}{ds}(z) = \sin\theta$

$$U_{me} = U_0$$

$$\lambda_t = \lambda_c = 1.16$$

$$B_e = D/\sqrt{2}$$

$$\frac{(t_m - t_a)_e}{(t_m - t_a)_0} = \frac{(\lambda_t^2 + 1)}{2\lambda_t^2}$$

$$\frac{(c_m - c_a)_e}{(c_m - c_a)_0} = \frac{(\lambda_c^2 + 1)}{2\lambda_c^2}$$

The value of S_e, relative to the point of discharge, is:

$$S_e/D = 6.2 \qquad F \geq 40$$

$$S_e/D = 3.9 + 0.057F^2 \qquad 5 \leq F < 40$$

$$S_e/D = 2.075 + 0.425F^2 \qquad 1 \leq F < 5$$

$$S_e/D = 0. \qquad 0 \leq F < 1$$

All that remains to be specified to integrate the equations downstream along the S coordinate are the entrainment function to be used, the ambient stratification condition, and the density equation of state.

The calculations used an IBM 360 and IBM 3033 computing system. The method of integration is a trapezoidal rule expression of the governing equations with adjustable step size. Two versions of the

general method were used here. The first is used to evaluate flows in unstratified ambients, or in ambients characterized by linear gradients in temperature, concentration, or density itself. No explicit equation of state is necessary, only β and γ. The second version, with the same computational technique, uses an accurate density equation.

Since the objective is to develop a predictive model applicable to large scale discharges in ocean water, the density equation used in version two is that of Gebhart and Mollendorf [11]. This relation correlates the temperature dependence of density as an expansion around the density extremum temperature at any given level of pressure and salinity. The resulting expression is fitted to a comprehensive set of experimental data over temperature, salinity and pressure maximums of $t = 20°C$, $s = 40\%$, and $p = 1000$ bars absolute. Density is in kg/m^3. This equation is given in Appendix C.

For each of these calculations, the density equation was first used to establish the density field in the ambient. This requires input of at least one reference temperature and salinity level and appropriate gradients, or specification of the complete temperature and salinity fields. The water surface pressure is assumed to be one atmosphere. The relation is first used at the surface, and density is calculated progressively downward, using hydrostatically integrated values of pressure along the way.

Once the ambient density field is established, the relation is then used to calculate the density terms in the vertical momentum equation at each calculational interval, using the jet temperature and concentration values predicted by their respective equations. Ambient density and pressure are assumed to be linear between the points calculated for the ambient.

The relation is also used to calculate the initial density difference between the jet and the ambient at the point of discharge, given temperature and salinity level, or to calculate the initial temperature of the jet, given Froude number and salinity.

The advantages of using an accurate density relation include:

(1) The full density dependence on temperature, salinity and pressure is taken into account in all calculations.

(2) The actual ambient density field of either a hypothetical or real circumstance is accurately established, utilizing appropriate temperature and salinity input.

(3) The relation is readily applicable to computerized analysis, and is computationally compact.

VI. RESULTS

Comparison between the jet trajectories and properties calculated here and earlier calculations, using the same entrainment function, has been generally good. This is in spite of differing computing techniques used in different studies. The resulting trajectories will be compared with earlier calculations.

A. UNSTRATIFIED, QUIESCENT AMBIENT

This jet/ambient system represents by far the most frequently modelled case. Comparison here is for horizontally discharged buoyant jets.

Figures (6-1) and (6-2) compare the trajectories predicted by these calculations, for F = 10 and 20, with the calculations of Abraham [3], both using $\alpha = 0.085$. Correspondence between the two is consistent, with the present method predicting slightly less horizontal penetration of the ambient than Abraham's model at all Froude numbers compared.

Figures (6-3) and (6-4) show the uniformly close correspondence between these calculations and those of Hirst [14], [15], both using Hirst's entrainment function, entry 3 in Table T3-2, for F = 4,6,8 and 10.

Figures (6-5) through (6-8) again compare present calculations with those of Hirst, but with both using the entrainment functions $\alpha = 0.057$ and $\alpha = 0.082$. Data of Fan is included for comparison where available. The results, combined with those in Figures (6-3) and (6-4) indicate that within the Froude number range compared, correspondence of present calculations with Hirst's model is very good regardless of the choice of entrainment function.

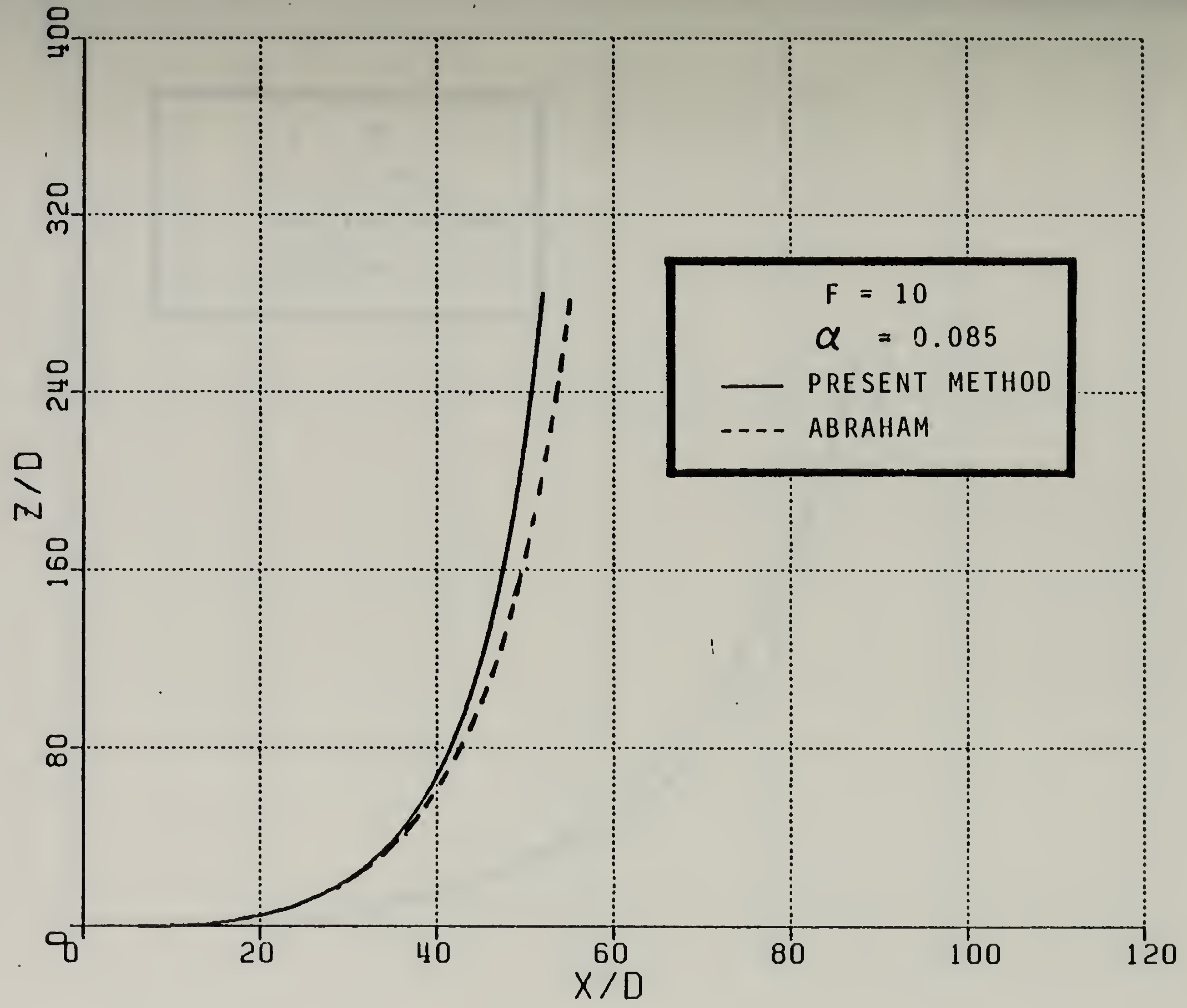

Figure 6-1. Comparison of present method with model of Abraham [3]

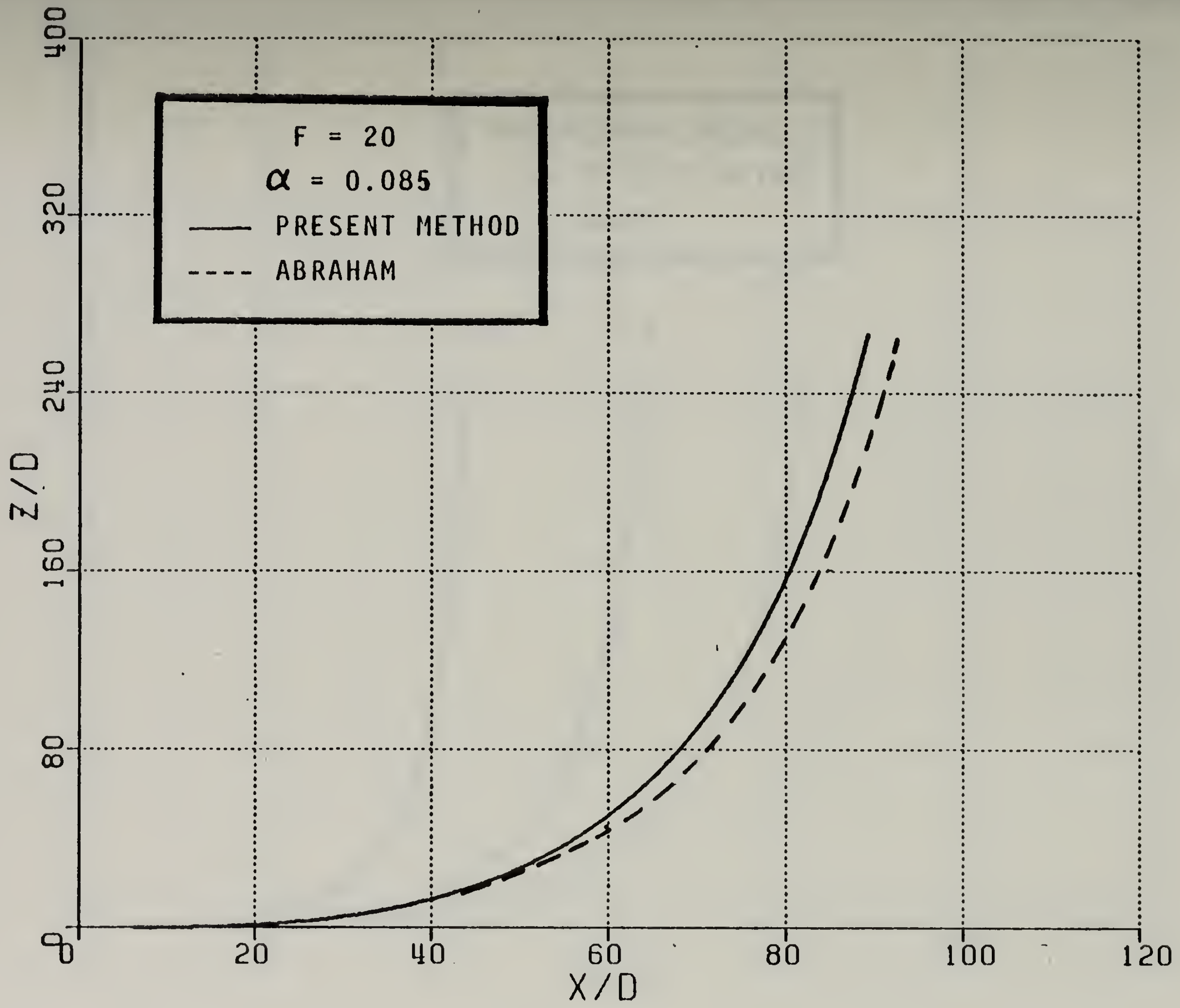

Figure 6-2. Comparison of present method with model of Abraham [3]

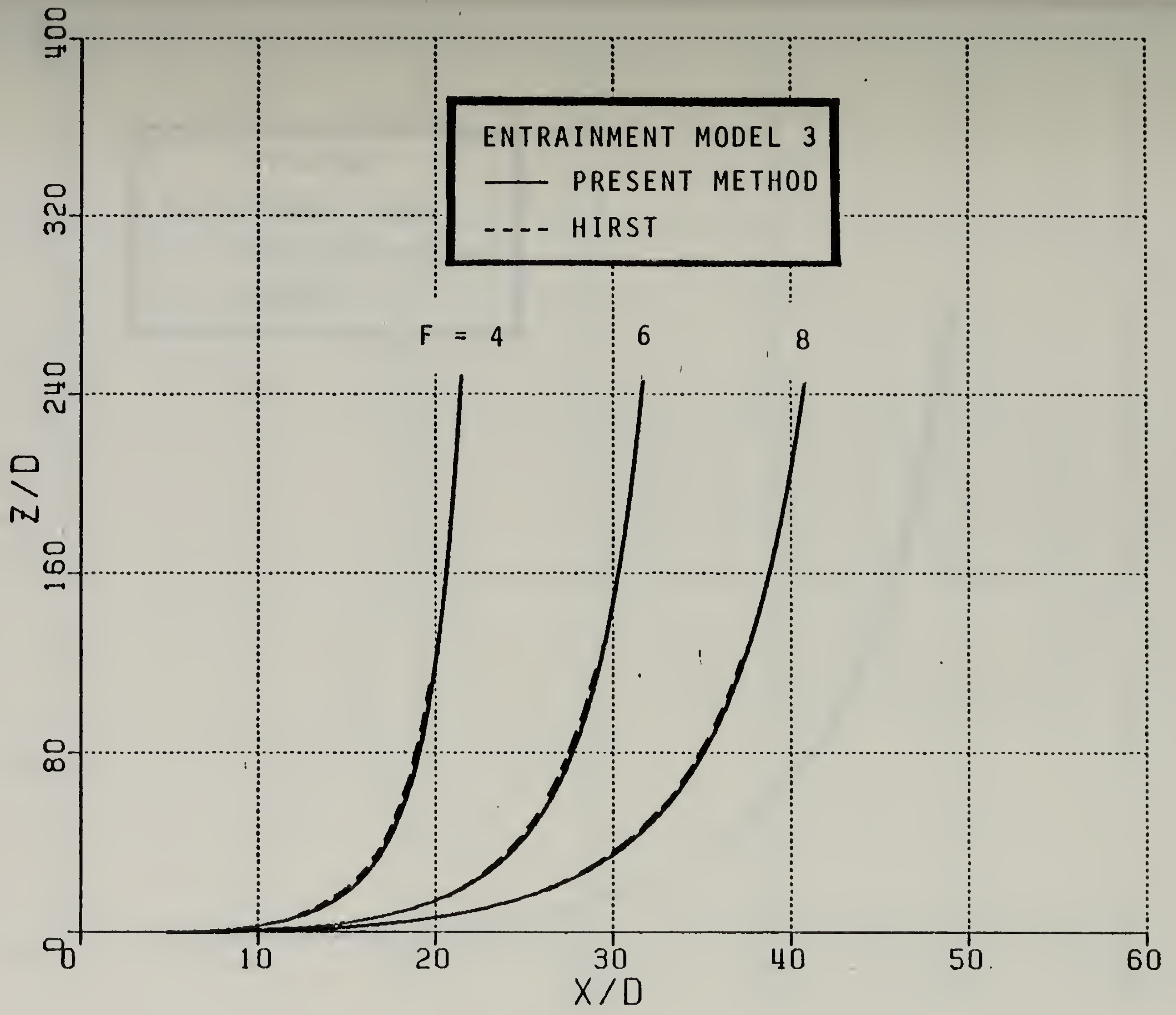

Figure 6-3. Comparison of present method with model of Hirst [13]

[illegible]

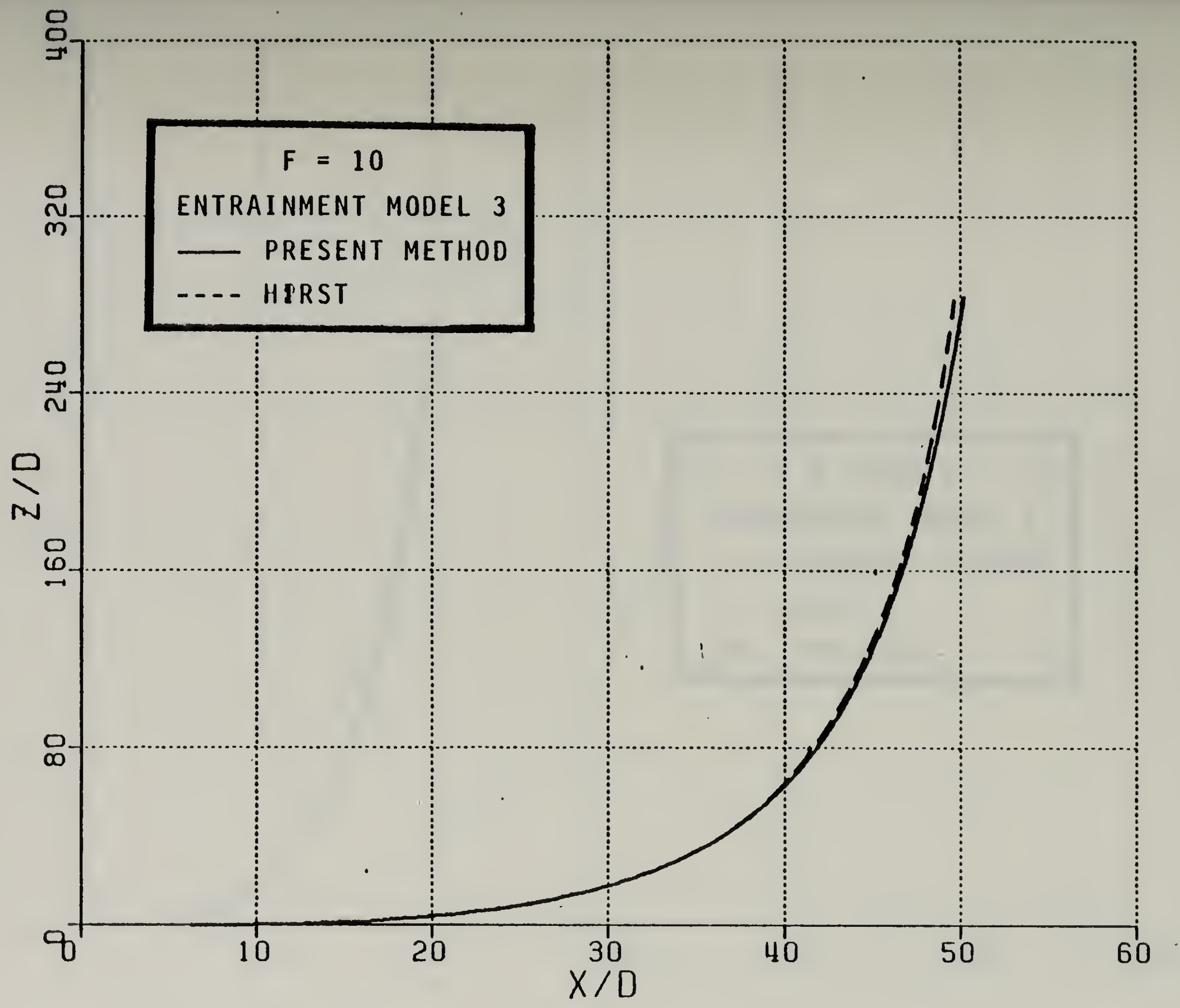

Figure 6-4. Comparison of present method with model of Hirst

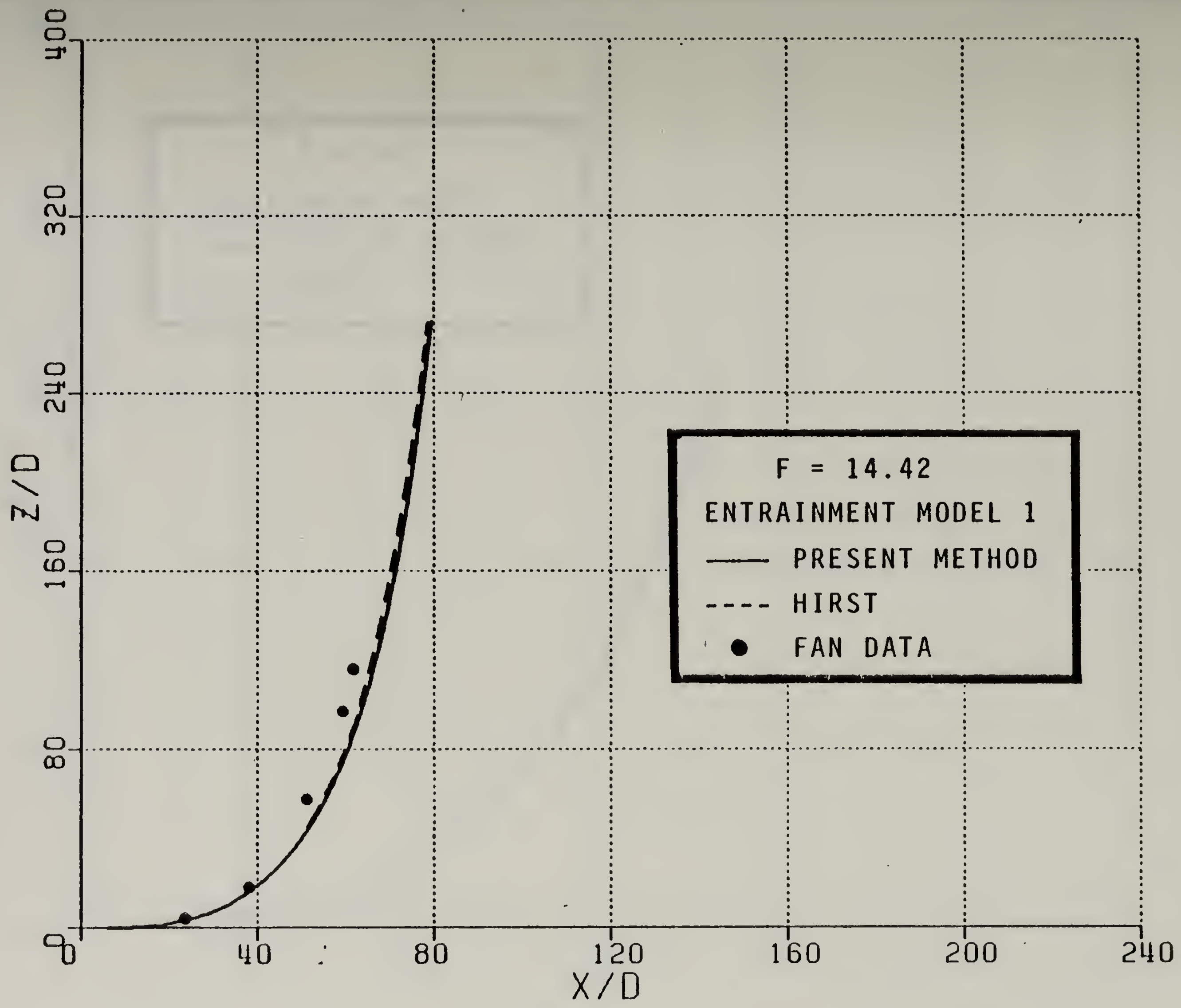

Figure 6-5. Comparison of present method and model of Hirst, both using $\alpha = 0.057$, and data of Fan [7]

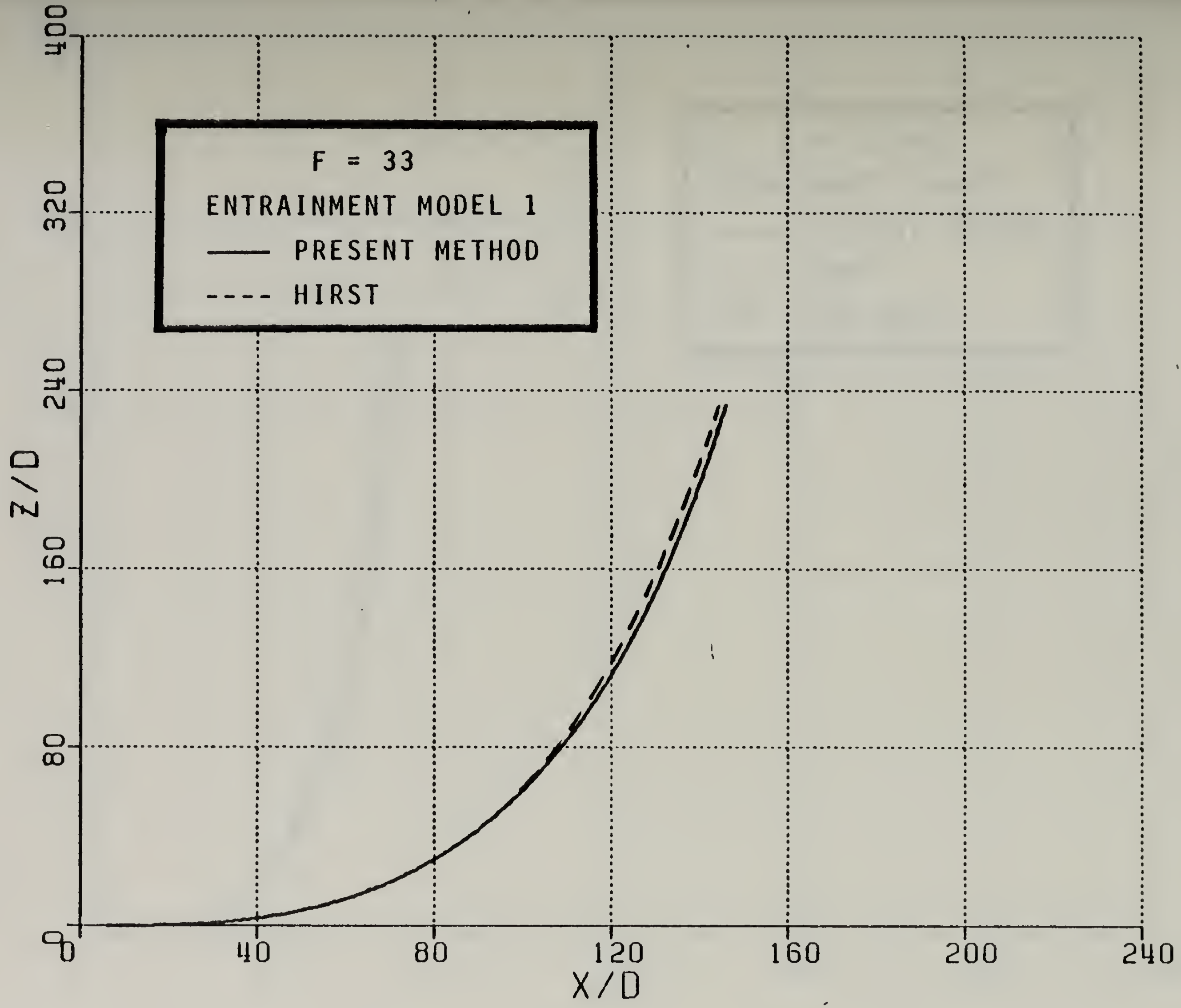

Figure 6-6. Comparison of present method and model of Hirst, both using $\alpha = 0.057$

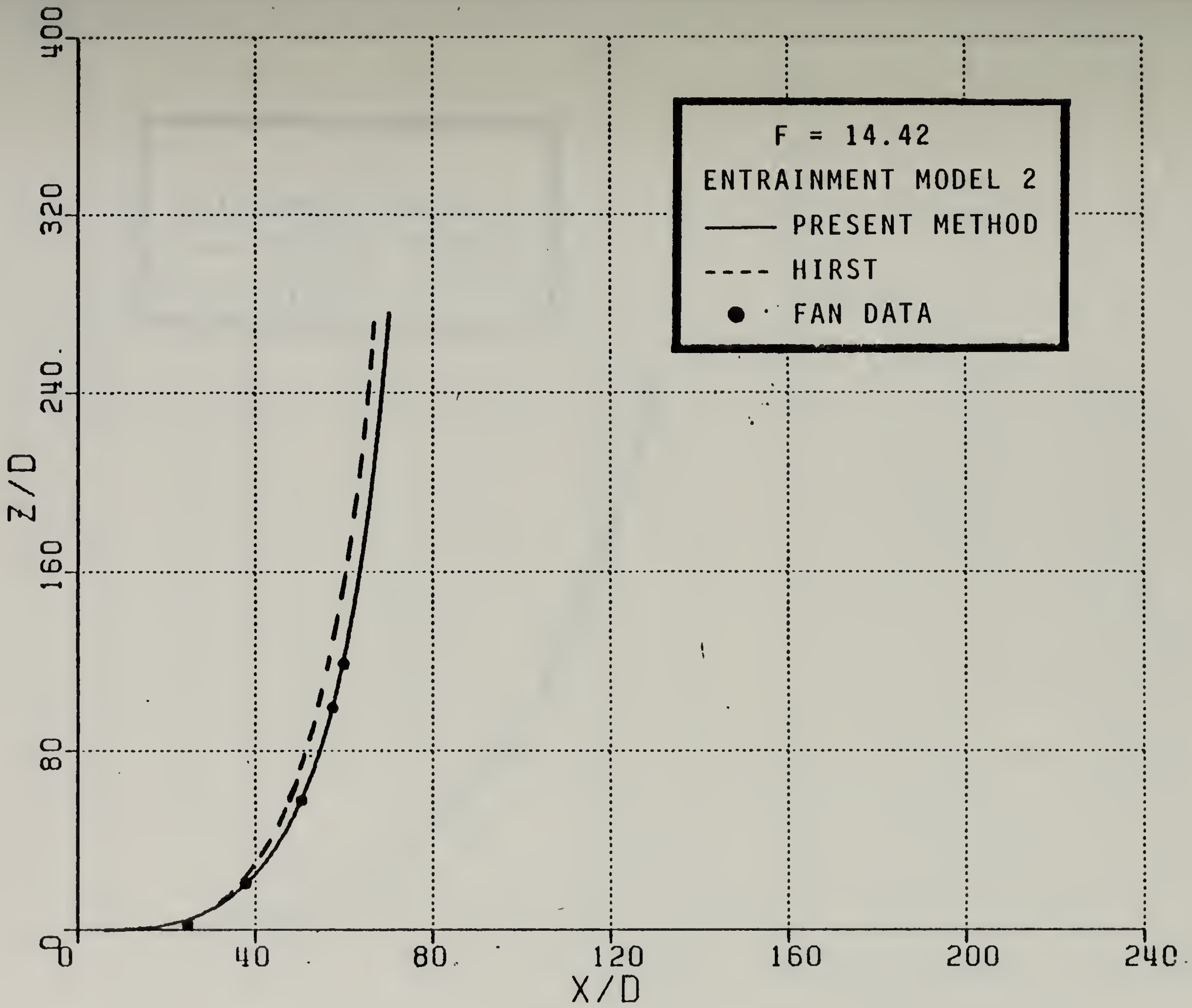

Figure 6-7. Comparison of present method and model of Hirst, both using α = 0.082, and data of Fan

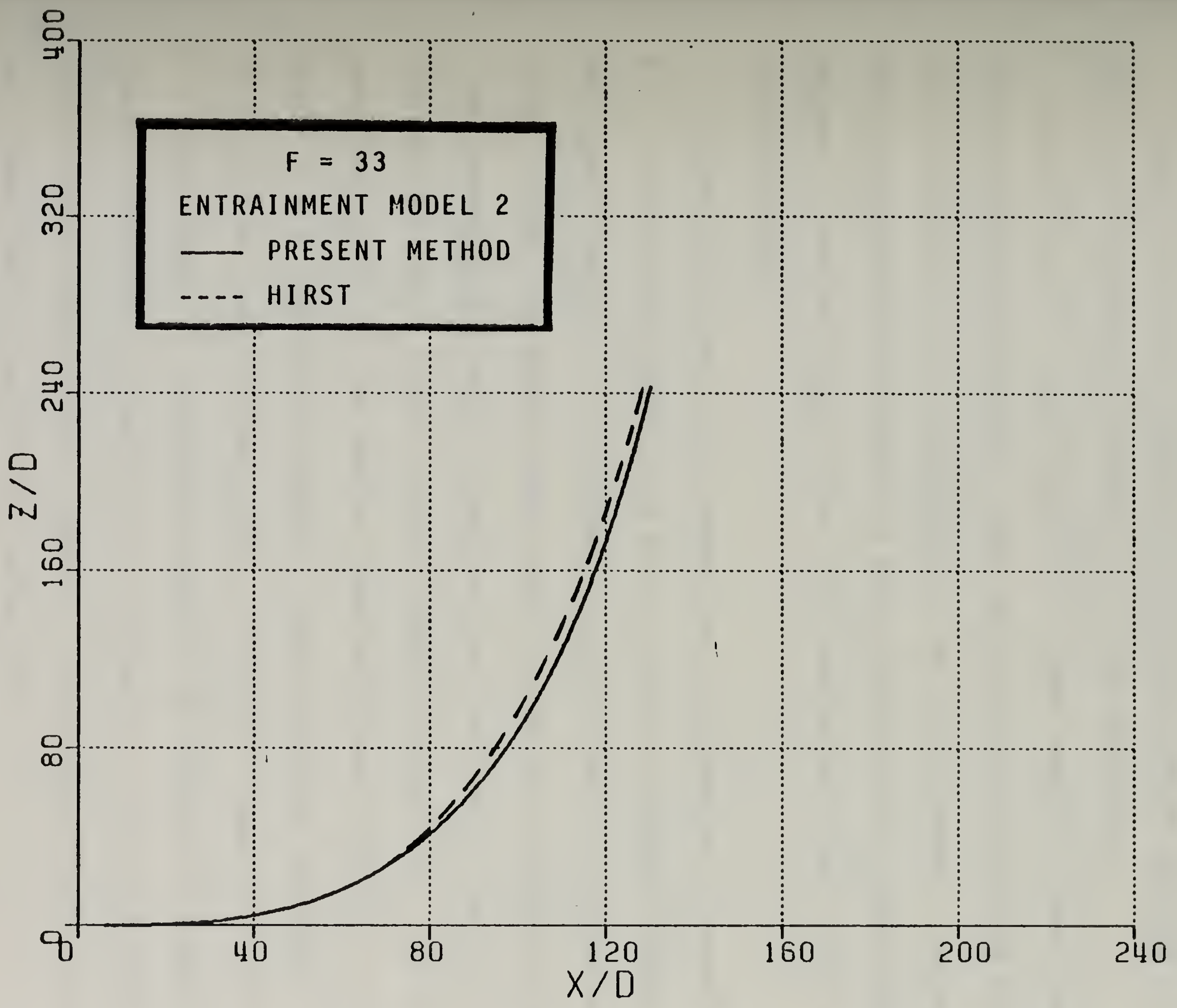

Figure 6-8. Comparison of present method and model of Hirst, both using α = 0.082

Comparison of calculations with those of Fan [9], using $\alpha = 0.082$, is shown in Figure (6-9). In this case, the present method predicts greater horizontal penetration of the jet and, therefore, somewhat less vertical penetration at most values of F.

A comparison of the present calculations, using no equation of state, with the calculations of Riester et al. [23], both using $\alpha = [(0.057 \cos\theta)^2 + (0.082 \sin\theta)^2]^{1/2}$, showed reasonably good agreement for high temperature ambients, where the β correction factor of Riester et al. resulted in little adjustment of the Froude number. Progressively poorer comparison was evident with their prediction for lower temperature ambients, where the Froude number adjustment became larger. This is shown in Figure (6-10).

Figures (6-11) and (6-12) compare the calculated jet trajectories at F = 1,2,4,6,8,10,50,100,150, and 200 for the five quiescent ambient entrainment functions. The ambient is unstratified and no equation of state is used. The models which relate to plume and non-buoyant jet flows understandably begin to deviate significantly from the norm of the trajectories when F is not in their intended range of use. This is particularly true for the buoyant plume entrainment function, $\alpha = 0.082$ (model 2). It consistently predicts lower entrainment and higher trajectory at all but the lowest Froude numbers. Albertson's momentum jet function, $\alpha = 0.057$, (model 1) consistently predicts the highest entrainment and, therefore flattest, trajectory at all values of F. The "end-point" correlation of Riester et al., model 5, is also seen to predict higher entrainment than the norm for all values of F.

The generally accepted values of entrainment functions for the extrema of Froude numbers are $\alpha = 0.082$ for $F = 0$, and $\alpha = 0.057$ for $F = \infty$. The

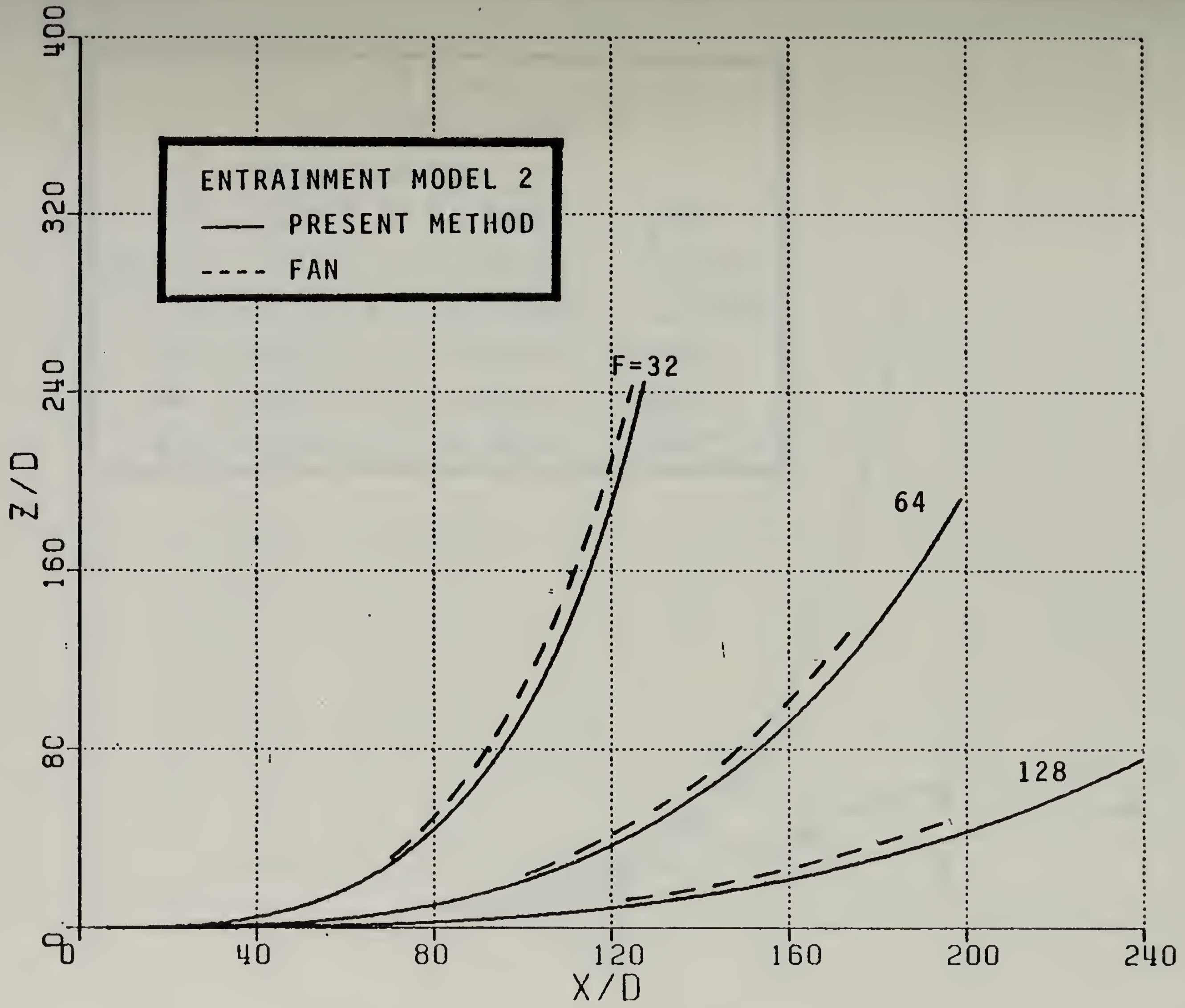

Figure 6-9. Comparison of present method with model of Fan [9]

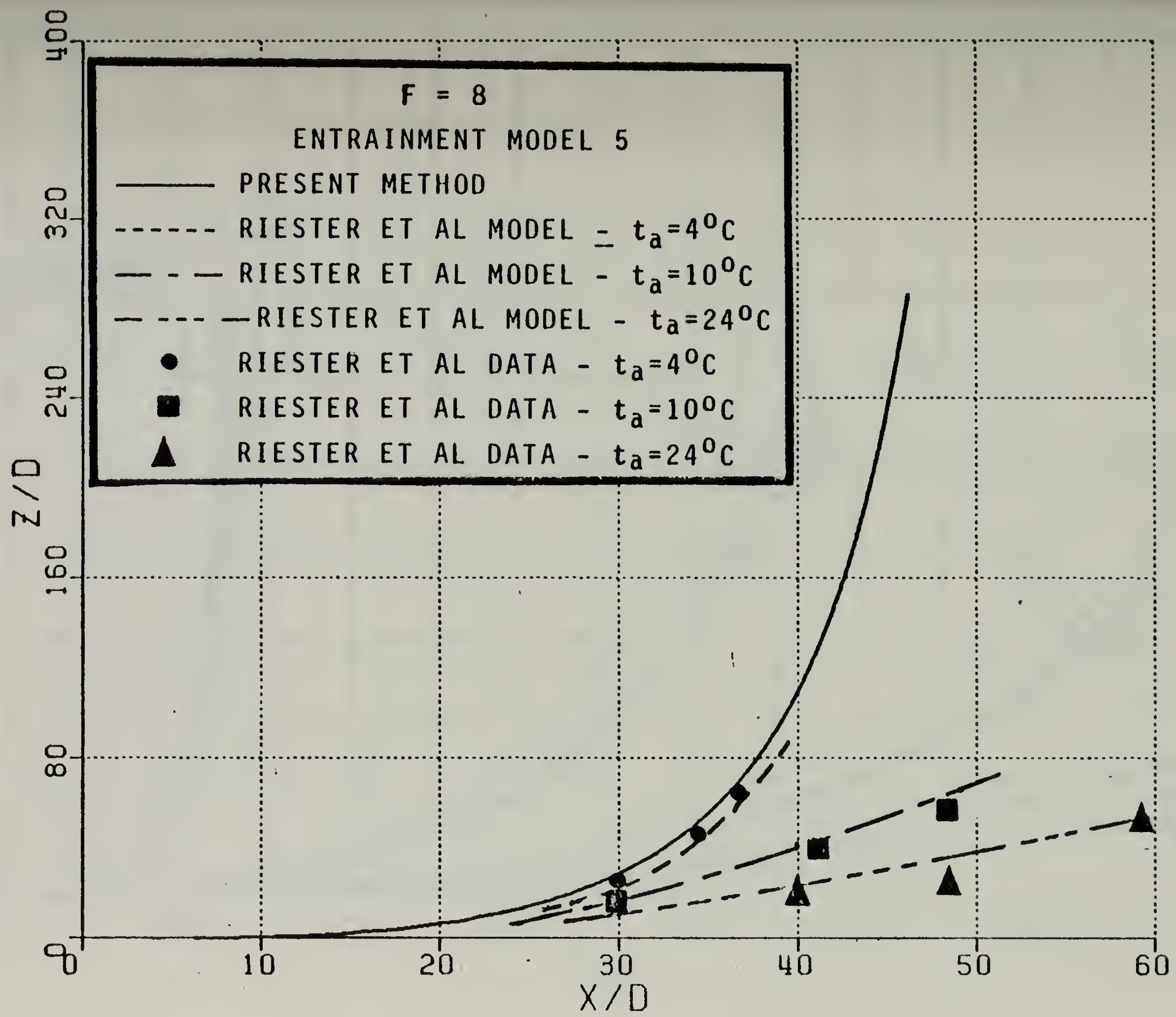

Figure 6-10. Comparison of present method with model and data of Riester et al. [23]

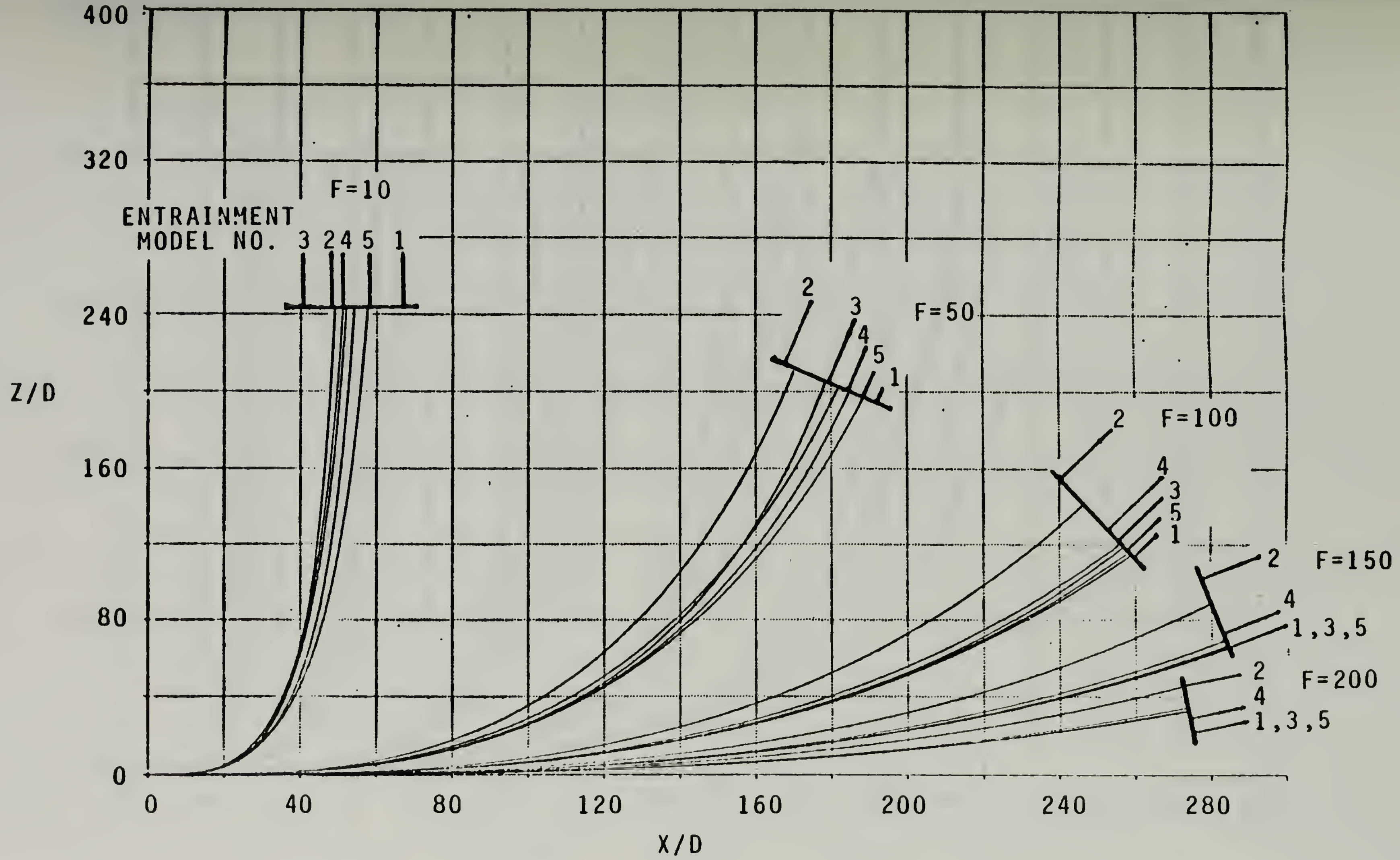

Figure 6-11. Comparison of entrainment models, quiescent ambient medium

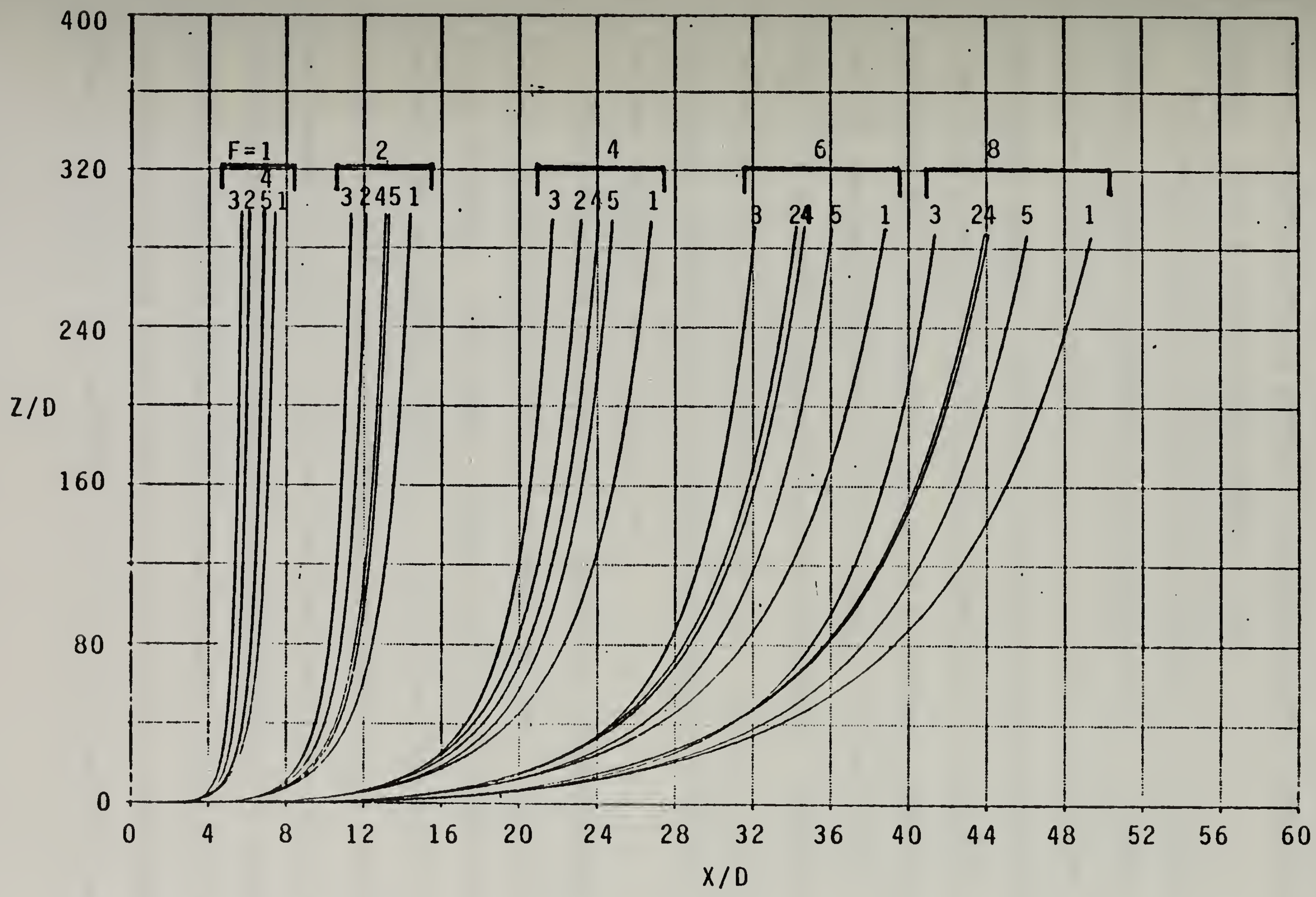

Figure 6-12. Comparison of entrainment models, quiescent ambient medium

two models which most closely reflect the Froude number/entrainment relation over the range of F considered here are the function of Hirst (model 3) and the empirically derived function of Davis et al. (model 4). Hirst's function actually predicts the most buoyant, least entraining behavior for the lowest Froude numbers (≤ 10).

All models predict strikingly similar behavior in the decay of centerline velocity, temperature, and concentration. The decay of jet properties along the pathlength S are not strongly dependent on F or entrainment function. Figure (6-13) shows the superposition of centerline velocity decay, U/U_0, for all jets depicted in Figure (6-11) ($F = 10, 50, 100, 150, 200$). The trend is seen to be an extremely rapid initial velocity decrease immediately after discharge. For jets with $F \geq 50$, $U/U_0 = 0.1$ around 50 diameters along the trajectory. Further downstream, the residual velocities decrease less rapidly. Figure (6-13) also shows that higher velocities persist downstream at smaller values of F, i.e., for more buoyant or less vigorous jets.

Close inspection of Figure (6-13) reveals an apparent anomaly. For $F = 10$, the Hirst model predicts the lowest residual velocity along most of the trajectory. The highest residual velocity is predicted for the buoyant plume entrainment function $\alpha = 0.082$. Yet Figure (6-11) for $F = 10$ shows that these two entrainment functions predict the highest, most buoyant trajectory, with the Hirst function representing the extreme. The behavior of the Hirst function, on one hand displaying buoyant characteristics indicative of low levels of entrainment, and on the other hand displaying high velocity decay indicative of high entrainment, seems to contradict the consistent behavior of the buoyant plume function.

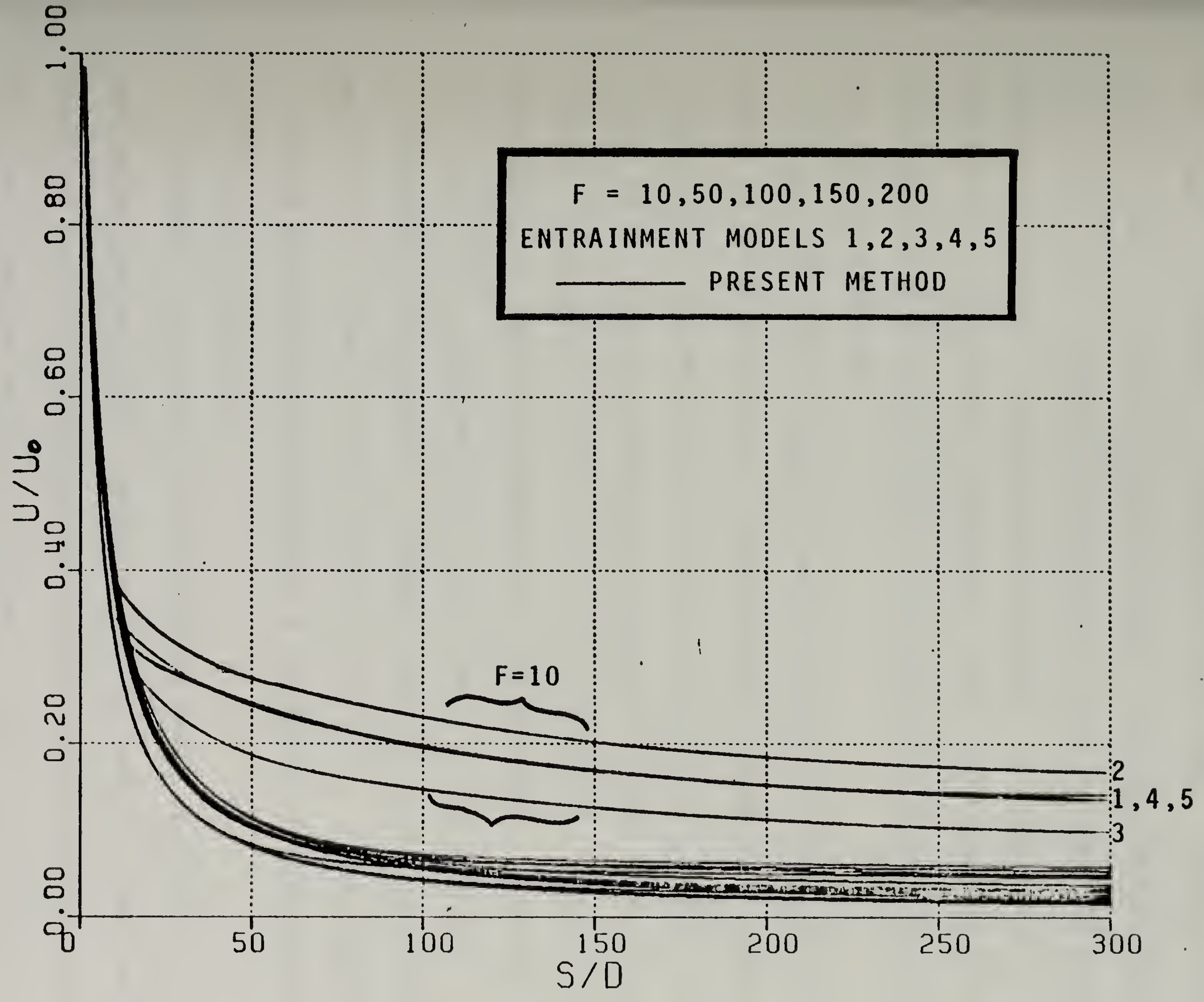

Figure 6-13. Velocity decay for 25 jets, F = 10 to 200, entrainment models 1 to 5

This behavior may be explained by close examination of Figure (6-14), an enlargement of the F = 10 results on (6-11). In the first 20 diameters of trajectory, the Hirst model is seen to be lower because of more rapid entrainment in comparison to the buoyant plume model. It then curves rapidly upward, displaying the most buoyant trajectory farther downstream. The velocity level apparently decreased early due to rapid entrainment. However, the jet still retained enough buoyancy to cause the sharp upturn characteristic of the later trajectory. These results are indicative of the importance of the early level of entrainment in determining properties much further downstream.

An even more uniform behavior among the group of 25 calculations considered in the illustration of velocity decay is shown in a superposition of temperature difference decay curves in Figure (6-15). Jets in this F range of 10 to 200 have temperature residuals of less than 0.2 at 20 diameters downstream and less than 0.1 at 50 diameters. Both of these decay curves are in close agreement with existing data. Note that in this formulation, concentration residuals decay in the same way.

An example of the radial or diameter growth of a jet, using entrainment model 2, is shown in Figures (6-16) and (6-17). These figures illustrate that the physical extent of a jet generally increases more rapidly with increasing F.

In summary, the various past entrainment models for jets in a quiescent ambient medium predict reasonably similar behavior. Most notable exceptions to this conclusion are the results using the buoyant plume entrainment function, model 2, at higher F. This is well outside the range of intended use. Further, all of the models are in reasonably close agreement with meager existing data for small diameter jets.

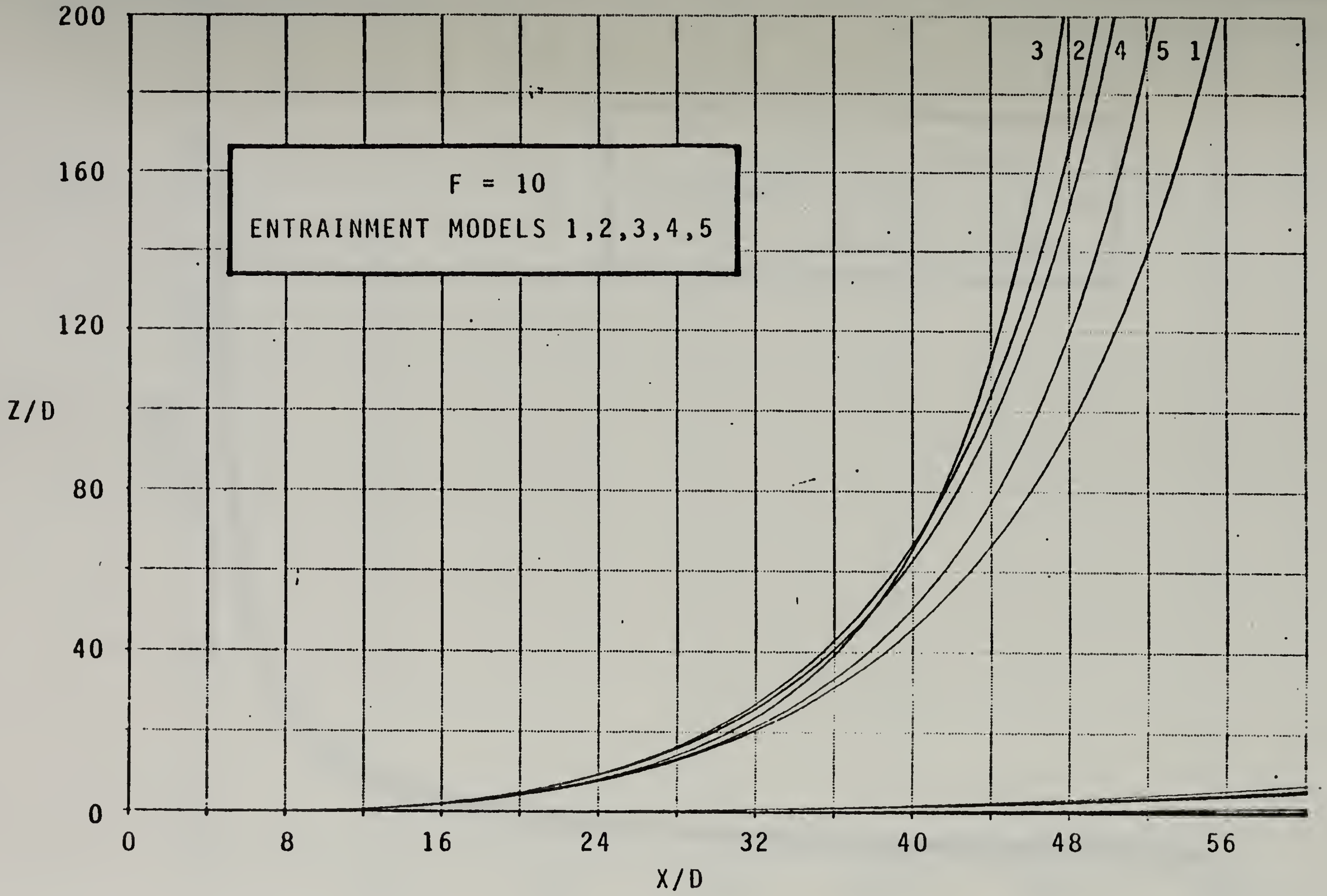

Figure 6-14. Comparison of entrainment models, quiescent ambient medium

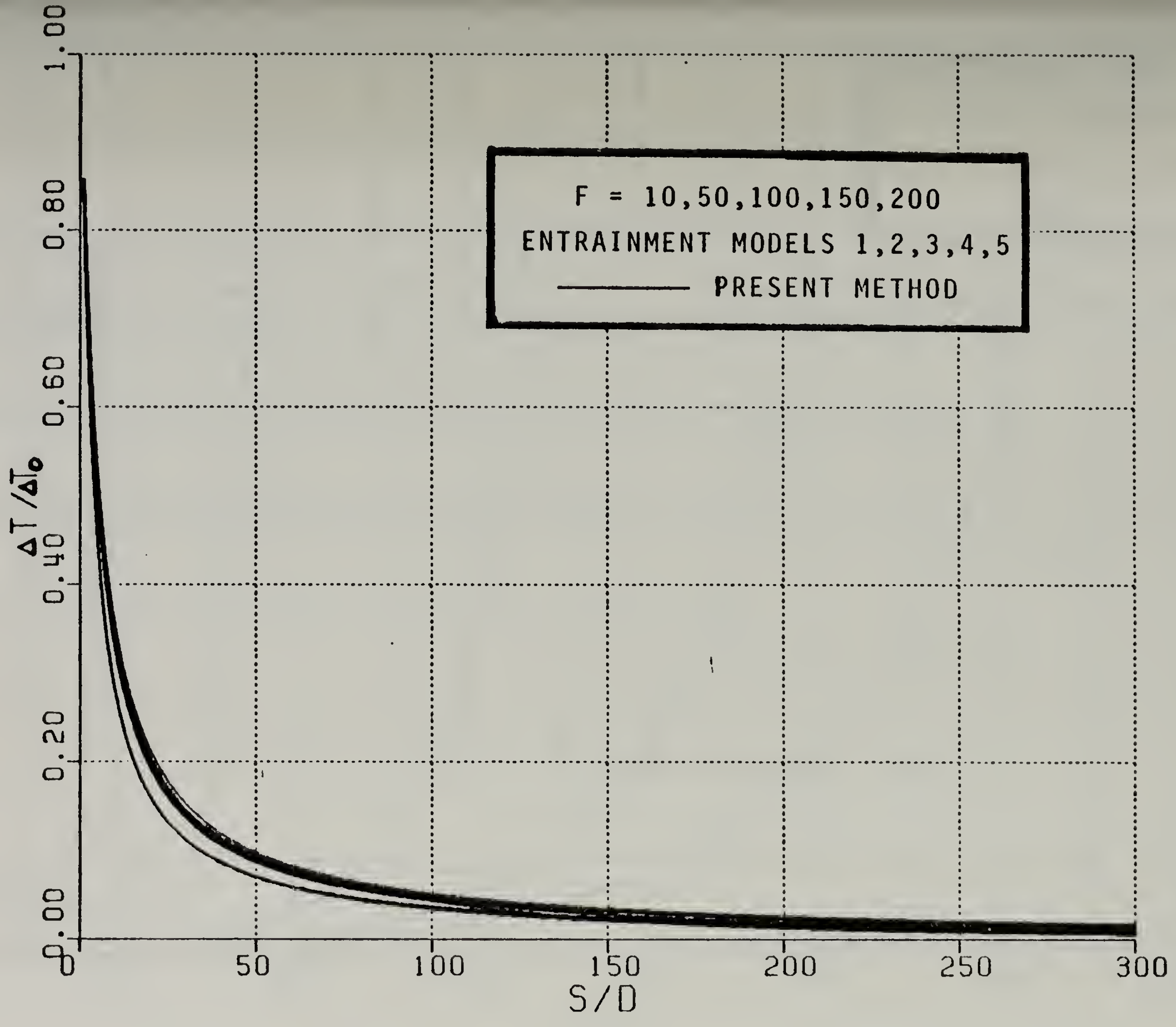

Figure 6-15. Temperature difference decay for a group of 25 jets, F = 10 to 200, entrainment models 1 to 5

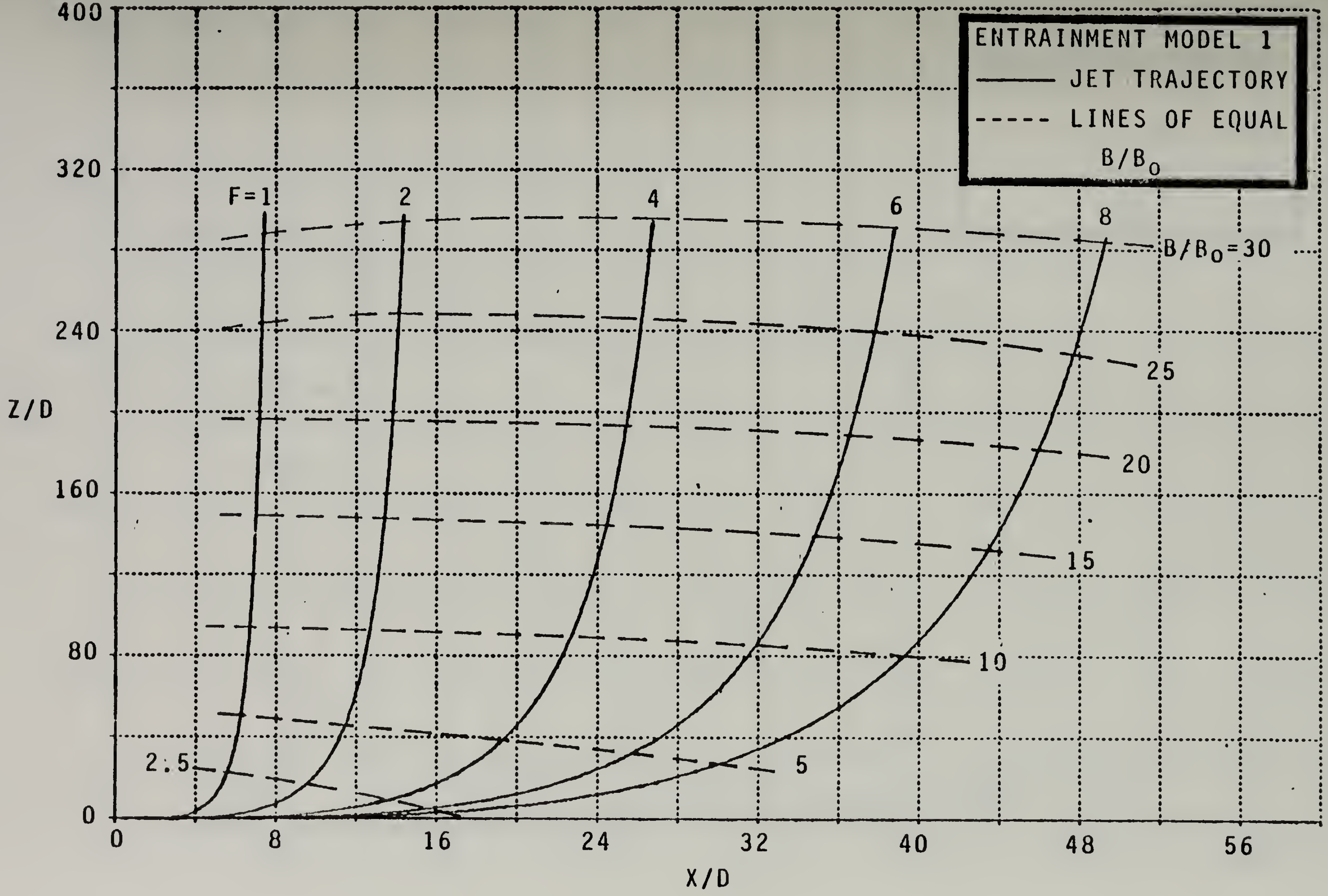

Figure 6-16. Radial growth of buoyant momentum jets, quiescent ambient medium

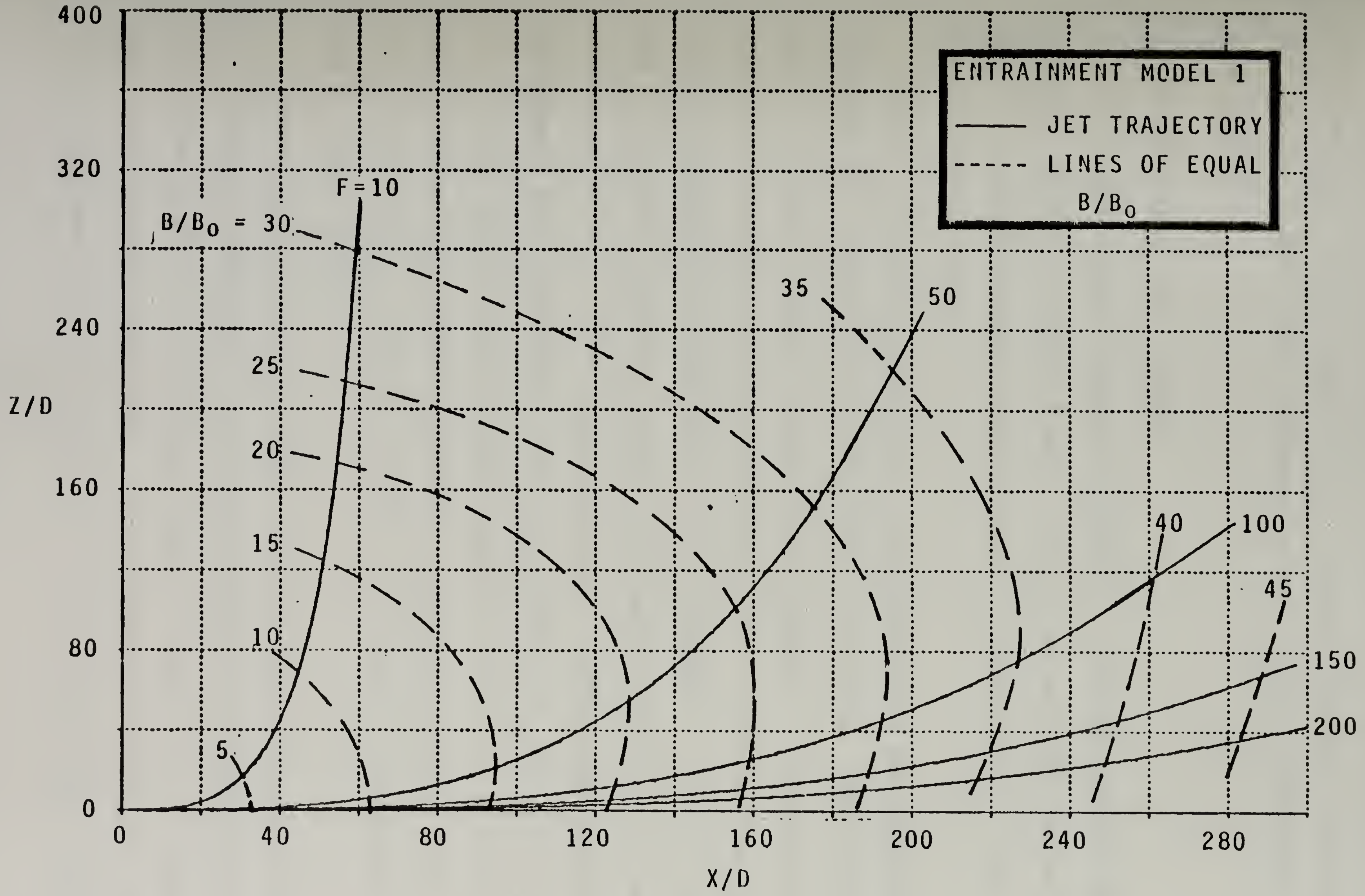

Figure 6-17. Radial growth of buoyant momentum jets, quiescent ambient medium

Twenty years of "entrainment function generation" in the literature not withstanding, it may be stated that in a quiescent ambient, predicted jet behavior is not strongly dependent on the particular entrainment model used.

B. FLOWING UNSTRATIFIED AMBIENT

The two entrainment functions proposed for a buoyant momentum jet in a flowing ambient are models 8 and 9. It will be seen that they do not result in agreement between predicted results characteristic of the quiescent ambient models.

Figure (6-18) shows the trajectory predicted by the two entrainment functions for a vertical jet in a horizontal cross flow. The conditions are $R = 0.25$ and $F = 2.83$, in an unstratified ambient. This set of values of R and F is especially significant because it is one of the few cases in which the models are known to be in close agreement. For all F less than 2.83, model 9 predicts a higher, more buoyant trajectory than model 8. Conversely, at $F > 2.83$, model 9 generally predicts lower trajectory and somewhat more rapid decay of velocity, temperature, and concentration. For $F = 2.83$, model 9 predicts lower trajectory for all $R < 0.25$, and vice versa. Figure (6-19) shows the effect of lessening the ambient flow rate to $R = 0.125$ for a jet of $F = 2.83$ with all other conditions the same as Figure (6-18).

Figures (6-20), (6-21) and (6-22) illustrate that the disparity between the trajectory predictions of the flowing ambient entrainment models is not limited to the case of discharge nromal to a cross flow. In these cases, the discharge angle is 45°. The same behavior is evident--reasonably good agreement for $F = 2.83$ and $R = 0.25$ as in Fig. 6-20. However

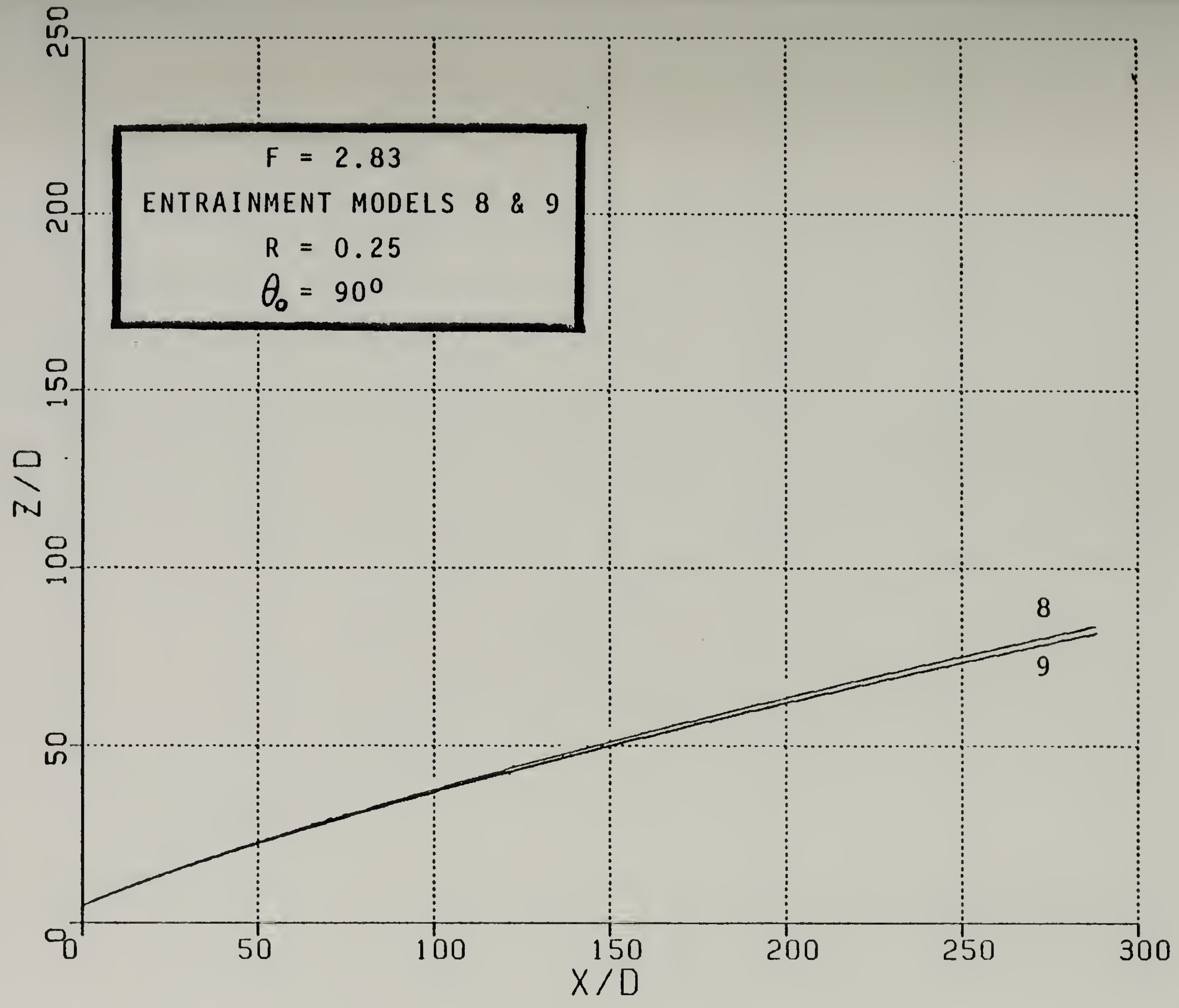

Figure 6-18. Comparison of flowing ambient entrainment models

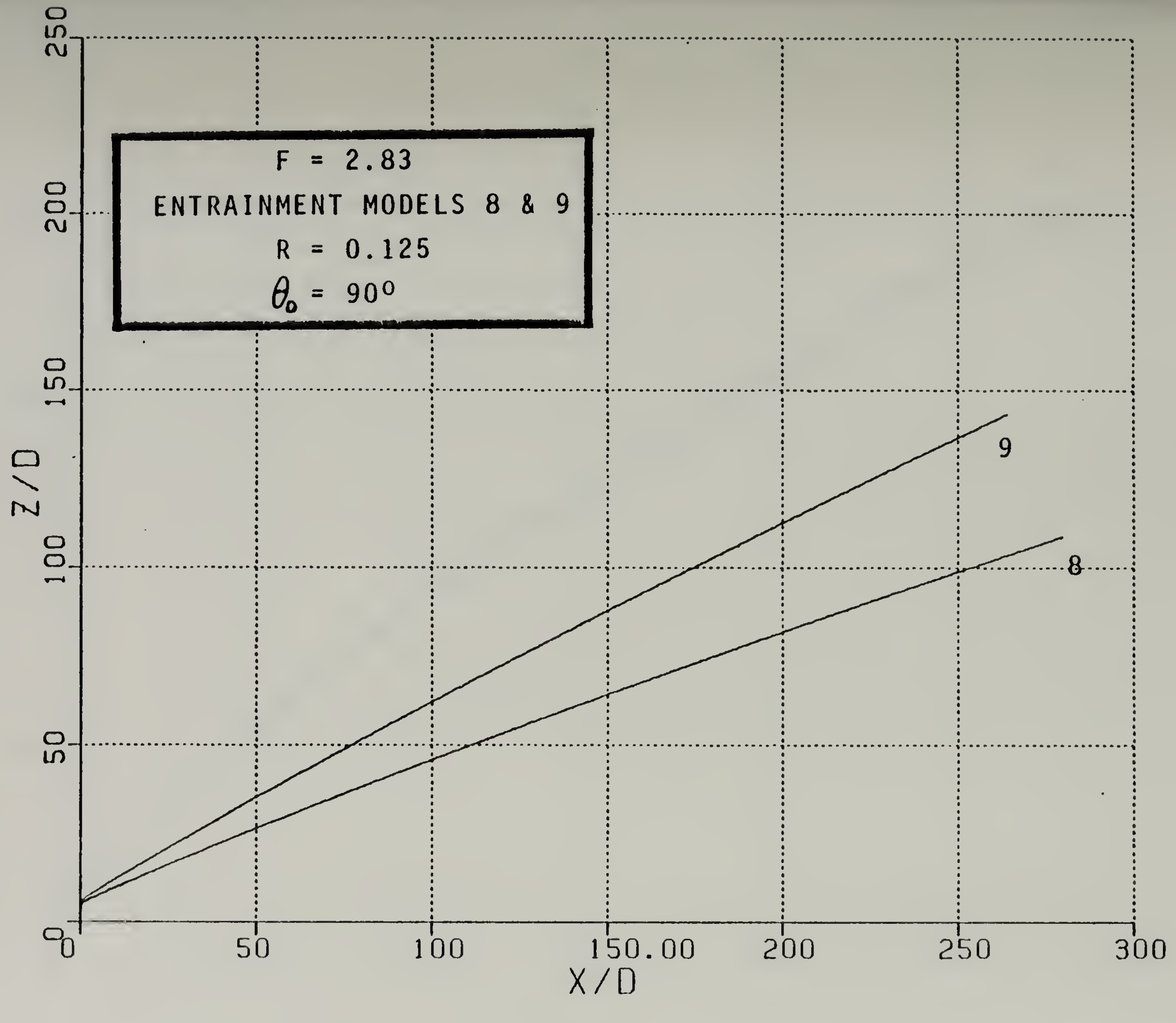

Figure 6-19. Comparison of flowing ambient entrainment models

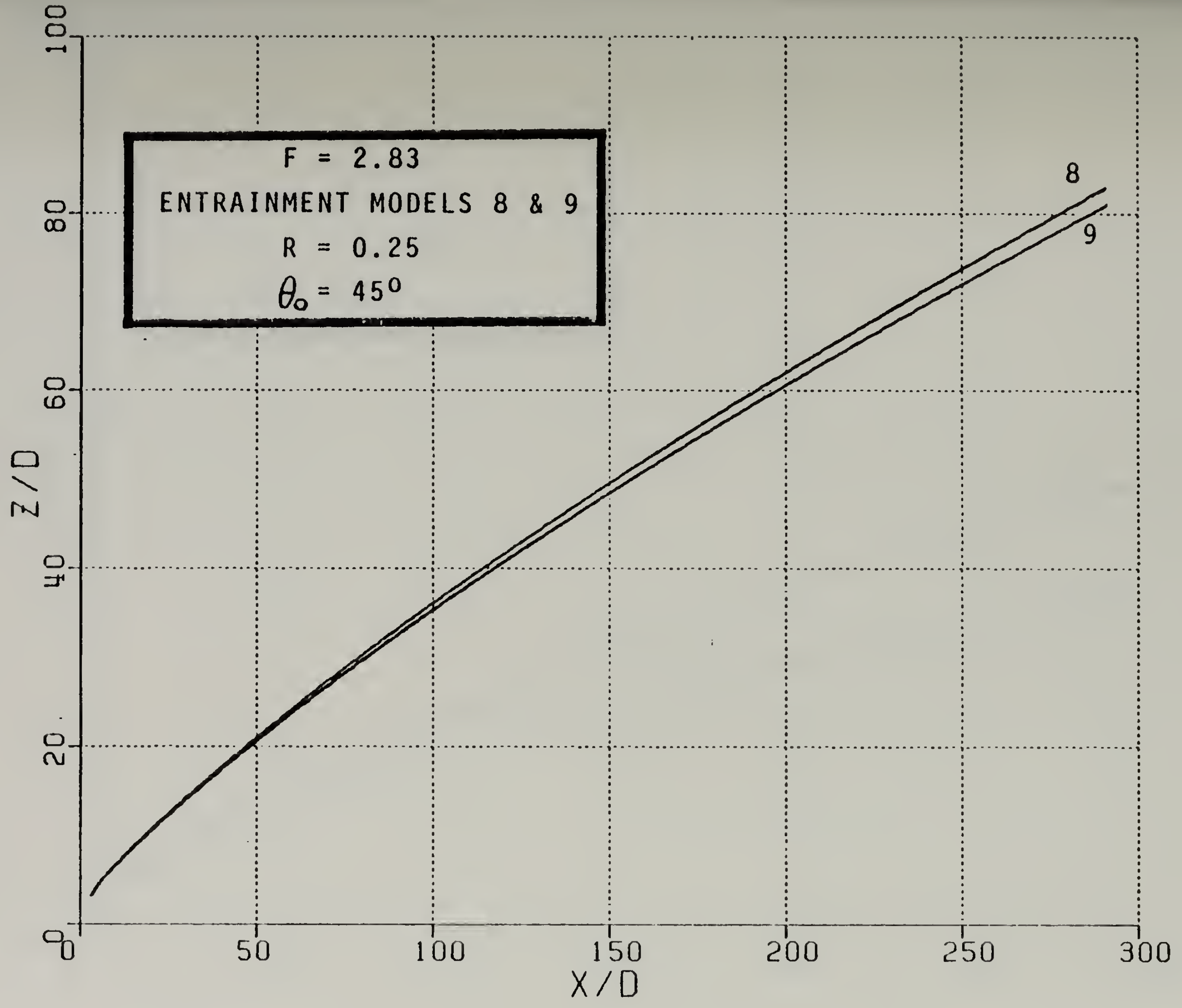

Figure 6-20. Comparison of flowing ambient entrainment models

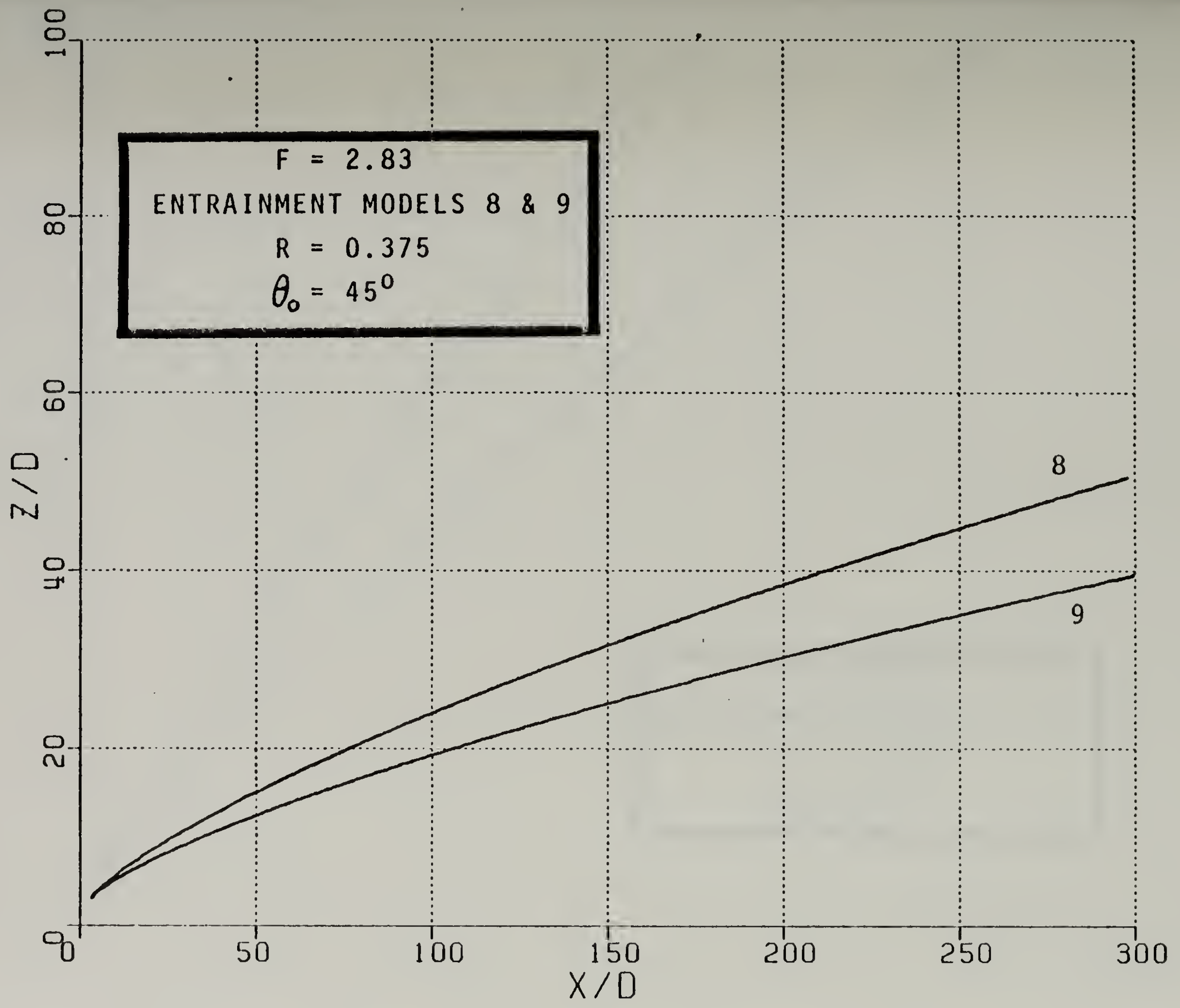

Figure 6-21. Comparison of flowing ambient entrainment models

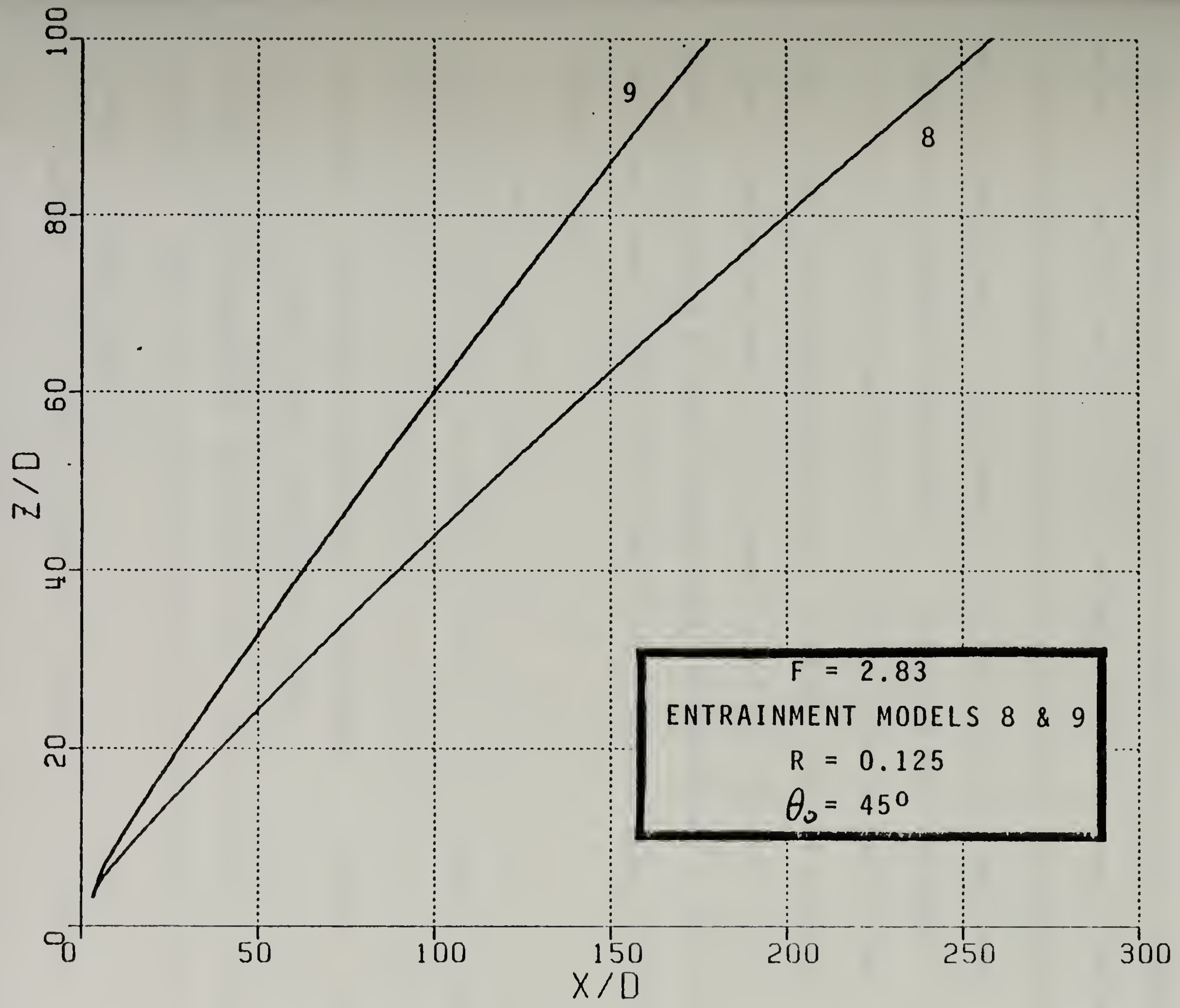

Figure 6-22. Comparison of flowing ambient entrainment models

model 8 predicts a higher trajectory for $R > 0.25$, Fig. (6-21), and model 9 a higher trajectory for $R < 0.25$, Fig. (6-22).

As F and R are increased, the upward penetration of the jet decreases. This is due to more rapid entrainment and lower initial buoyancy of the high Froude number jets, as well as the stronger horizontal "sweeping" effect of the more rapidly flowing ambients. In most cases, however, the increase in these effects do not lessen the disparity between the relative magnitudes of rise predicted by the two entrainment models. Figure (6-23) depicts another case of relatively good agreement at $F = 10$, $R = 0.125$, $\theta_0 = 90°$, compared with the data of Fan at these values. However, Figure (6-24) shows that model 8 diverges from the other two indicated trajectories when R is increased to 0.25 at the same value of F. Figure (6-25) shows the same disagreement between models 8 and 9 at $\theta_0 = 45°$. For higher Froude numbers, the disparity persists, as shown in Figures (6-26) to (6-31).

The results for initial pure "coflow", in which the jet is discharged horizontally parallel to the ambient flow, $\theta_0 = 0$, are shown in Figures (6-32) to (6-37). The conditions are $F = 20$ and 40 for $R = 0.125$, 0.25, 0.4 and 0.8. The same characteristic disagreement is evident. At small values of R, the disagreement between the models is 15 to 40%. At larger R values, the disagreement approaches 100%. The two models are inconsistent throughout. These high R values are beyond the data used in the fit by Ginsberg and Ades in model 9.

In summary, the disparity between the predicted jet trajectory using the two flowing ambient entrainment functions is generally most apparent in flows with significant vertical components in their trajectory. Obviously, the models are very sensitive to how the cross flow entrainment

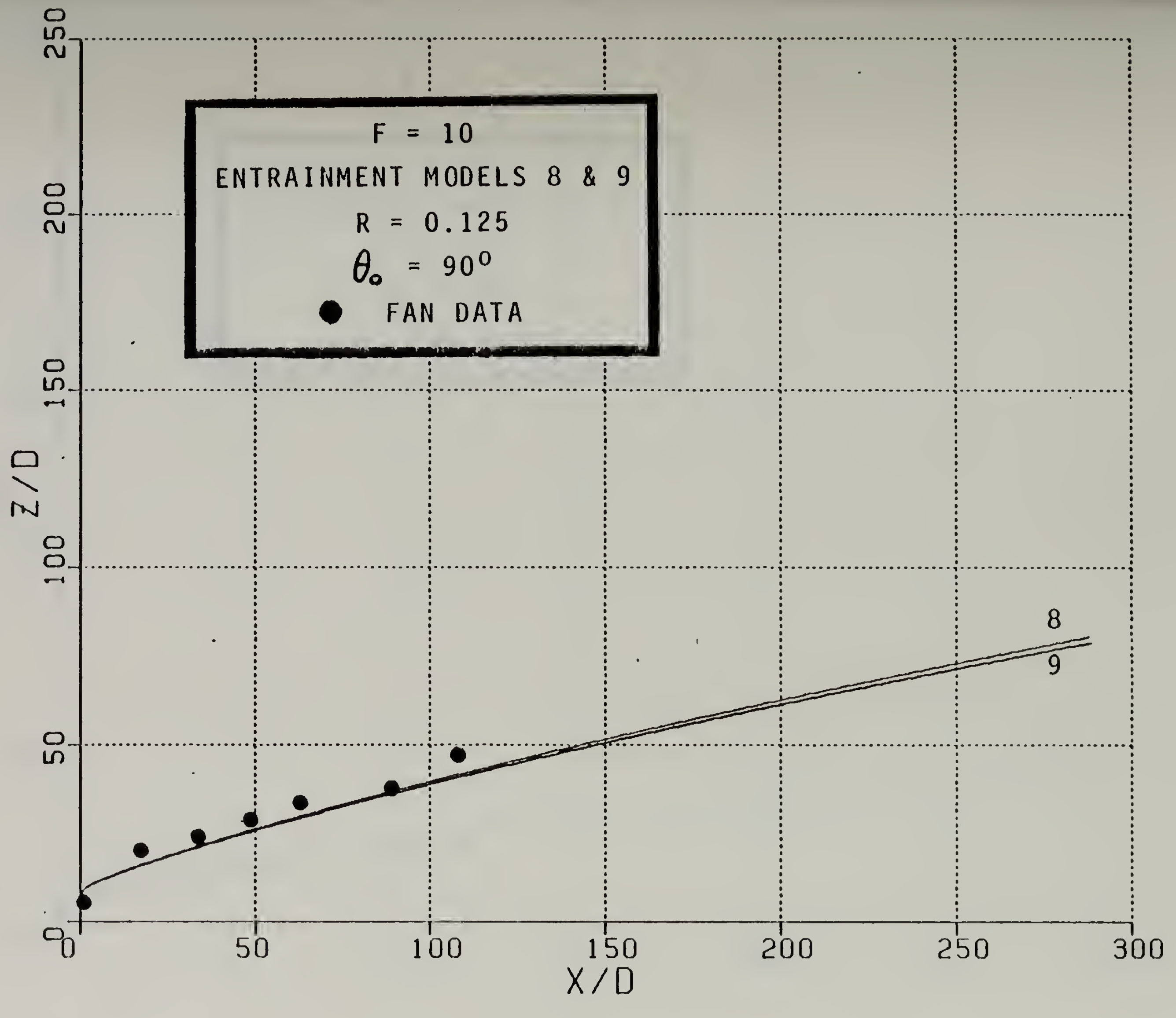

Figure 6-23. Comparison of flowing ambient entrainment models and the data of Fan

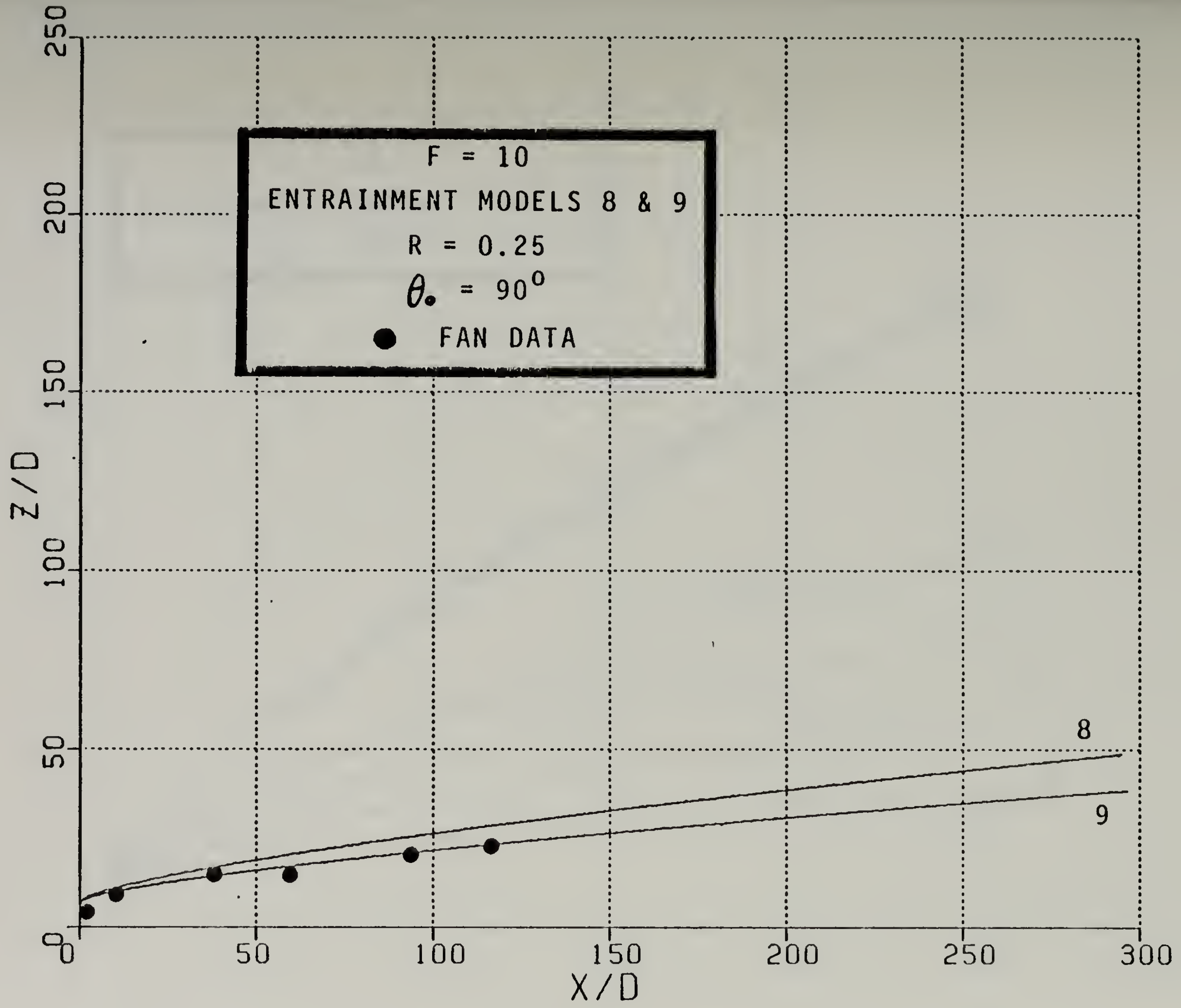

Figure 6-24. Comparison of flowing ambient entrainment models

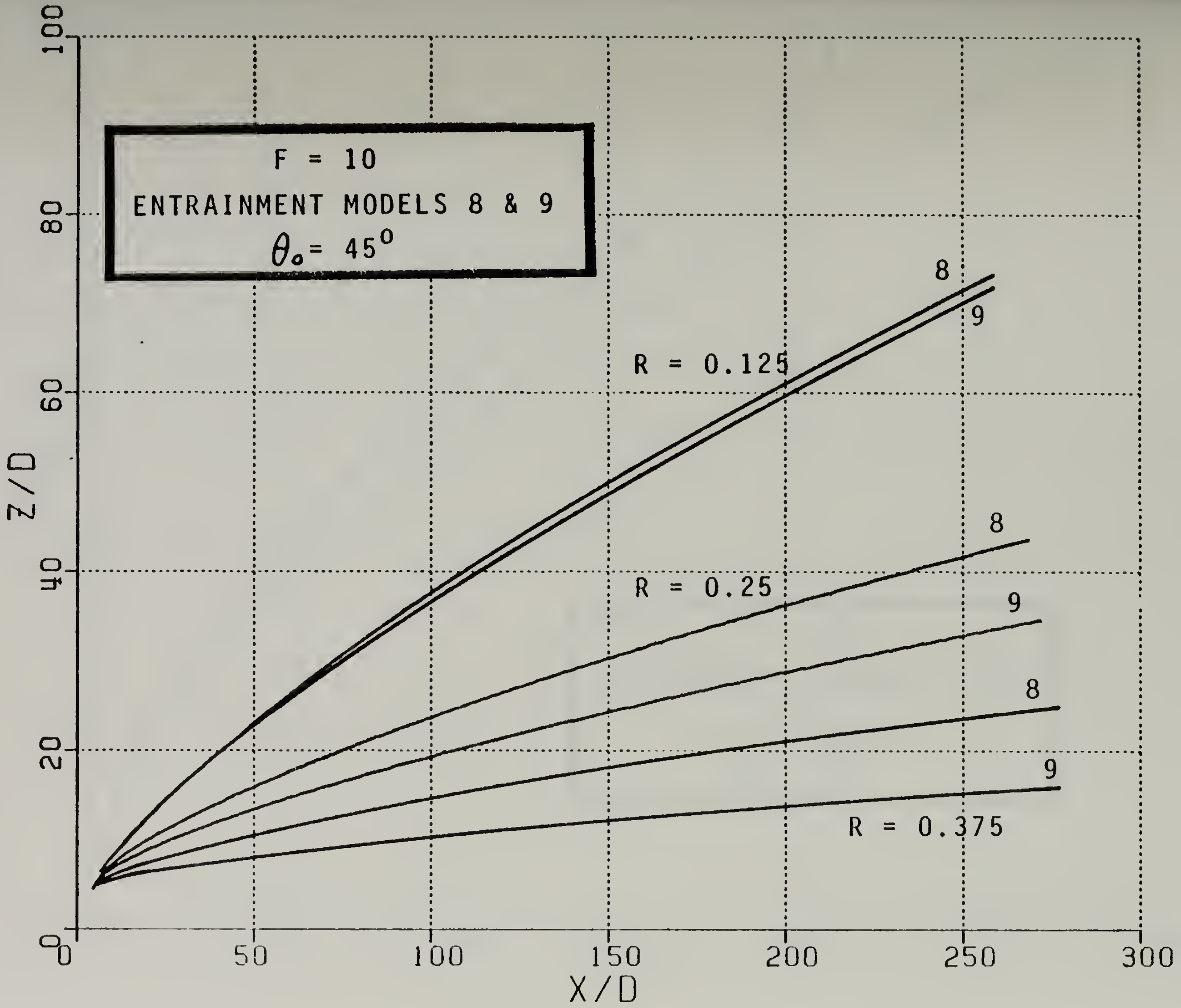

Figure 6-25. Comparison of flowing ambient entrainment models

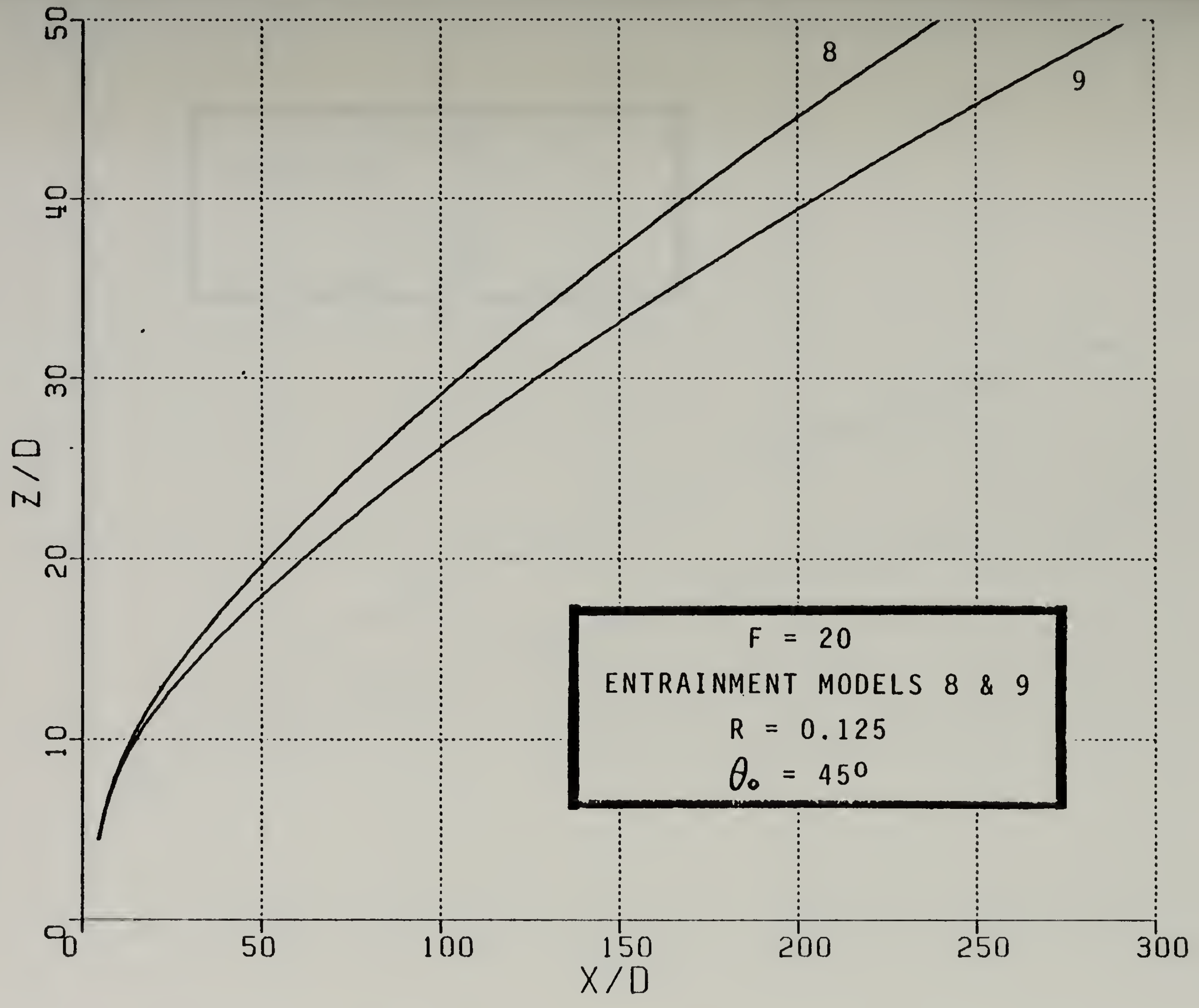

Figure 6-26. Comparison of flowing ambient entrainment models

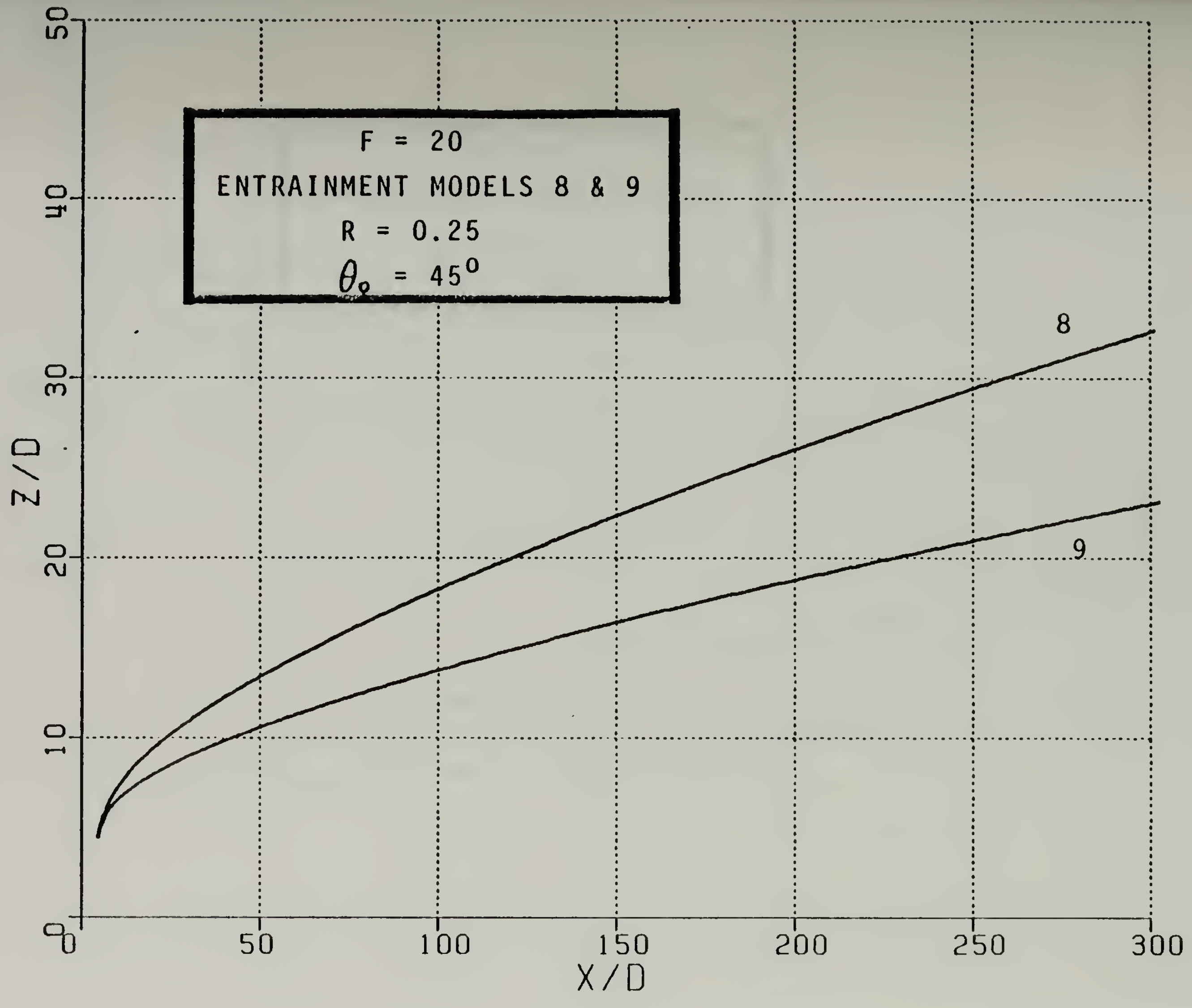

Figure 6-27. Comparison of flowing ambient entrainment models

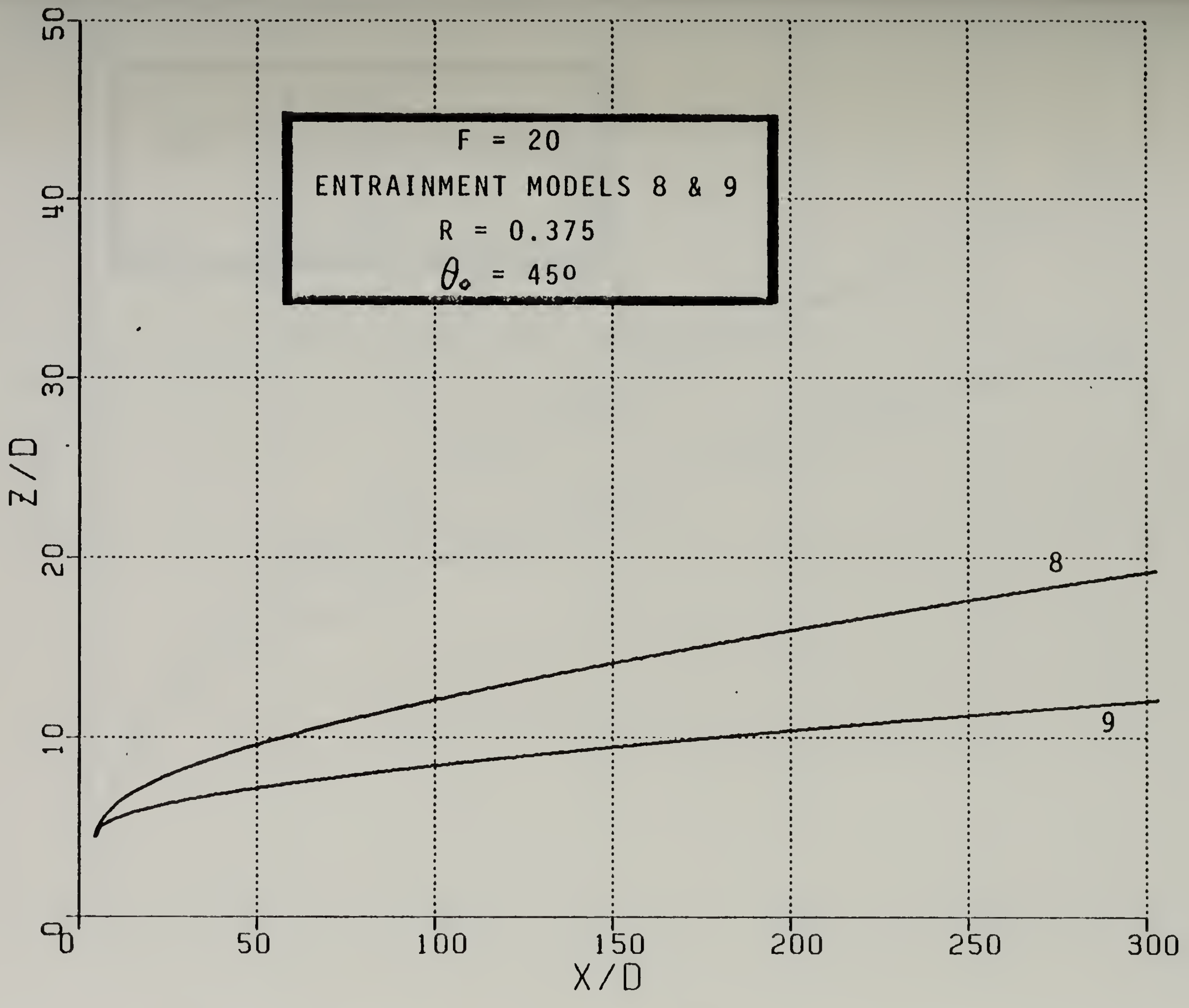

Figure 6-28. Comparison of flowing ambient entrainment models

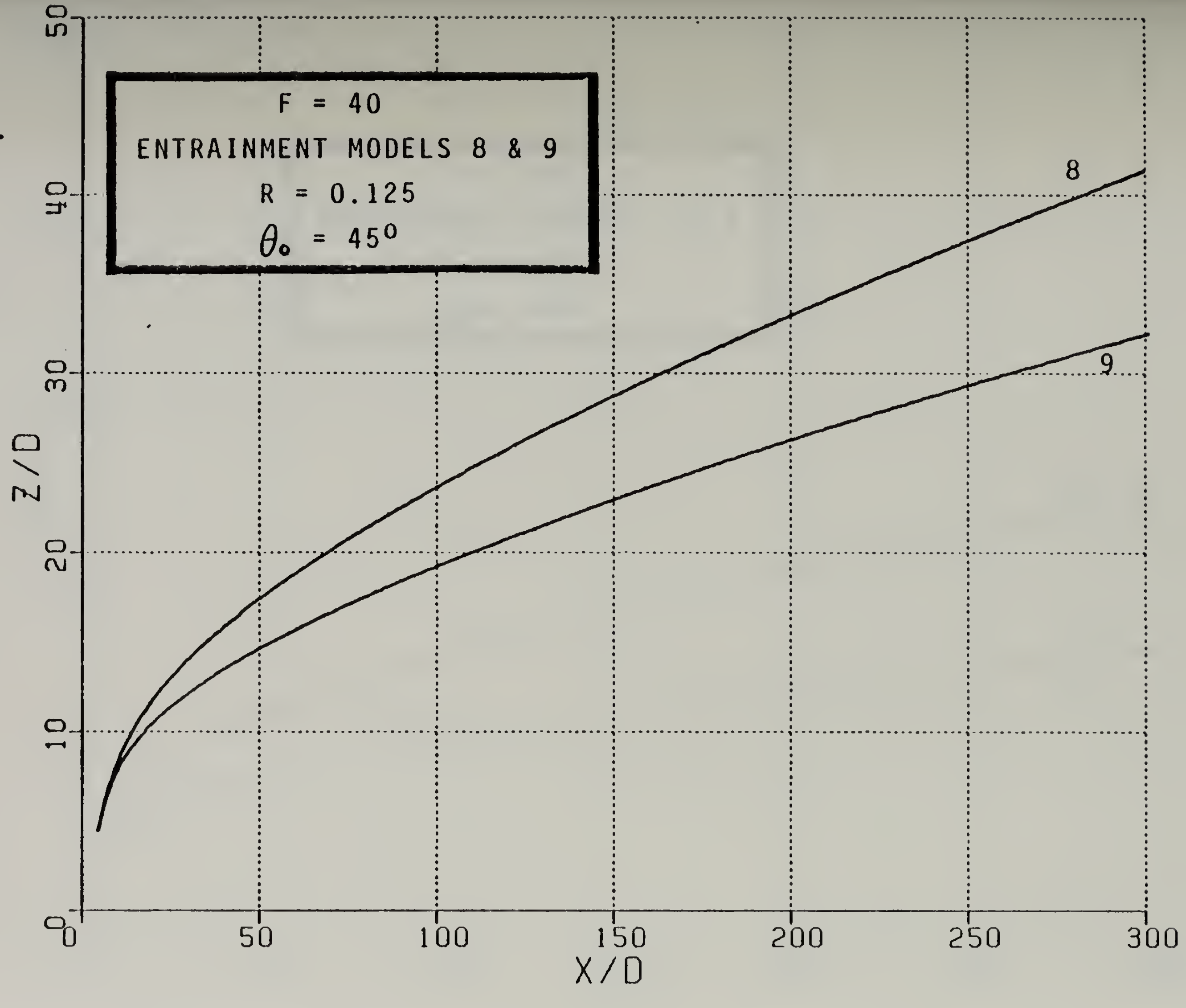

Figure 6-29. Comparison of flowing ambient entrainment models

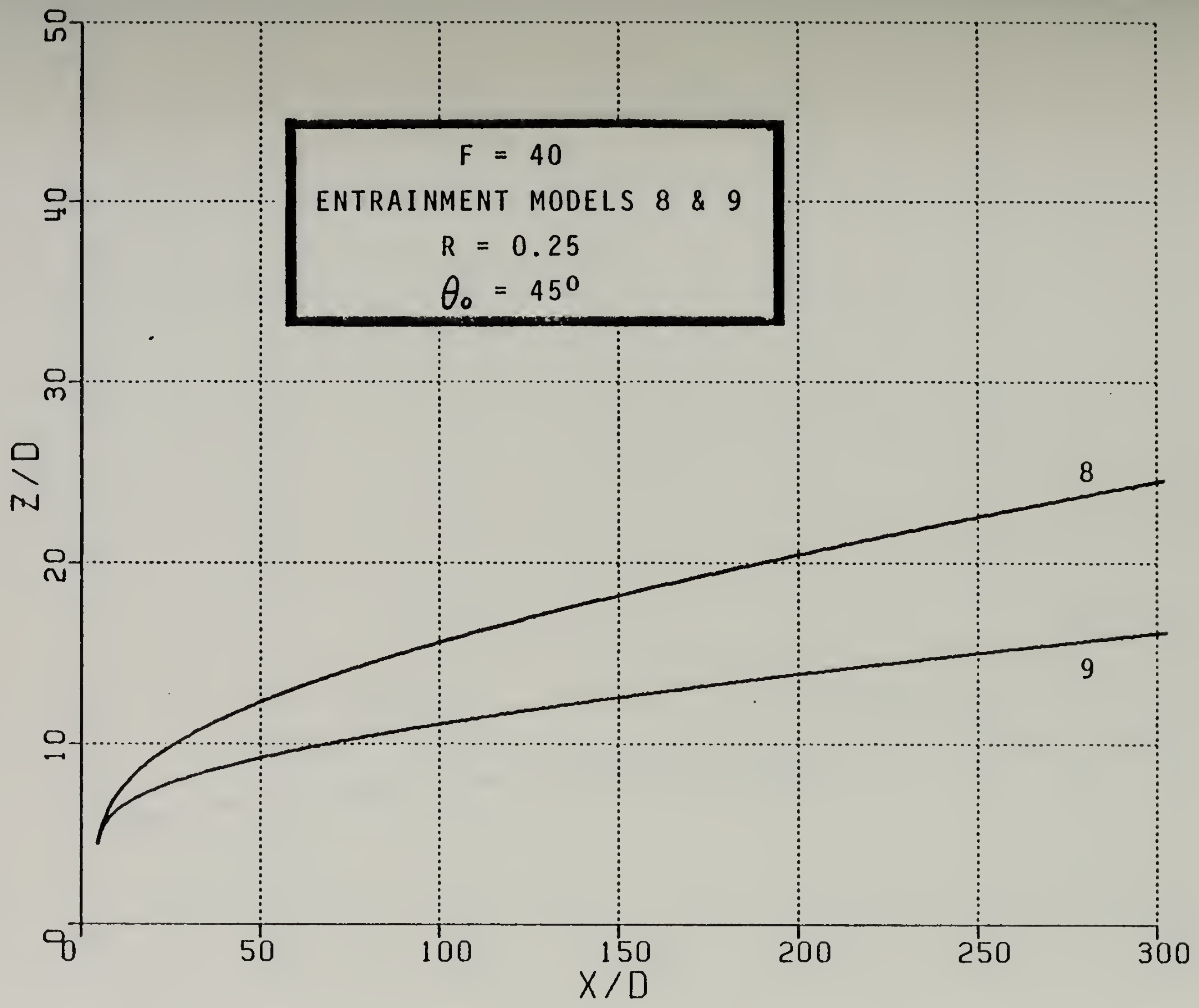

Figure 6-30. Comparison of flowing ambient entrainment models

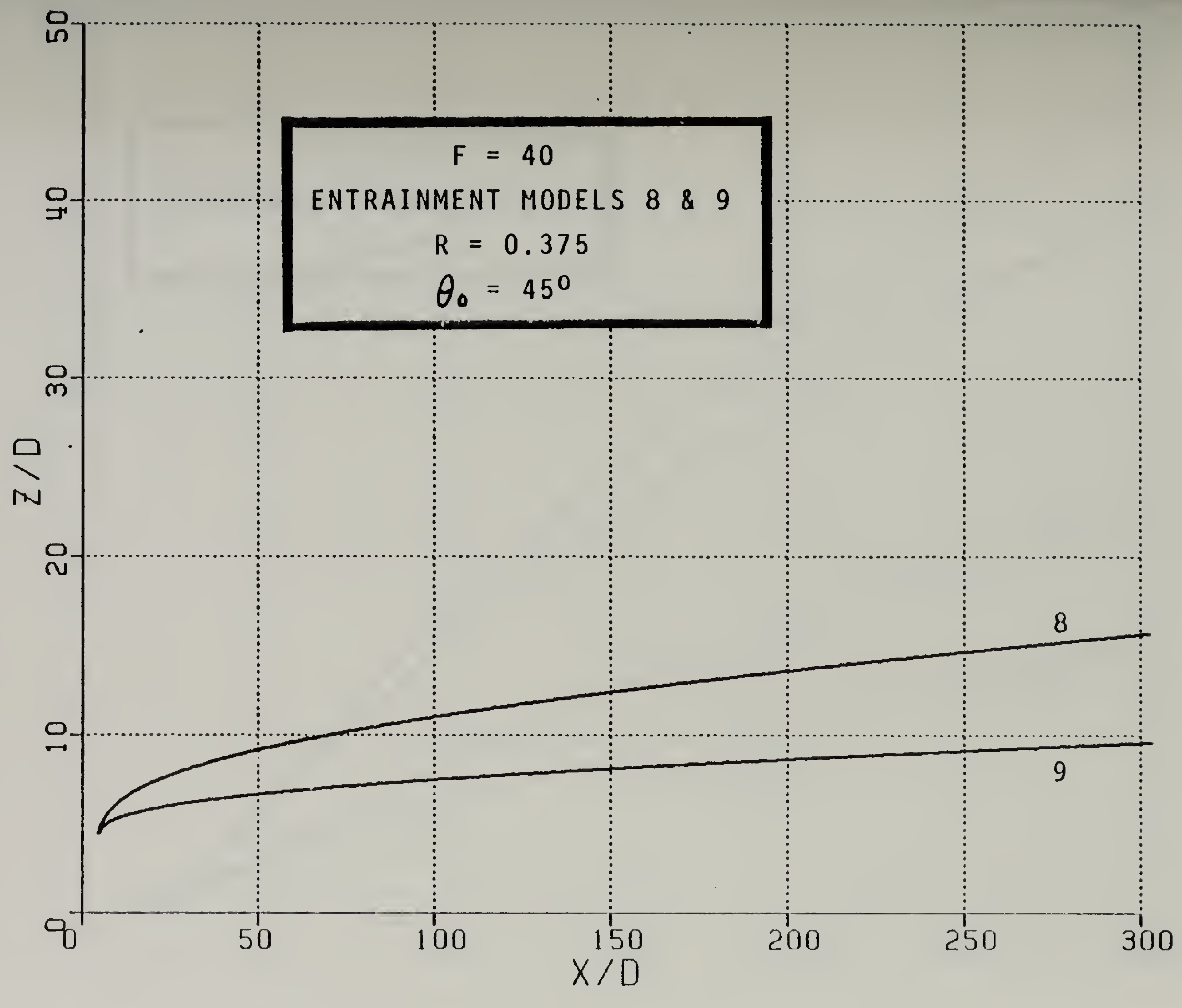

Figure 6-31. Comparison of flowing ambient entrainment models

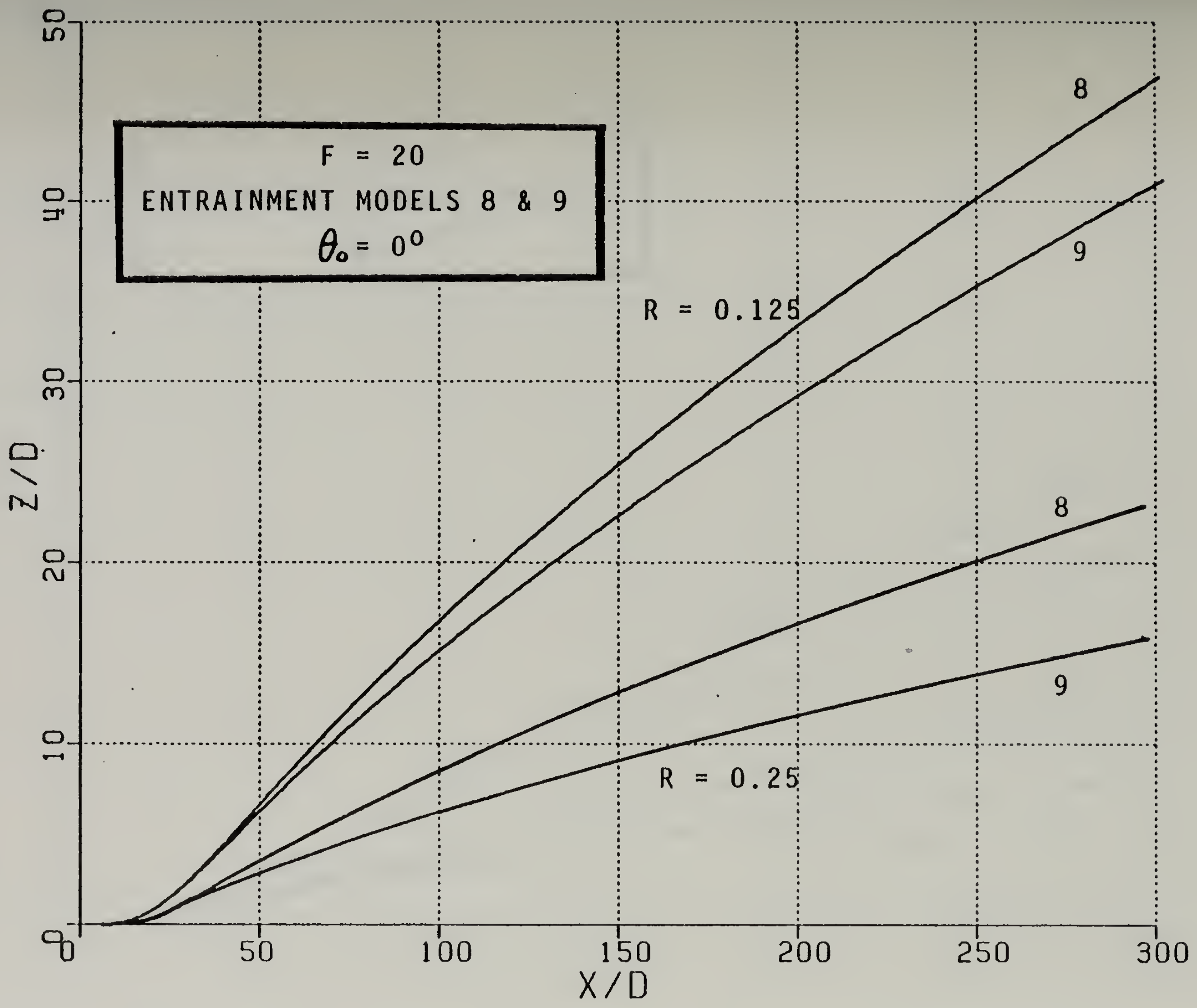

Figure 6-32. Comparison of flowing ambient entrainment models for case of pure coflow

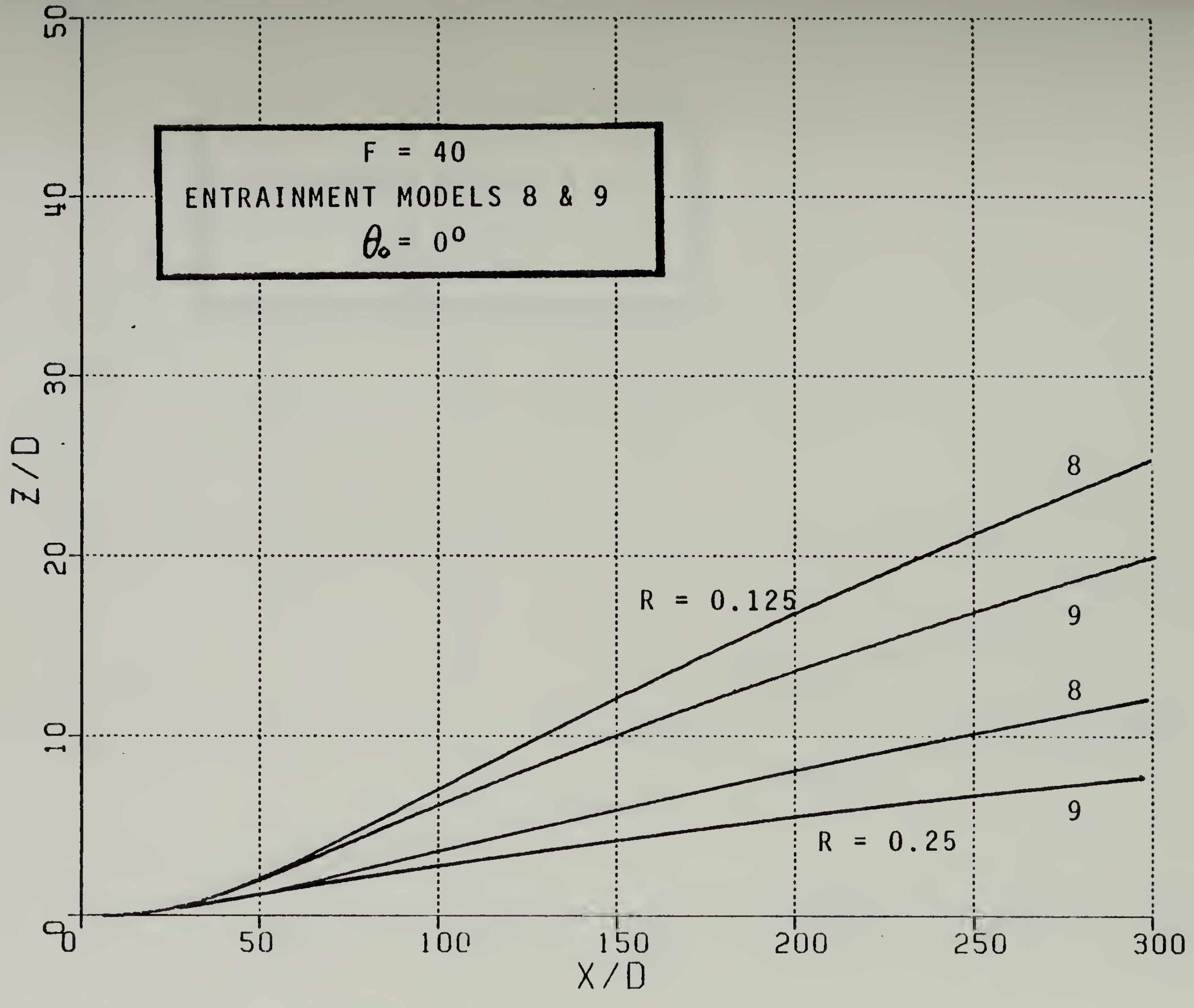

Figure 6-33. Comparison of flowing ambient entrainment models for case of pure coflow

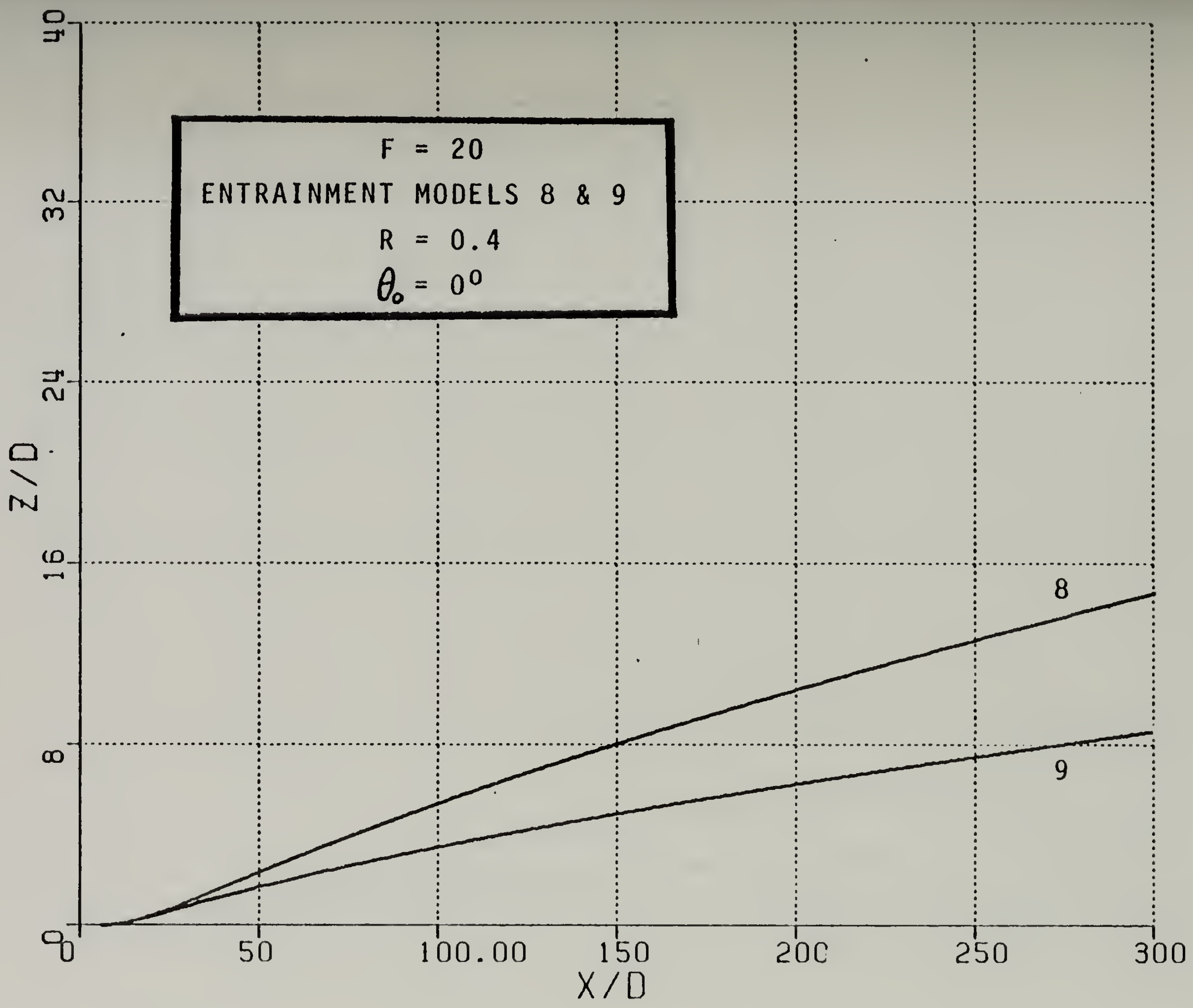

Figure 6-34. Comparison of flowing ambient entrainment models for case of pure coflow

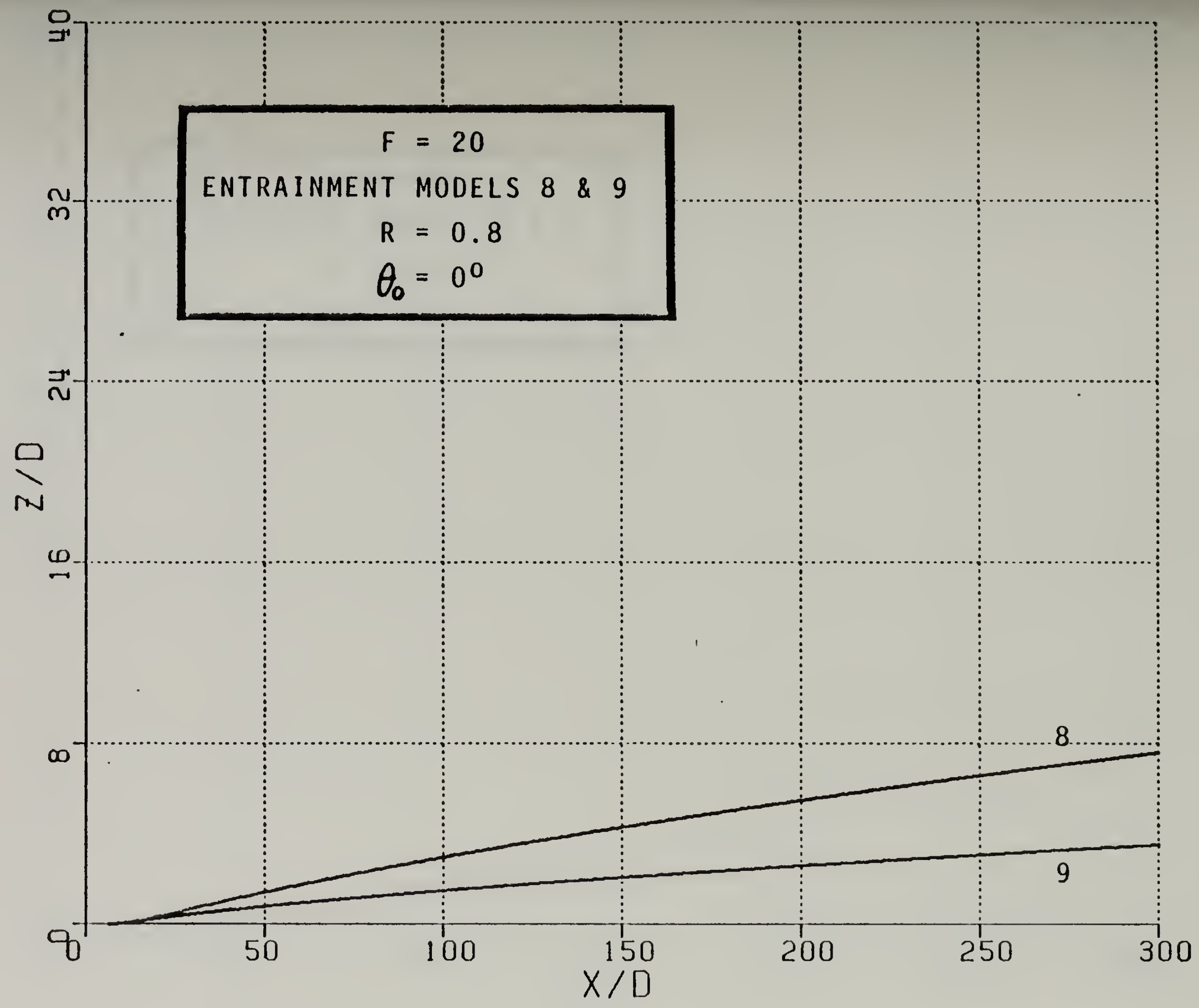

Figure 6-35. Comparison of flowing ambient entrainment models for case of pure coflow

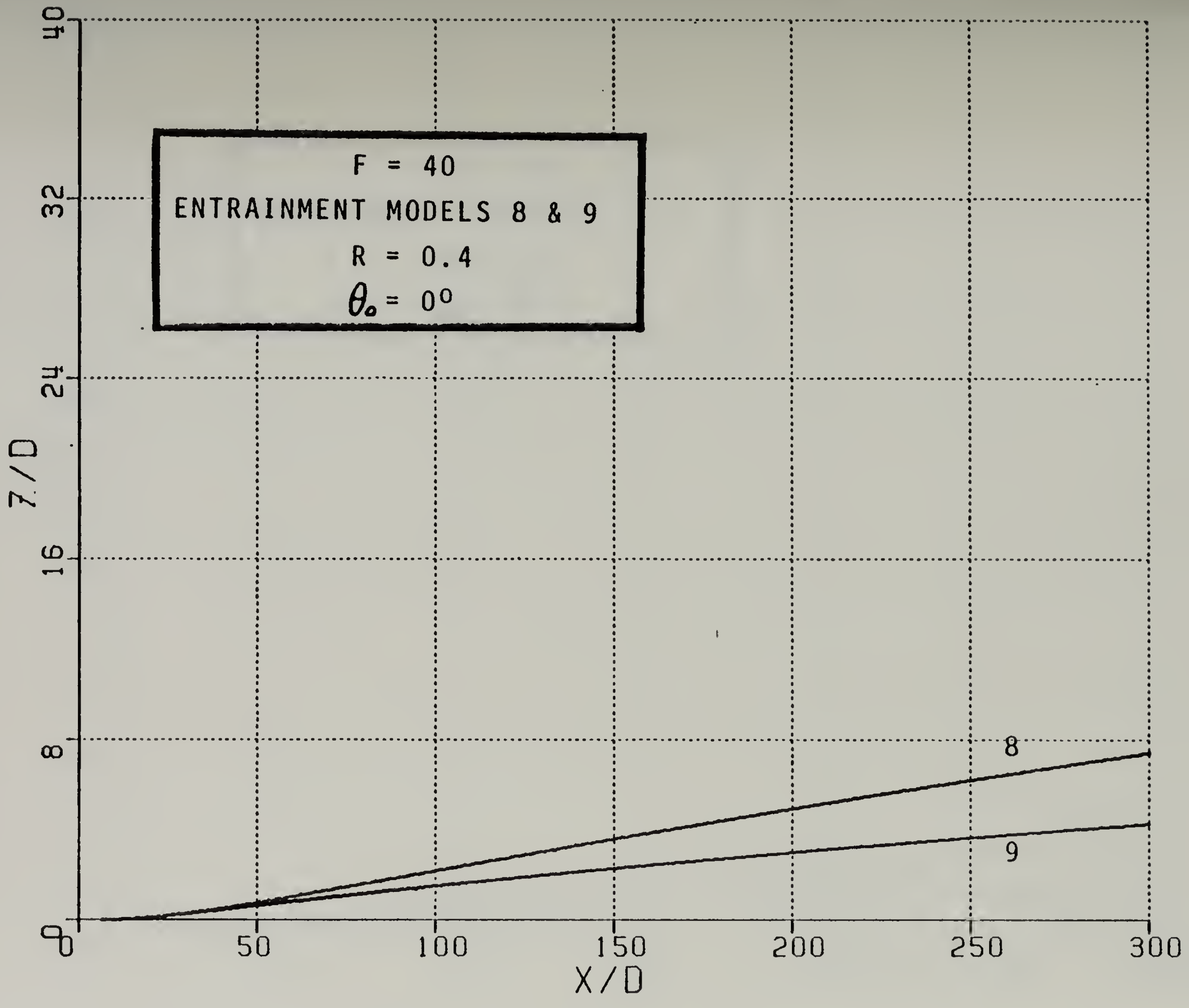

Figure 6-36. Comparison of flowing ambient entrainment models for case of pure coflow

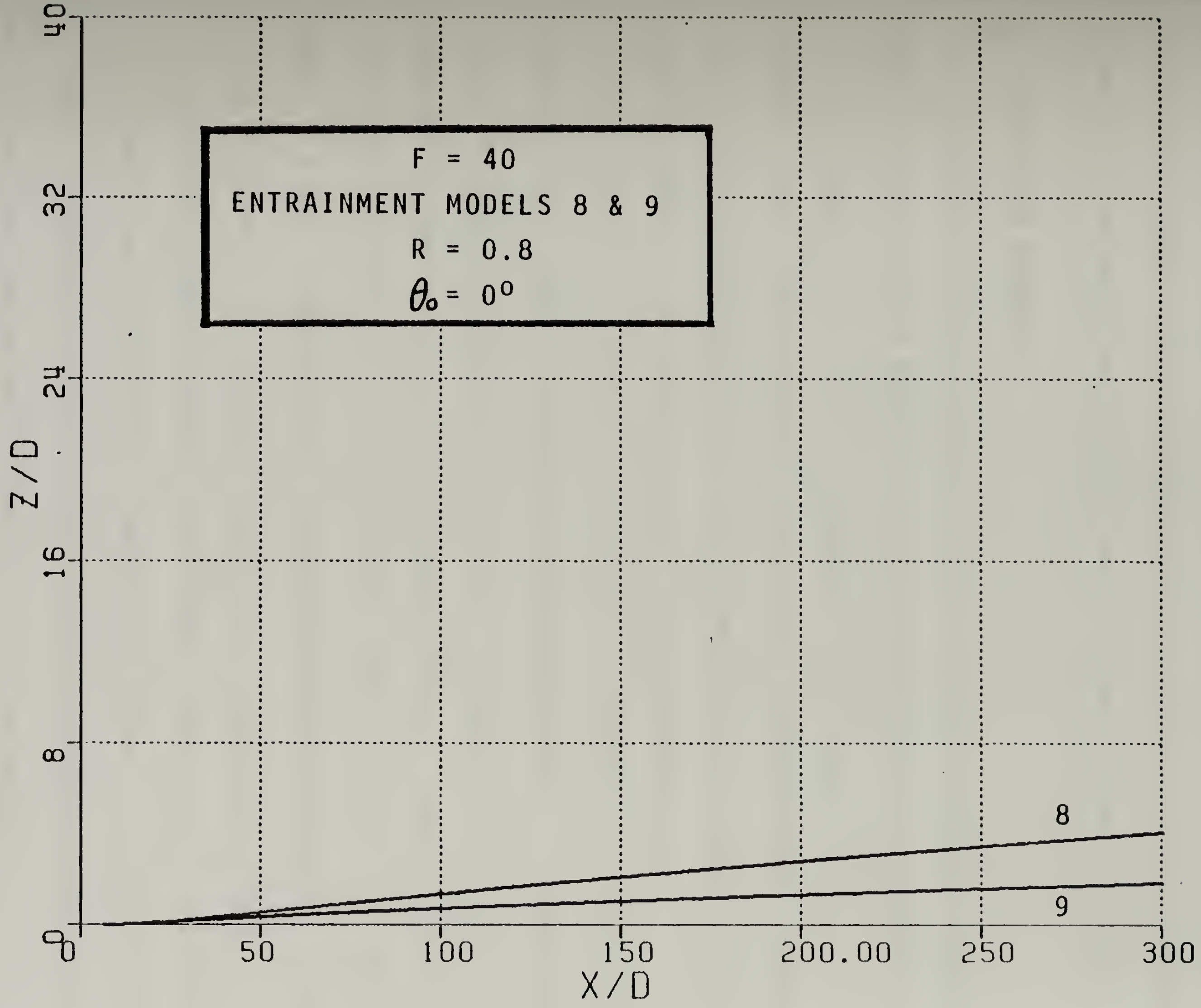

Figure 6-37. Comparison of flowing ambient entrainment models for case of pure coflow

effect is accounted for. These low Froude number, low R flows often result in calculated differences of vertical rise of many diameters in magnitude. This disagreement is found at all discharge angles. At higher values of F and R, the absolute difference in predicted vertical rise becomes small, but relative to the total rise of the jet, the difference may be many times greater than for lower values of F and R.

C. STRATIFIED AMBIENTS

A stable stratified ambient, in which density increases with increasing depth, has the general effect of restricting the vertical motion of an initially buoyant jet. This is because of the compound effect of stratification and of the jet losing buoyancy due to entrainment of ambient fluid. This occurs regardless of the direction of buoyancy, ambient stratification, or of the magnitude of the stratification.

Figure (6-38) illustrates the effect of increasingly strong stable stratification, due to an ambient temperature gradient. The calculation is for an upwardly buoyant jet of F = 50, discharged horizontally into a quiescent ambient. For the least stratification, A, the jet has followed a trajectory similar to the unstratified case, replotted from Figure 6-11. There is a very slight vertical restriction of the trajectory. In case B, near the end of the computed trajectory, a noticeable change in trend, or re-bending of the trajectory, is evident. The point of inflection in this curve is very significant. Calculations show that this is the vertical level at which the jet has become neutrally buoyant, due to entrainment on one hand and the decreasing density of the surrounding fluid on the other. Further upward rise beyond this point is due solely to the momentum then existing in the jet. This momentum is gradually decreased by the downward force of negative buoyancy.

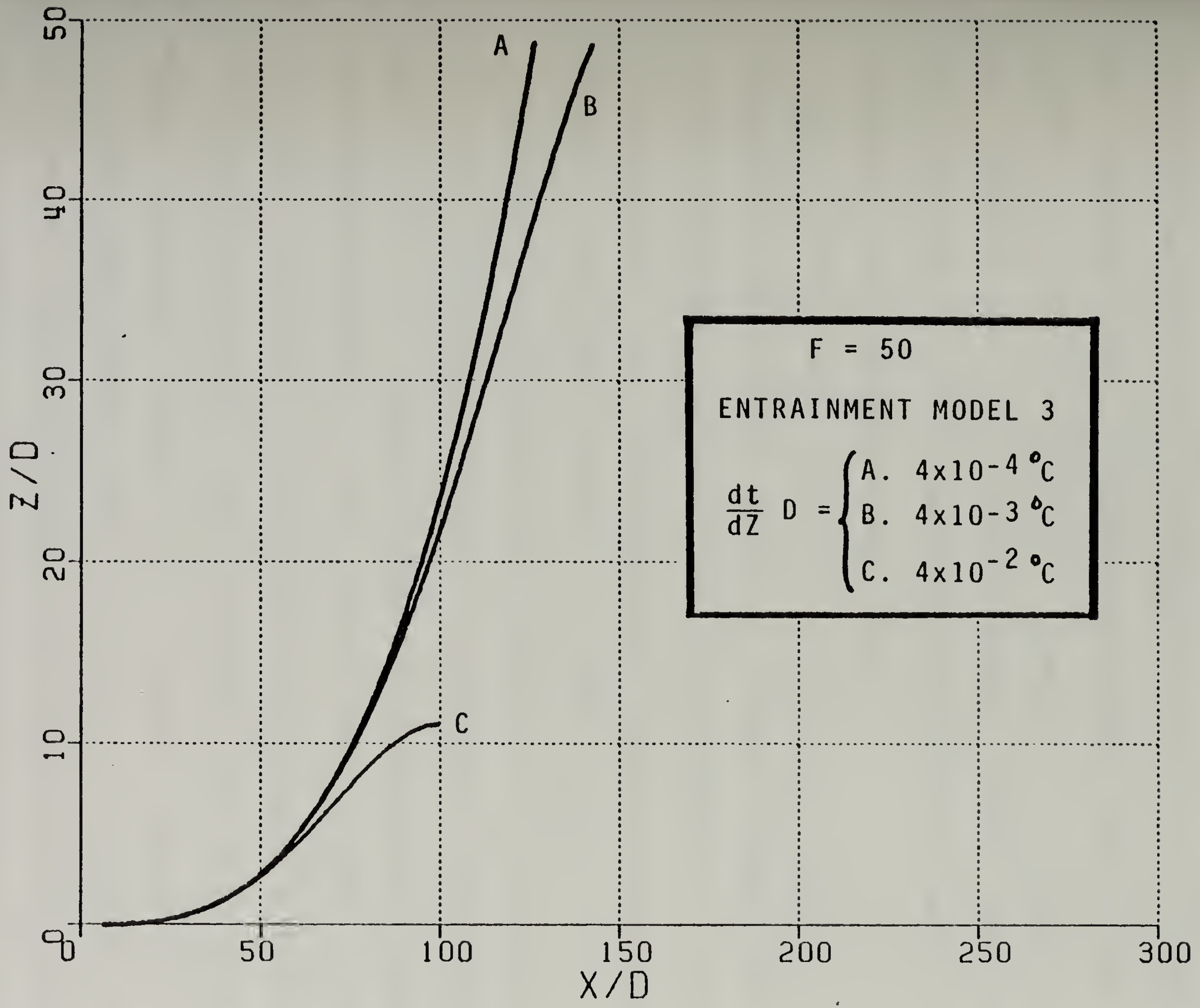

Figure 6-38. Buoyant jet behavior in a stratified ambient

Case (C) shows the eventual course of events for a jet which has become vertically "trapped", due to increased ambient stratification. The trajectory has undergone complete re-bending, to horizontal flow with no buoyancy. Standard practice in entrainment modelling, which will be followed here, is to halt computation at the point of maximum rise. Beyond this point, all but the most vigorous jets will have acquired "far field" characteristics. Assumptions of axisymmetric jet shape, tenuous at best in a stratified ambient, certainly cannot be made beyond this point, and initial momentum and buoyancy have become largely irrelevant to future behavior in most cases.

Figures (6-39), (6-40), and (6-41) illustrate the effect of the same degrees of stratification on jets at a higher discharge Froude number, F = 100, 150 and 200. The general behavior characteristics are similar to those previously noted, with ambient stratification further restricting the vertical rise already limited by low initial buoyancy.

The intuitive reasoning that the trajectory of initially more buoyant jets is less affected by stratification is supported by these calculations. Figures (6-42), (6-43), and (6-44) compare the trajectories of various Froude number discharges in an environment of three different stratification levels. The lowest F jets are seen to be negligibly affected over this range of stratification, while the higher F jets exhibit varying degrees of trajectory flattening, vertical trapping, and terminal rise. Given strong enough stratification in the ambient, of course, any initially buoyant jet will eventually experience negative buoyancy and terminate its rise at some elevation in a sufficiently extensive ambient. No elevation overshoot is seen.

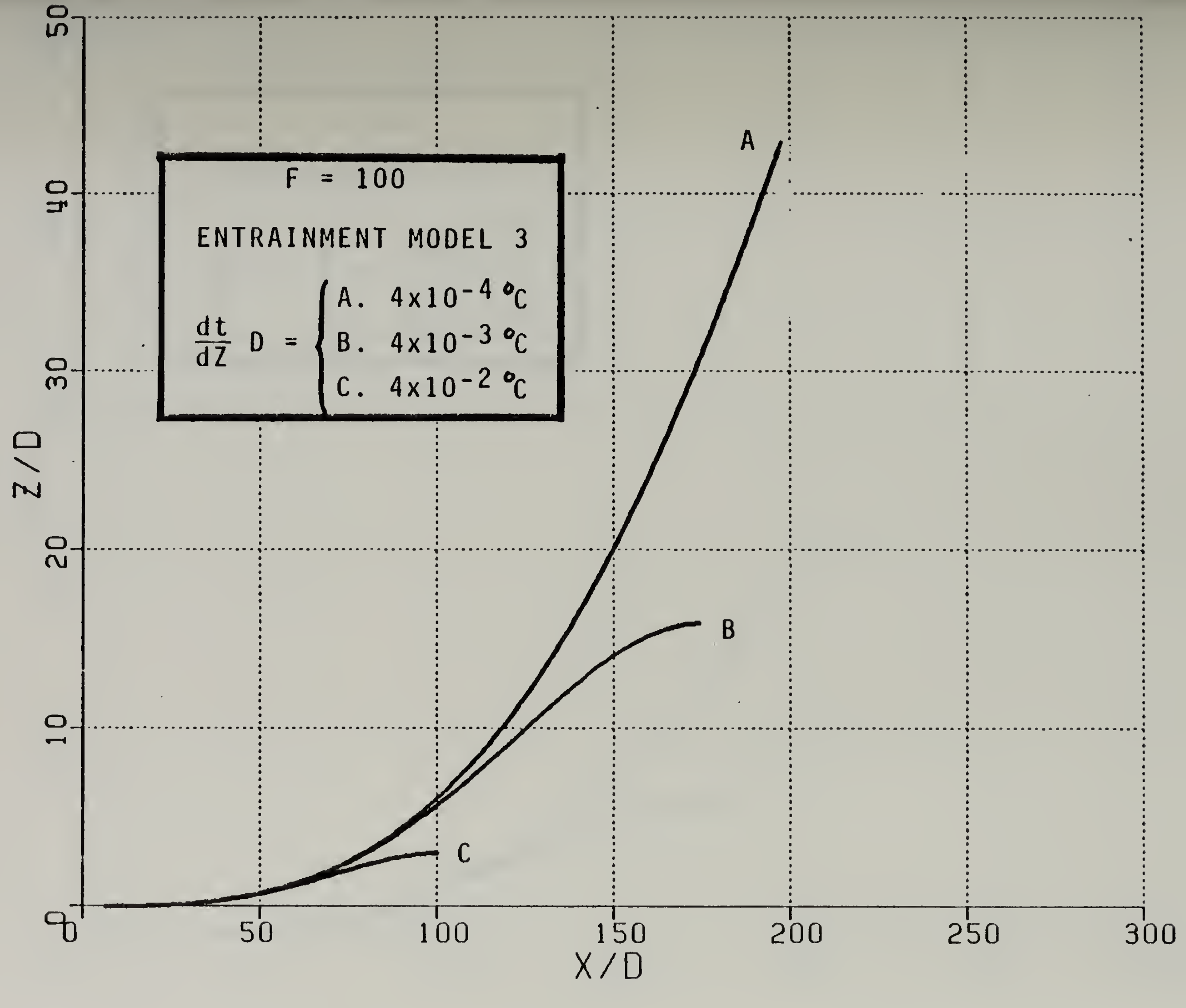

Figure 6-39. Jet behavior in a stratified ambient

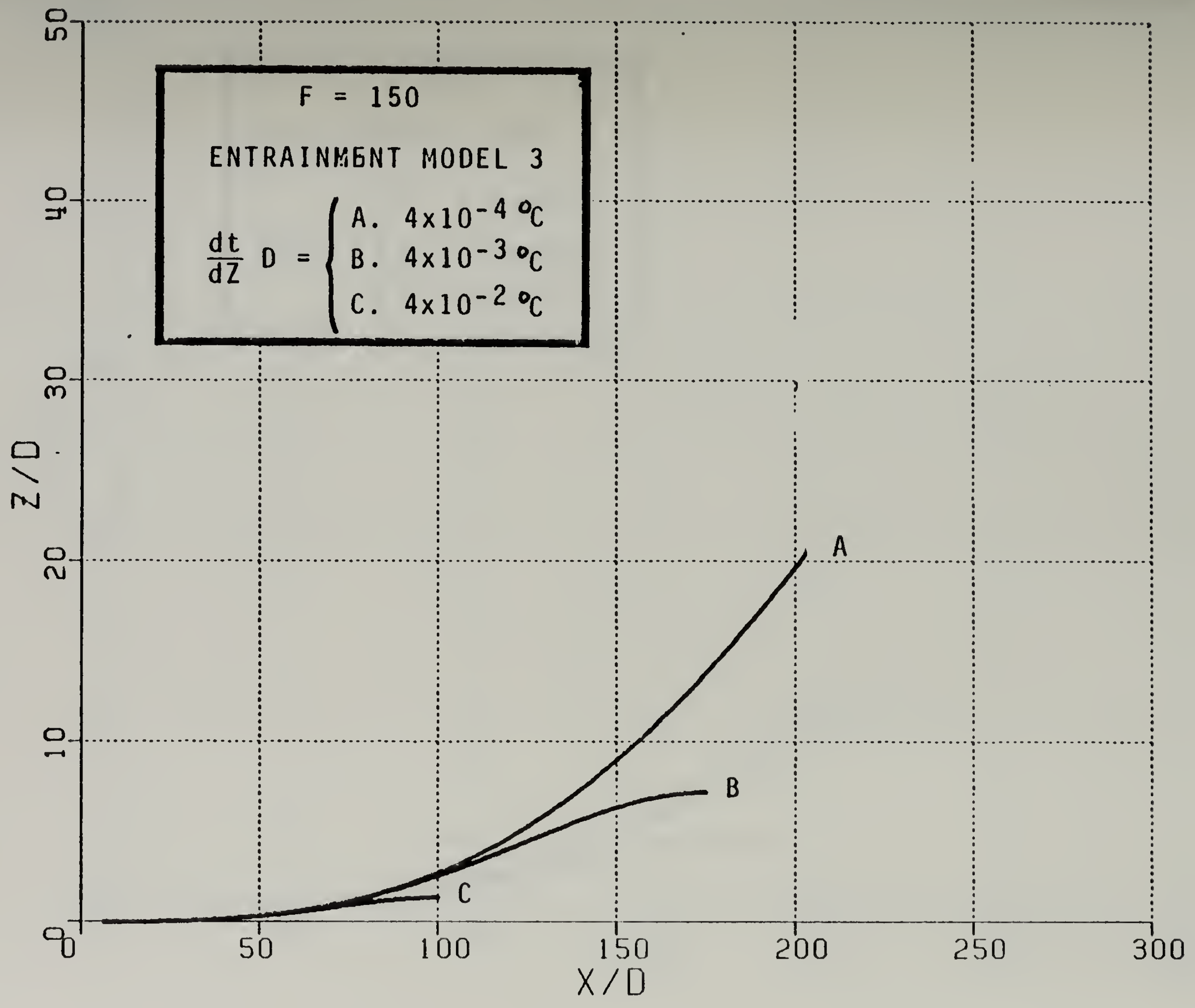

Figure 6-40. Jet behavior in a stratified ambient

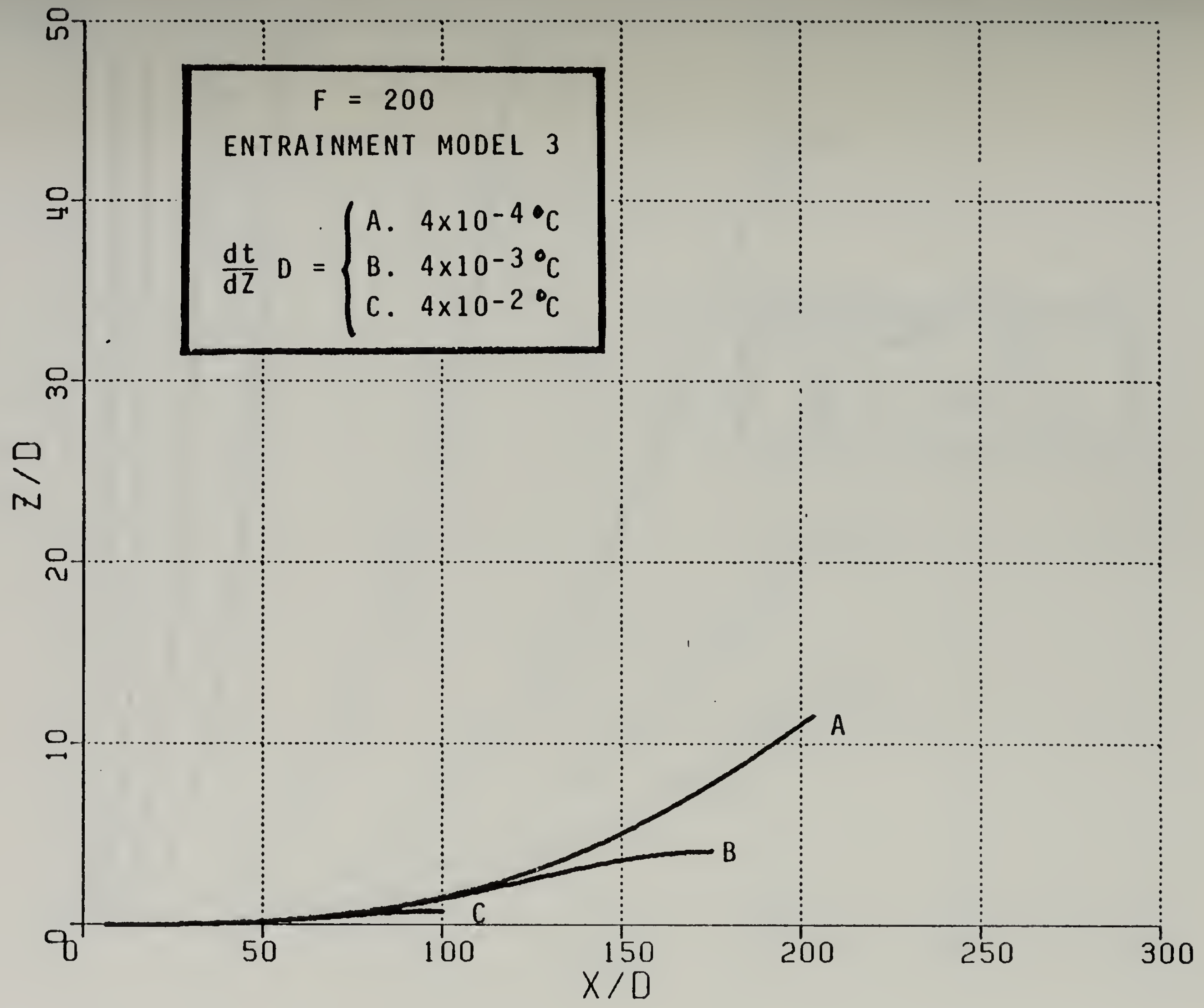

Figure 6-41. Jet behavior in a stratified ambient

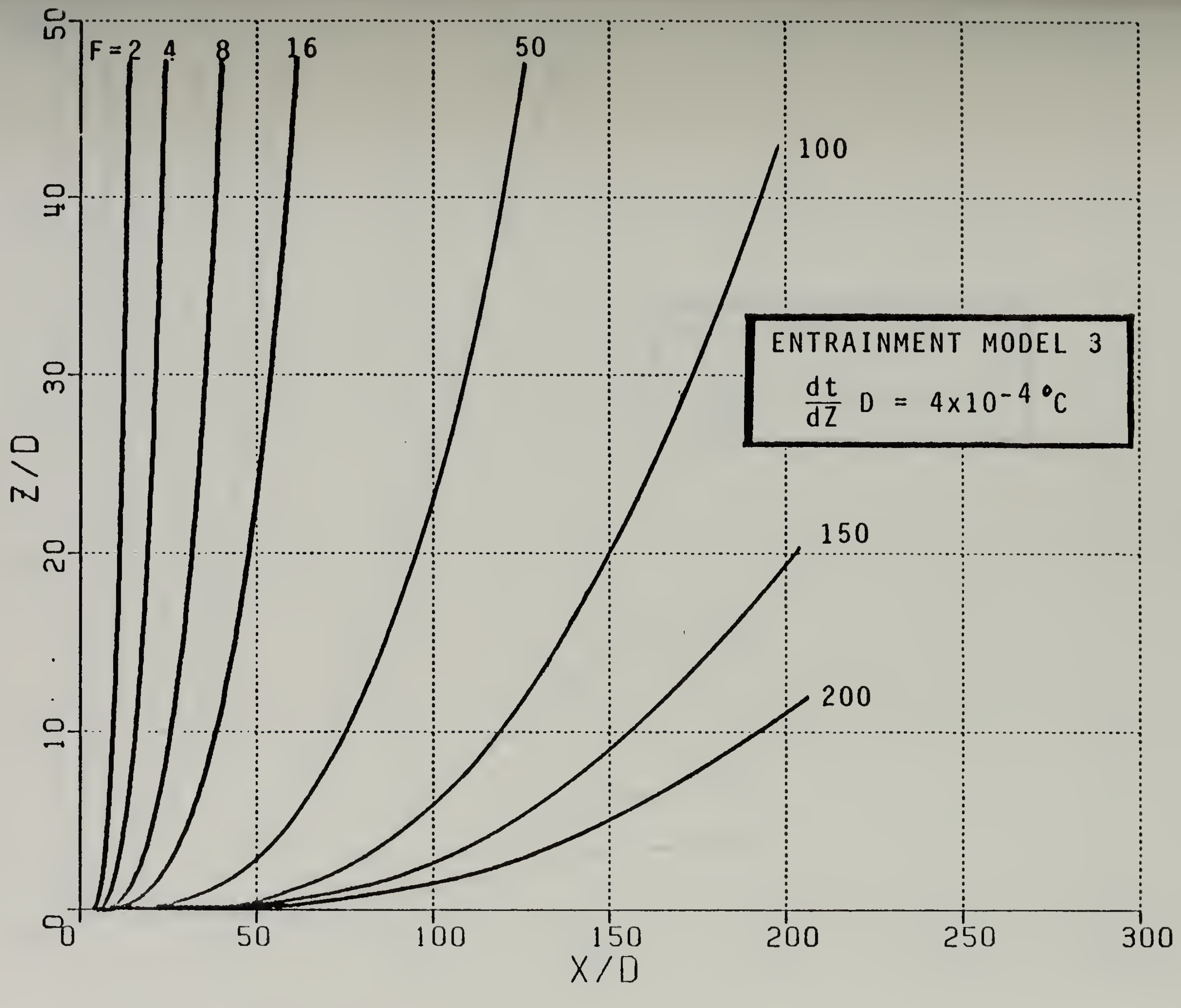

Figure 6-42. Effect of stratification on jet behavior

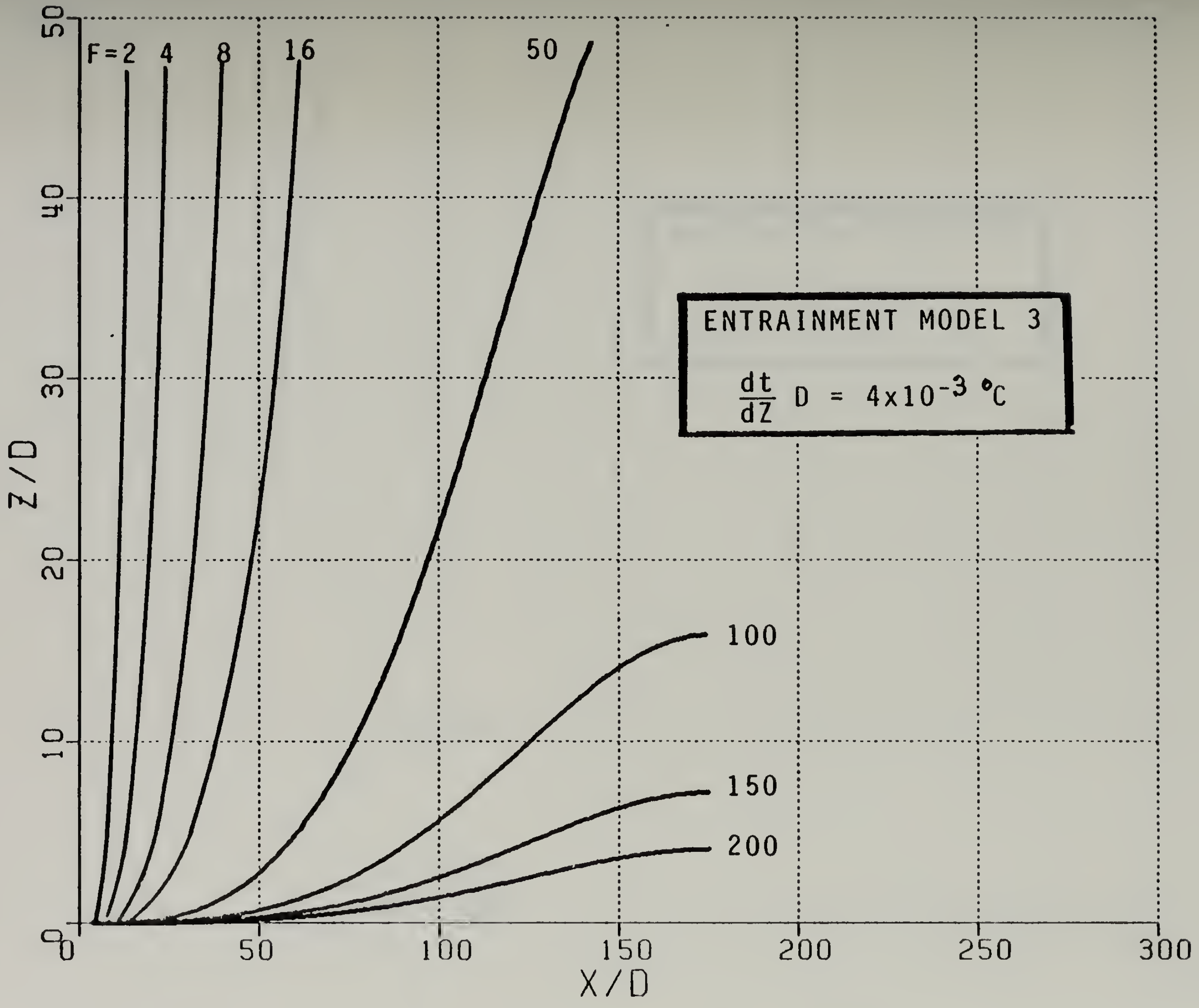

Figure 6-43. Effect of stratification on jet behavior

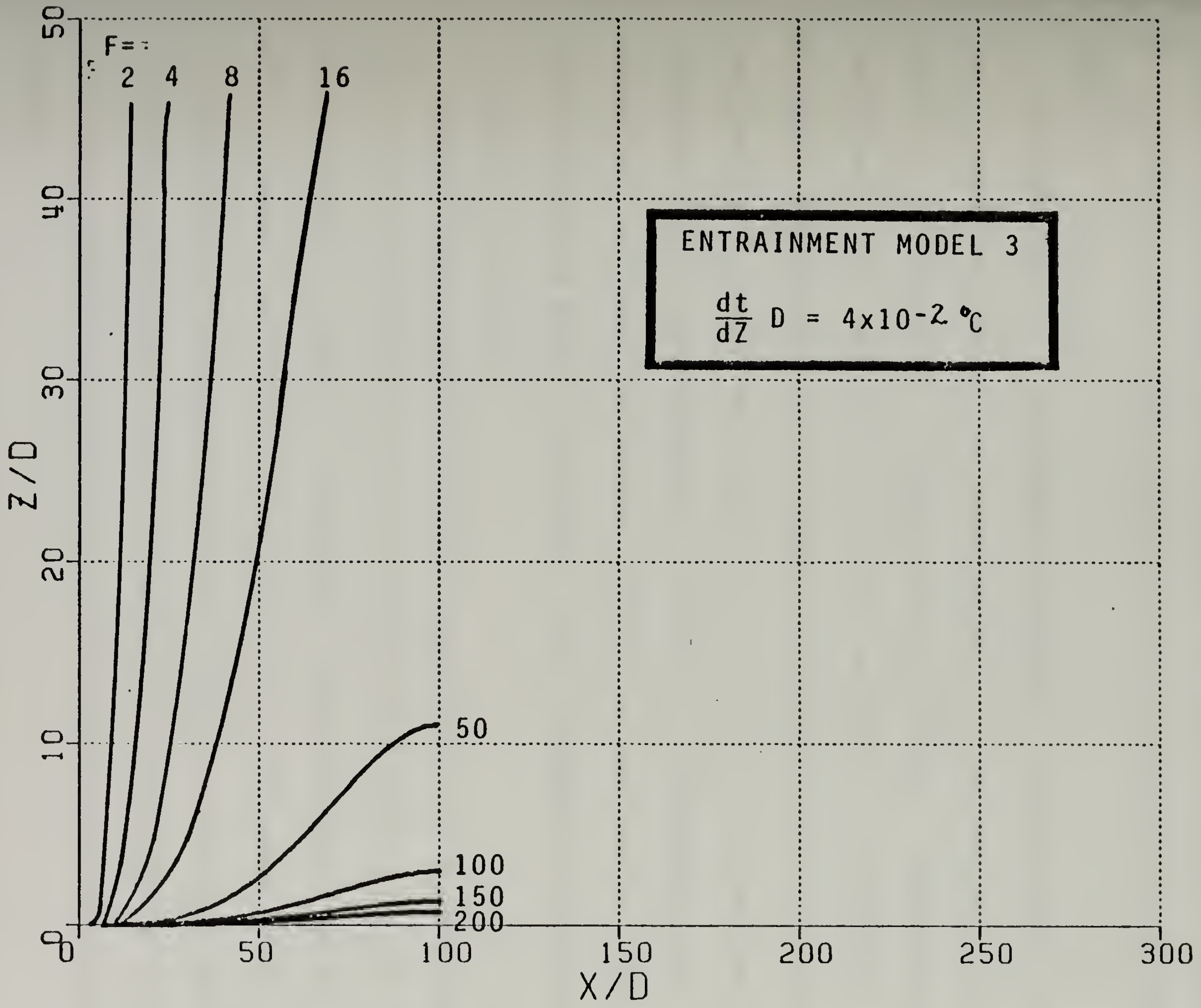

Figure 6-44. Effect of stratification on jet behavior

The above circumstances demonstrated are typical of past jet modelling in a stratified ambient. Stratification, as indicated in the earlier discussion of equations of state, is usually represented in terms of a single, constant temperature, salinity, or density gradient. Rarely, as in Reference [15], temperature and salinity gradients may be treated together.

The capability of a comprehensive equation of state to more realistically describe a particular water ambient and the behavior of a jet within it is illustrated in Figures (6-45) to (6-50). Figure (6-45) characterizes the temperature, salinity, and density stratification of an area of the Northern Pacific Ocean to a depth of 500 m. June temperature and salinity data for a point 53° 04' N, 175° 35' W were taken from Reference [4], and approximated by a series of 5 temperature and 4 salinity gradients. The Gebhart-Mollendorf relation was then used to establish the corresponding density field shown, which includes the contribution of hydrostatic pressure.

Figure (6-46) shows the predicted trajectories of 5 buoyant momentum jets, for F = 10,20,30,40 and 50, discharged horizontally in this density field at a depth of 200 m. In each case, the initial jet diameter is 1 m., while F ranges from 10 to 50. Initial salinity difference between the jet and ambient was assumed to be zero. Buoyancy was due to elevated temperature, however the effect of the salinity stratification gradient is included in the calculation of jet density and buoyancy along the trajectory.

All five of these jets exhibit the progression from positive to negative buoyancy, as well as a level of maximum upward penetration. All display a rather smooth curvature and re-curvature, due to the relatively

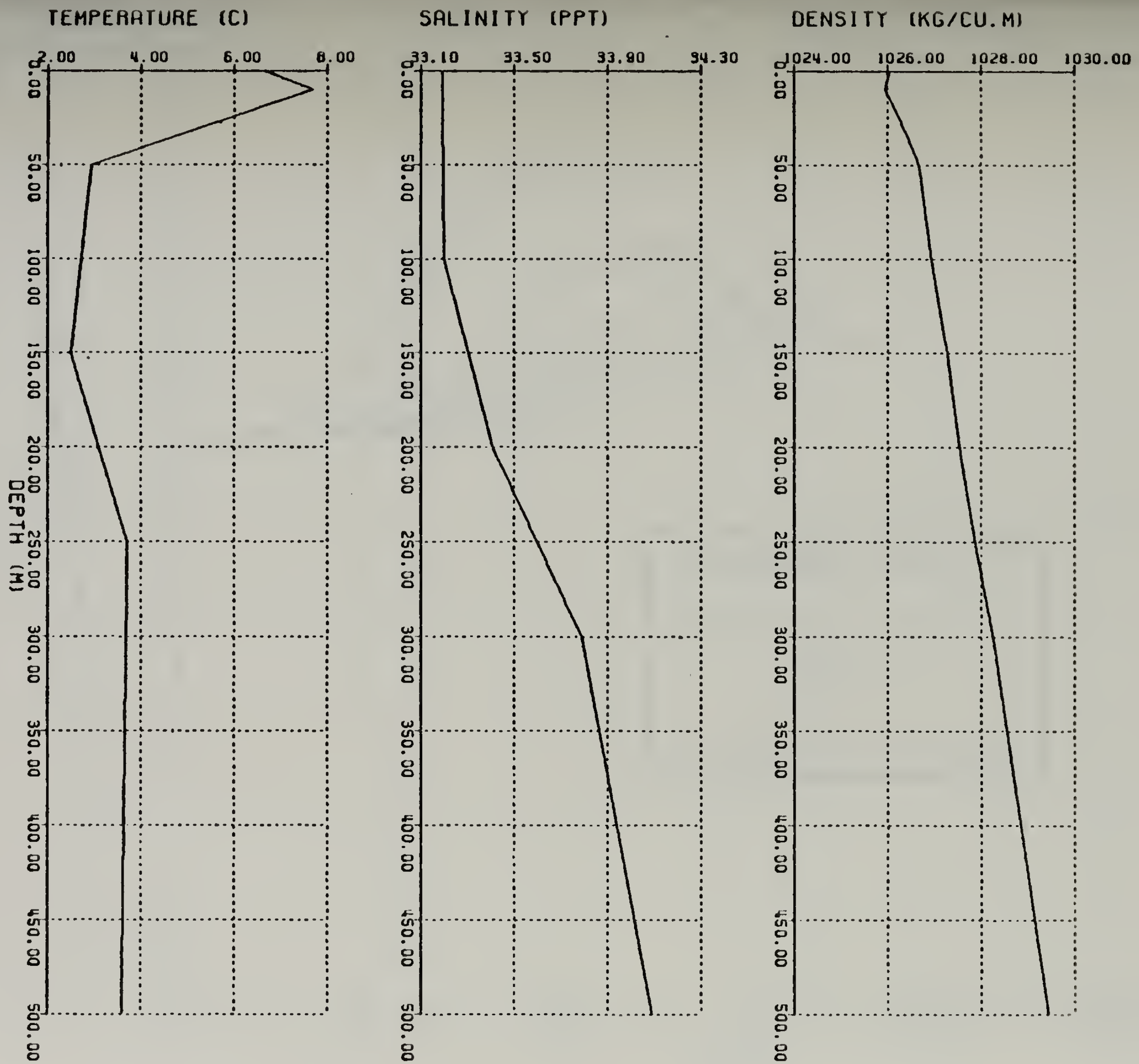

Figure 6-45. Temperature, salinity and density for Northern Pacific Ocean, 53° 04' N, 175° 35' W, June

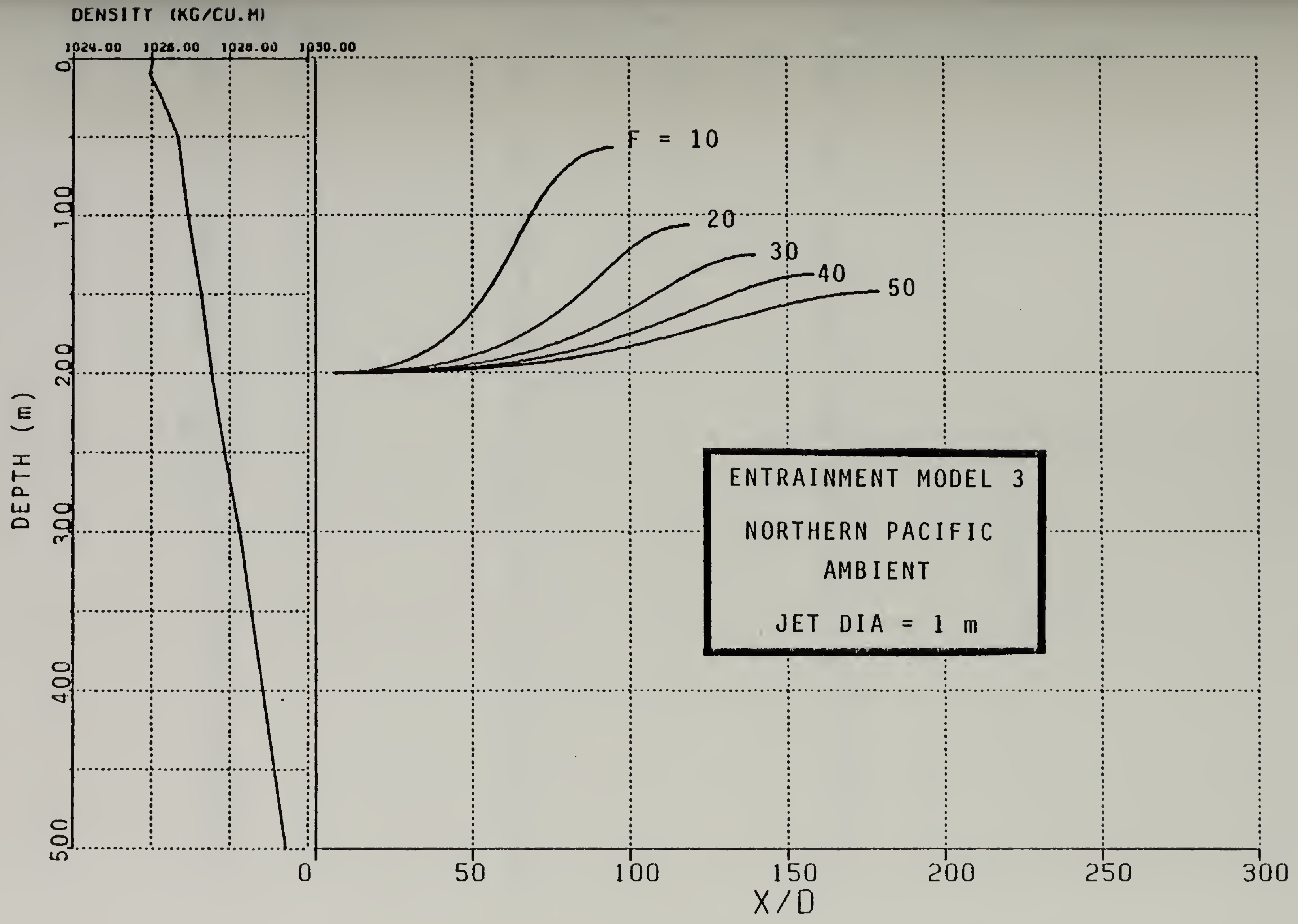

Figure 6-46. Trajectory of 5 jets discharged into the ambient of Figure 6-45

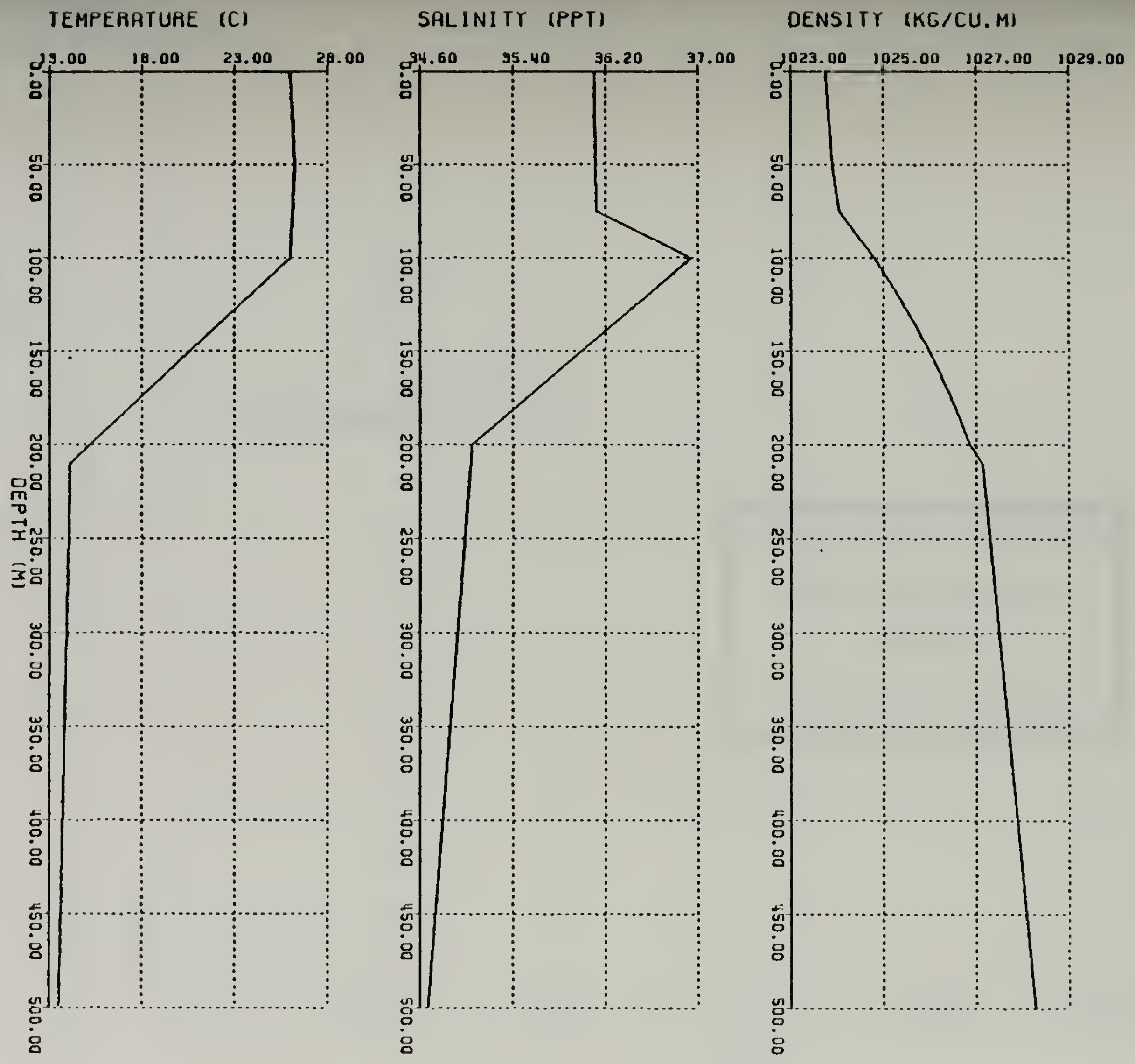

Figure 6-47. Temperature, salinity, and density profiles for tropical Atlantic Ocean, 02° 03' S, 39 °20' W, February.

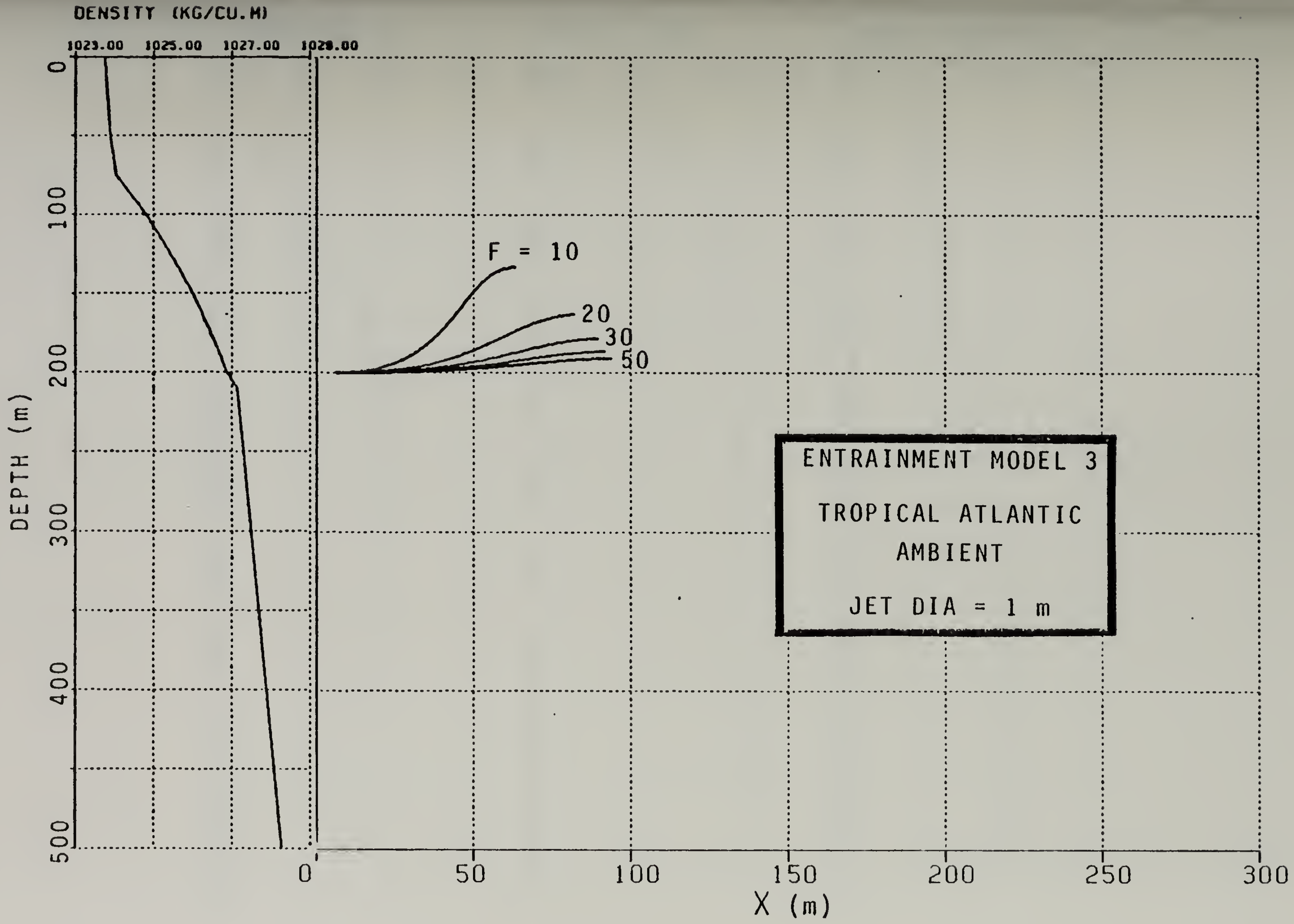

Figure 6-48. Trajectory of 5 jets discharged into the ambient of figure 6-47

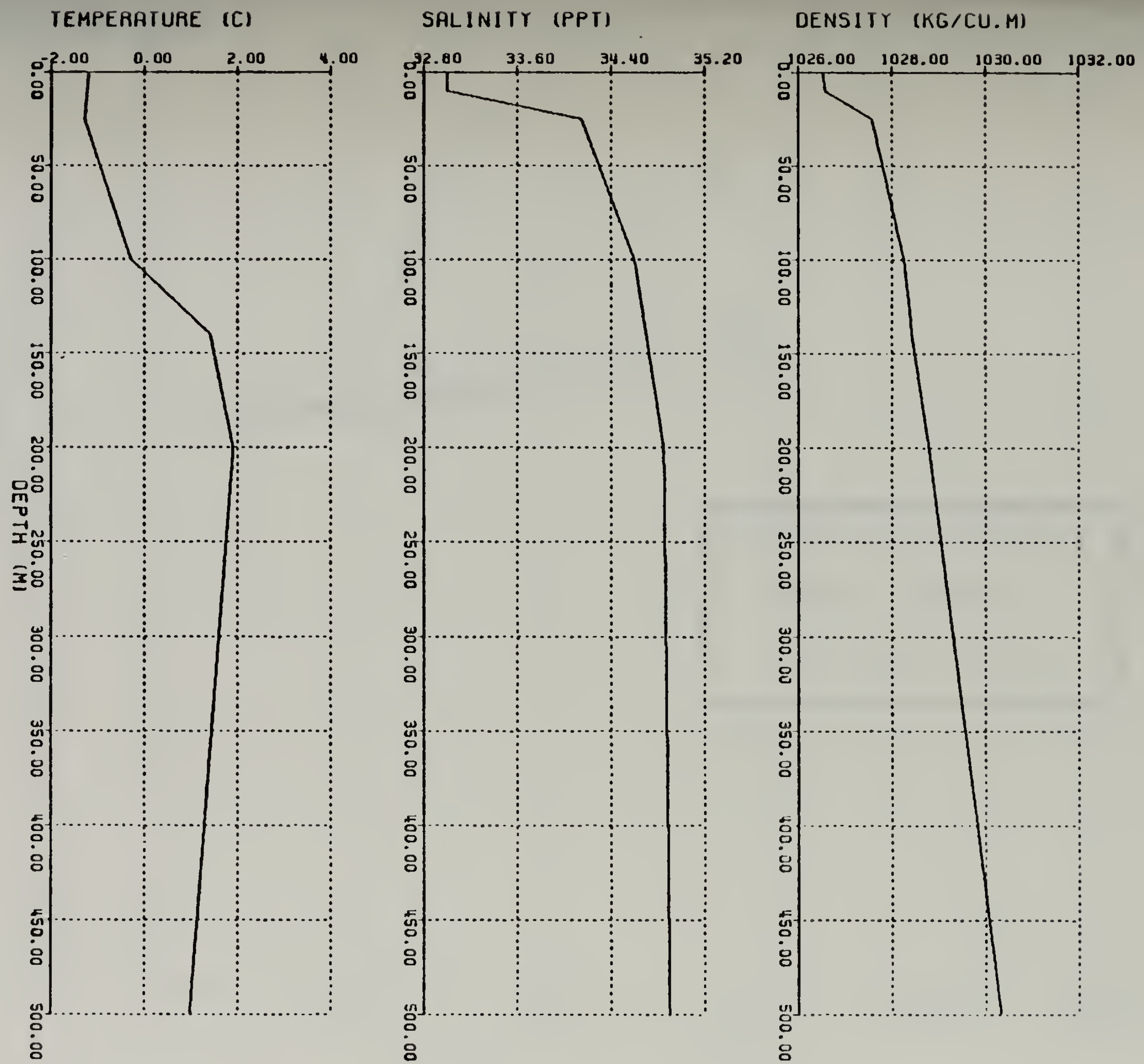

Figure 6-49. Temperature, salinity, and density profiles for Arctic Ocean, 81° 28' N, 8° 05' E, October

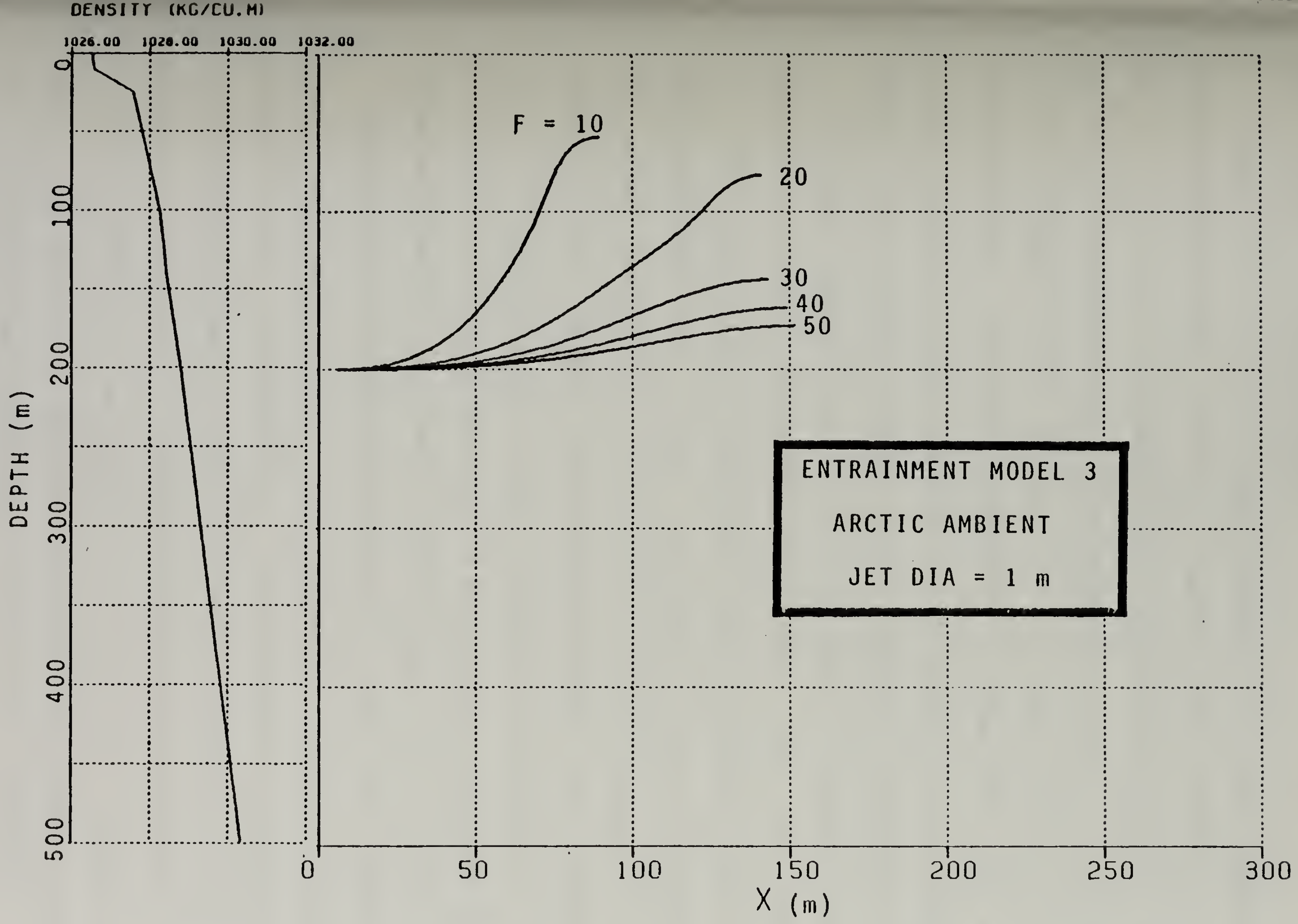

Figure 6-50. Trajectories of 5 jets discharged into the ambient of figure 6- 49

constant density gradient encountered in the vertical range of penetration. Again, no overshoot occurs.

Figure (6-47) illustrates another characteristic oceanic temperature-salinity-density field, in this case from the tropical Atlantic at a point 02° 03' S, 39° 20' W. The data for this construction was taken in February and is from Reference [21]. The trajectory of jets F = 10,20,30,40 and 50 discharged into this density field at a depth of 200 m. is shown in Figure (6-48). The vertical penetration of these jets in this case is significantly less than calculated for the Northern Pacific density profile, due to the much stronger density gradient in the tropical ocean.

An October temperature-salinity-density field for the Arctic Ocean at 81° 28' N, 8° 05' E is shown in Figure (6-49). Data is from Reference [17]. The strong salinity discontinuity near the surface is due to melt from the adjacent Arctic ice pack. The behavior of jets discharged into this ambient, Figure (6-53), is especially interesting compared to Figures (6-49) and (6-51), because of the varying recurvature rates encountered. For F = 30, the jets exhibit a smooth curvature and recurvature. The F = 10 and F = 20 jets, however, show a much sharper recurvature because of the encounter with the steeper density gradient above the 100 m. level.

These examples illustrate the advantage of using a full equation of state in entrainment modelling. The dependence of the model on assumed values of β and γ is eliminated, as is the requirement to express ambient stratification in terms of constant temperature, salinity, or density gradients. The accuracy of the ambient density characterization is limited only by the availability and spacing of the field data. Ultimately, the use of a full equation of state can reduce one of the primary uncertainties in entrainment modelling--that of evaluating the temperature-salinity-pressure-density relationship.

VII. EXTRAPOLATION OF PRESENT METHODS TO PARAMETERS OF INTEREST

In reviewing the progress to date in entrainment modelling of buoyant momentum jets, some rather striking matters become apparent. The first of these is the very small physical scale of the experimental studies which has been made to underlie subsequent modelling schemes. Jet discharge diameters were mostly about 1 cm, the largest being 3.9 cm. The entire jet trajectories were usually only a few meters in length. Great lengths arose in some of the experiments done with flowing ambients, but even these studies used similarly small diameter discharges. These limitations, of course, arose, at least in part, through the innate limitation in size and economy which applies to experimental work.

Still, the data base from these small scale discharges are often used to develop models for real world jets, such as power plant discharges and sewer outfalls. These are commonly hundreds to thousands of times larger. Such upscaling of the implications of the experiments implies a faith in the similarity properties of the densimetric Froude number. This may or may not be justified. Further, such a large scale difference between supporting data and real system projection, in the case of an underwater momentum jet, does not necessarily imply similar scaling in turbulence within the jet and in the immediately surrounding ambient. Fan [7] found that the effect of ambient turbulence on jet behavior was profound. It is not unreasonable to expect that the scale of turbulence within the jet, or the relative scale between ambient turbulence and jet dimensions, may not have equally important effects.

The second striking aspect of experimental and analytical work is the relatively low densimetric Froude number range used. Admittedly, more

buoyant, lower Froude number jets are more "interesting" in terms of possible trajectories, and may be of more importance in many environmental modelling situations. Froude numbers in the range of 10 to 40 are common in the literature. Values as high as 100 are rare. There are a number of "real" cases, however, in which entrainment modelling might be used, where Froude numbers might be in this higher range. Very basic calculations dealing with unclassified physical and propulsive properties of submarines, for instance, indicate that the propeller outflow, with all condenser efflux entrained and mixed within, might represent a Froude number in the range of 50 to 200. Ship or submarine condenser efflux by itself might be expected to have a range inclusive of all Froude numbers to about 200, depending on discharge size, flow rate, and thermal loading.

A third limitation in the present state of entrainment modelling is the inconsistent predictive quality of the collection of available flowing ambient entrainment functions in their supposed range of applicability. A fourth shortcoming is the range of R in which data is available to guide modelling. Very little experimental data exists for R greater than 0.25. Almost no data exist for an initially co-flowing ambient. The data is not sufficient to definitively select either a general entrainment function or even one valid over a restricted range of F and R.

Given the limitations of the current background data to support any modelling technique, a high level of confidence in predicting large scale jet trajectories, involving conditions of ambient flow, turbulence, or high Froude number discharges is unwarranted. There are simply too many unknowns to proceed confidently, limited by contemporary methods and information.

Toward the objective of developing large scale entrainment modelling, the following suggestions are made.

VIII. RECOMMENDATIONS

If entrainment modelling is to be made applicable to large scale discharges involving relatively high ambient flow velocities, a more comprehensive data base than now exists needs to be established. Such a data base would include:

(1) higher Froude number flows, up to a range of 200.

(2) larger scale discharges, with particular attention to turbulence scale and its effects.

(3) higher R coflows.

Future analytical models, drawing from such an enhanced data base, need to specifically address:

(1) determination of a dependable entrainment function for submerged jets discharged to a flowing ambient.

(2) determination of methods to include turbulence effects in the model.

(3) inclusion of an accurate and comprehensive equation of state, such as the one proposed here, in the model.

APPENDIX A

A. ASSUMED GAUSSIAN DISTRIBUTIONS

$$U = U_m \exp[\frac{-r^2}{B^2}] \qquad (2\text{-}1)$$

$$\frac{T-T_a}{T_m-T_a} = \exp[\frac{-r^2}{\lambda^2 B^2}] \qquad (2\text{-}2)$$

$$\frac{C-C_a}{C_m-C_a} = \exp[\frac{-r^2}{\lambda^2 B^2}] \qquad (2\text{-}3)$$

$$\frac{\rho_a-\rho}{\rho_a-\rho_m} = \exp[\frac{-r^2}{\lambda^2 B^2}]$$

B. DEVELOPMENT OF THE GOVERNING EQUATIONS

1. Continuity

$$\frac{d}{dS}\{\int_0^{2\pi}\int_0^{\infty} Urdrd\phi\} = 2\pi\alpha U_m B \qquad (5\text{-}1)$$

$$\frac{d}{dS}\{2\pi\int_0^{\infty} Urdr\} = 2\pi\alpha U_m B$$

Substituting Equation (2-1)

$$\frac{d}{dS}\{\int_0^{\infty} U_m \exp[\frac{-r^2}{B^2}]rdr\} = \alpha U_m B$$

$$\frac{d}{dS}\{U_m \frac{B^2}{2}\} = \alpha U_m B$$

$$\frac{d}{dS}\{U_m B^2\} = 2\alpha U_m B \qquad (A-1)$$

For the case of a coflowing ambient, the entrainment rate is expressed as a function of jet centerline velocity and jet width which is more complex than the simple linear relationship of the quiescent ambient case. For coflowing ambients,

$$\frac{d}{dS}\{\int_0^{2\pi} \int_0^{\infty} U r dr d\phi\} = 2\pi f(\alpha, U_m, B, R)$$

By development identical to the quiescent ambient case,

$$\frac{d}{dS}\{U_m B^2\} = 2f(\alpha, U_m, B, R) \qquad (A-2)$$

2. Conservation of Energy

$$\frac{d}{dS}\{\int_0^{2\pi} \int_0^{\infty} U(t-t_a) r dr d\phi\} = -\frac{dt_a}{dS}\{\int_0^{2\pi} \int_0^{\infty} U r dr d\phi\} \qquad (5-4)$$

Integrating and substituting Equations (2-1) and (2-2),

$$\frac{d}{dS}\{2\pi \int_0^{\infty} U_m \exp[\frac{-r^2}{B^2}](t_m - t_a)\exp[\frac{-r^2}{\lambda^2 B^2}] r dr\}$$

$$= -\frac{dt_a}{dS}\{2\pi \int_0^{\infty} U_m \exp[\frac{-r^2}{B^2}] r dr\}$$

$$\frac{d}{dS}\{U_m(t_m-t_a)\int_0^\infty \exp[\frac{-r^2(\lambda^2+1)}{\lambda^2B^2}]rdr\}$$

$$= -\frac{dt_a}{dS}\{U_m\int_0^\infty \exp[\frac{-r^2}{B^2}]rdr\}$$

$$\frac{d}{dS}\{U_m(t_m-t_a)[\frac{\lambda^2B^2}{2(\lambda^2+1)}]\} = -\frac{dt_a}{dS}\{U_m\frac{B^2}{2}\} \qquad (A-3)$$

3. Conservation of Concentration or Other Scalar Species

$$\frac{d}{dS}\{\int_0^{2\pi}\int_0^\infty U(c-c_a)rdrd\phi\}$$

$$= -\frac{dc_a}{dS}\{\int_0^{2\pi}\int_0^\infty Urdrd\phi\} \qquad (5-5)$$

By development identical to conservation of energy in (2) above, using Equation (2-3),

$$\frac{d}{dS}\{U_m(c_m-c_a)[\frac{\lambda^2B^2}{2(\lambda^2+1)}]\} = -\frac{dc_a}{dS}\{U_m\frac{B^2}{2}\} \qquad (A-4)$$

4. Conservation of Horizontal Momentum

For the case of the quiescent ambient,

$$\frac{d}{dS}\{\int_0^{2\pi}\int_0^\infty U^2\cos\theta rdrd\phi\} = 0 \qquad (5-2)$$

$$\frac{d}{dS}\{2\pi\int_0^\infty U^2\cos\theta rdr\} = 0$$

Substituting Equation (2-1),

$$\frac{d}{dS}\{2\pi U_m^2\cos\theta \int_0^\infty \exp[\frac{-2r^2}{B^2}]rdr\} = 0$$

$$\frac{d}{dS}\{2\pi U_m^2\cos\theta[\frac{1}{2}\frac{B^2}{2}]\} = 0$$

$$\frac{d}{dS}\{U_m^2B^2\cos\theta\} = 0 \qquad (A-5)$$

For the case of the flowing ambient,

$$\frac{d}{dS}\{\int_0^{2\pi}\int_0^\infty U^2\cos\theta\, rdrd\phi\} = 2\pi f(\alpha,U_m,B,R)U_a$$

$$\frac{d}{dS}\{2\pi\int_0^\infty U^2\cos\theta\, rdr\} = 2\pi f(\alpha,U_m,B,R)U_a$$

Substituting Equation (2-1),

$$\frac{d}{dS}\{U_m^2\cos\theta\int_0^\infty \exp[\frac{-2r^2}{B^2}]rdr\} = f(\alpha,U_m,B,R)U_a$$

$$\frac{d}{dS}\{U_m^2\cos\theta[\frac{1}{2}\frac{B^2}{2}]\} = f(\alpha,U_m,B,R)U_a$$

$$\frac{d}{dS}\{U_m^2\cos\theta B^2\} = 4f(\alpha,U_m,B,R)U_a \qquad (4-6)$$

5. Conservation of Vertical Momentum

$$\frac{d}{dS}\{\int_0^{2\pi}\int_0^\infty \rho U^2\sin\theta\, rdrd\phi\} = \int_0^{2\pi}\int_0^\infty (\rho_a-\rho)grdrd\phi \qquad (5-3)$$

$$\frac{d}{dS}\{2\pi \int_0^\infty U^2 \sin\theta r dr\} = 2\pi \int_0^\infty (\frac{\rho_a - \rho}{\rho}) g r dr$$

Substituting Equations (2-1) and (2-2),

$$\frac{d}{dS}\{U_m^2 \sin\theta \int_0^\infty \exp[\frac{-2r^2}{B^2}] r dr\} = \frac{\rho_a - \rho_m}{\rho} g \int_0^\infty \exp[\frac{-r^2}{\lambda^2 B^2}] r dr$$

$$\frac{d}{dS}\{U_m^2 \sin\theta [\frac{1}{2} \frac{B^2}{2}]\} = \frac{\rho_a - \rho_m}{\rho} g (\frac{\lambda^2 B^2}{2})$$

$$\frac{d}{dS}\{U_m^2 \sin\theta B^2\} = \frac{\rho_a - \rho_m}{\rho}(2g\lambda^2 B) \tag{A-7}$$

6. Horizontal Trajectory

$$dX = dX \cos\theta$$

$$\frac{d}{dS} X = \cos\theta \tag{A-8}$$

7. Vertical Trajectory

$$dZ = dS \sin\theta$$

$$\frac{d}{dS} Z = \sin\theta \tag{A-9}$$

APPENDIX B

A. DIMENSIONLESS VARIABLES

The following dimensionless quantities will be used in the nondimensionalization of the governing equations:

$$u = \frac{U}{U_0}$$

$$u_m = \frac{U_m}{U_0}$$

$$b = \frac{B}{D}$$

$$s = \frac{S}{D}$$

$$x = \frac{X}{D}$$

$$z = \frac{Z}{D}$$

$$\frac{\Delta t_a}{\Delta t_0} = \frac{(t_{a2}-t_{a1})}{(t_0-t_{a0})}$$

$$\frac{\Delta c_a}{\Delta c_0} = \frac{(c_{a2}-c_{a1})}{(c_0-c_{a0})}$$

$$\frac{\Delta t_m}{\Delta t_0} = \frac{(t_m-t_a)}{(t_0-t_{a0})}$$

$$\frac{\Delta c_m}{\Delta t_0} = \frac{(c_m-c_a)}{(c_0-c_{a0})}$$

$$R = \frac{U_a}{U_0}$$

B. NONDIMENSIONALIZATION OF THE GOVERNING EQUATIONS

1. Continuity

For the case of the quiescent ambient,

$$\frac{d}{dS}\{U_m B^2\} = 2\alpha U_m B \qquad \text{(A-1)}$$

Substituting,

$$\frac{d}{ds\ D}\{u_m U_0 b^2 D^2\} = 2\alpha u_m U_0 b D$$

$$\frac{d}{ds}\{u_m b^2\} = 2\alpha u_m b \qquad \text{(B-1)}$$

For the case of the flowing ambient,

$$\frac{d}{dS}\{U_m B^2\} = 2f(\alpha, U_m, B, R) \qquad \text{(A-2)}$$

$$f(\alpha, U_m, B, R) = (0.057 + \frac{.97}{F_L}\sin\theta)B(|U_m - U_a\cos\theta| + a_3 U_a \sin\theta)$$

$$\frac{d}{dS}\{U_m B^2\} = 2(0.057 + \frac{.97}{F_L}\sin\theta)B(|U_m - U_a\cos\theta| + a_3 U_a \sin\theta)$$

Substituting,

$$\frac{d}{ds\ D}\{u_m U_m b^2 D^2\}$$

$$= 2(0.057 + \frac{.97}{F_L}\sin\theta)bD\ (|u_m U_m - RU_0\cos\theta| + a_3 RU_0 \sin\theta)$$

$$\frac{d}{ds}\{u_m b^2\} = 2(0.057 + \frac{.97}{F_L}\sin\theta)b(|u_m - R\cos\theta| + a_3 R\sin\theta) \qquad \text{(B-2)}$$

2. Conservation of Energy

$$\frac{d}{dS}\{U_m(t_m - t_a)\ [\frac{\lambda^2 B^2}{2(\lambda^2+1)}]\} = -\frac{dt_a}{dS}\{\frac{U_m B^2}{2}\} \qquad \text{(A-3)}$$

Substituting,

$$\frac{d}{ds\ D}\{u_m U_0\ \frac{\Delta t_m}{\Delta t_0}(t_0 - t_{a0})\ \frac{\lambda^2 b^2 D^2}{2(\lambda^2+1)}\}$$

$$= \ -\ \frac{\Delta t_a}{\Delta t_0}\ \frac{(t_0 - t_{a0})}{ds\ D}\{u_m U_0\ \frac{b^2 D^2}{2}\}$$

$$\frac{d}{ds}\{u_m\ \frac{\Delta t_m}{\Delta t_0}\ \frac{\lambda^2 b^2}{(\lambda^2+1)}\} \ = \ -\ \frac{\Delta t_a}{\Delta t_0\ ds}\{u_m b^2\} \qquad \text{(B-3)}$$

3. Conservation of Concentration or Other Scalar Species

$$\frac{d}{dS}\{U_m(c_m - c_a)\ \frac{\lambda^2 B^2}{2(\lambda^2+1)}\} \ = \ -\ \frac{dc_a}{dS}\{U_m\ \frac{B^2}{2}\} \qquad \text{(A-4)}$$

By development identical to conservation of energy in (2) above,

$$\frac{d}{ds}\{u_m\ \frac{\Delta c_m}{\Delta c_0}\ \frac{\lambda^2 b^2}{(\lambda^2+1)}\} \ = \ -\ \frac{\Delta c_a}{\Delta c_0\ ds}\{u_m b^2\} \qquad \text{(B-4)}$$

4. Conservation of Horizontal Momentum

For the case of the quiescent ambient,

$$\frac{d}{dS}\{U_m^2 B^2 \cos\theta\} \ = \ 0 \qquad \text{(A-5)}$$

Substituting,

$$\frac{d}{ds\ D}\{u_m^2 U_0^2 b^2 D^2 \cos\theta\} \ = \ 0$$

$$\frac{d}{ds}\{u_m^2 b^2 \cos\theta\} \ = \ 0 \qquad \text{(B-5)}$$

For the case of the flowing ambient,

$$\frac{d}{dS}\{U_m^2\cos\theta B^2\} = 4f(\alpha,U_m,B,R)U_a \tag{A-6}$$

$$f(\alpha,U_mB,R) = (0.057+\frac{.97}{F_L}\sin\theta)B(|U_m-U_a\cos\theta|+a_3U_a\sin\theta)$$

$$\frac{d}{dS}\{U_m^2\cos\theta B^2\} =$$

$$4U_a(0.057+\frac{.97}{F_L}\sin\theta)B(|U_m-U_a\cos\theta|+a_3U_a\sin\theta)$$

Subsituting,

$$\frac{d}{ds\ D}\{u_m^2U_0^2b^2D^2\cos\theta\} =$$

$$4RU_0(0.057+\frac{.97}{F_L}\sin\theta)bD\ (|u_mU_0-RU_0\cos\theta|+a_3RU_0\sin\theta)$$

$$\frac{d}{ds}\{u_m^2b^2\cos\theta\} = 4R(0.057+\frac{.97}{F_L}\sin\theta)b(|u_m-R\cos\theta|+a_3R\sin\theta) \tag{B-6}$$

5. Conservation of Vertical Momentum

$$\frac{d}{dS}\{U_m^2\sin\theta B^2\} = \frac{\rho_a-\rho_m}{\rho}(2g\lambda^2B) \tag{A-7}$$

The denominator of the density term on the right side of Equation (A-7) was transposed from the Bousinenesq term on the left side of the equation. It will be assigned a value equal to the reference discharge density. Substituting dimensionless terms,

$$\frac{d}{ds\ D}\{u_m^2 U_0^2 b^2 D^2 \sin\theta\} = \frac{\rho_a - \rho_m}{\rho}(2g\lambda^2 b^2 D^2)$$

$$\frac{d}{ds}\{u_m^2 b^2 \sin\theta\} = \frac{\rho_a - \rho_m}{\rho_0}\left(\frac{\rho_{a0} - \rho_{m0}}{\rho_{a0} - \rho_{m0}}\right) \frac{2g\lambda^2 b^2 D}{U_0^2}$$

$$\frac{d}{ds}\{u_m^2 b^2 \sin\theta\} = \left(\frac{\rho_a - \rho_m}{\rho_{a0} - \rho_{m0}}\right) \frac{2\lambda^2 b^2}{F^2} \qquad \text{(B-7)}$$

6. Horizontal Trajectory

$$\frac{d}{dS} X = \cos\theta \qquad \text{(A-8)}$$

Substituting,

$$\frac{d}{ds\ D} x\ D = \cos\theta$$

$$\frac{d}{ds} x = \cos\theta \qquad \text{(B-8)}$$

7. Vertical Trajectory

$$\frac{d}{dS} Z = \sin\theta \qquad \text{(A-9)}$$

Substituting,

$$\frac{d}{ds\ D} z\ D = \sin\theta$$

$$\frac{d}{ds} z = \sin\theta \qquad \text{(B-9)}$$

APPENDIX C

The Gebhart-Mollendorf relation for the density of saline water [11] is of the form

$$\rho(t,s,p) = \rho_m(s,p)[1-\alpha(s,p)|t-t_m(s,p)|^{q(s,p)}]$$

where t is temperature (°C), s is salinity (‰), p is pressure (bars absolute), $\rho_m(s,p)$ is the density extremum at the given values of s and p, $t_m(s,p)$ is the temperature corresponding to the density extremum for the same s and p values, $\alpha(s,p)$ is a temperature term coefficient, and $q(s,p)$ is a temperature term exponent. These values are in turn given by

$$\rho_m(s,p) = \rho_m(0,1)[1+f_1(p)+sg_1(p)+s^2h_1(p)]$$

$$a(s,p) = a(0,1)[1+f_2(p)+sg_2(p)+s^2h_2(p)]$$

$$t_m(s,p) = t_m(0,1)[1+f_3(p)+sg_3(p)+s^2h_3(p)]$$

$$q(s,p) = q(0,1)[1+f_4(p)+sg_4(p)+s^2h^4(p)]$$

where

$$f_i(p) = \sum_{j=1}^{3} f_{ij}(p-1)^j \quad , \quad g_i(p) = \sum_{j=0}^{3} g_{ij}(p-1)^j$$

$$h_i(p) = \sum_{j=0}^{3} h_{ij}(p-1)^j$$

$\rho_m(0,1) = 999.972$ kg m^{-3}

$t_m(0,1) = 4.029325$ °C

$\alpha(0,1) = 9.297173 \times 10^{-6}$ $°C^{-q}$

$q(0,1) = 1.894816$

and the values of f_{ij}, g_{ij}, and h_{ij} are given in tabular form in Table (TC-1).

The relation is fitted in the range of temperature to 20°C, pressure to 1000 bars absolute, and salinity to 40 ‰.

Comparison of the density predicted by this relation with the data of Chen and Millero [5] is shown in Figure (C-1). The overall rms difference between the relation and this data, for pure and saline water at all temperatures and pressures considered, is reported to be 9.0 ppm.

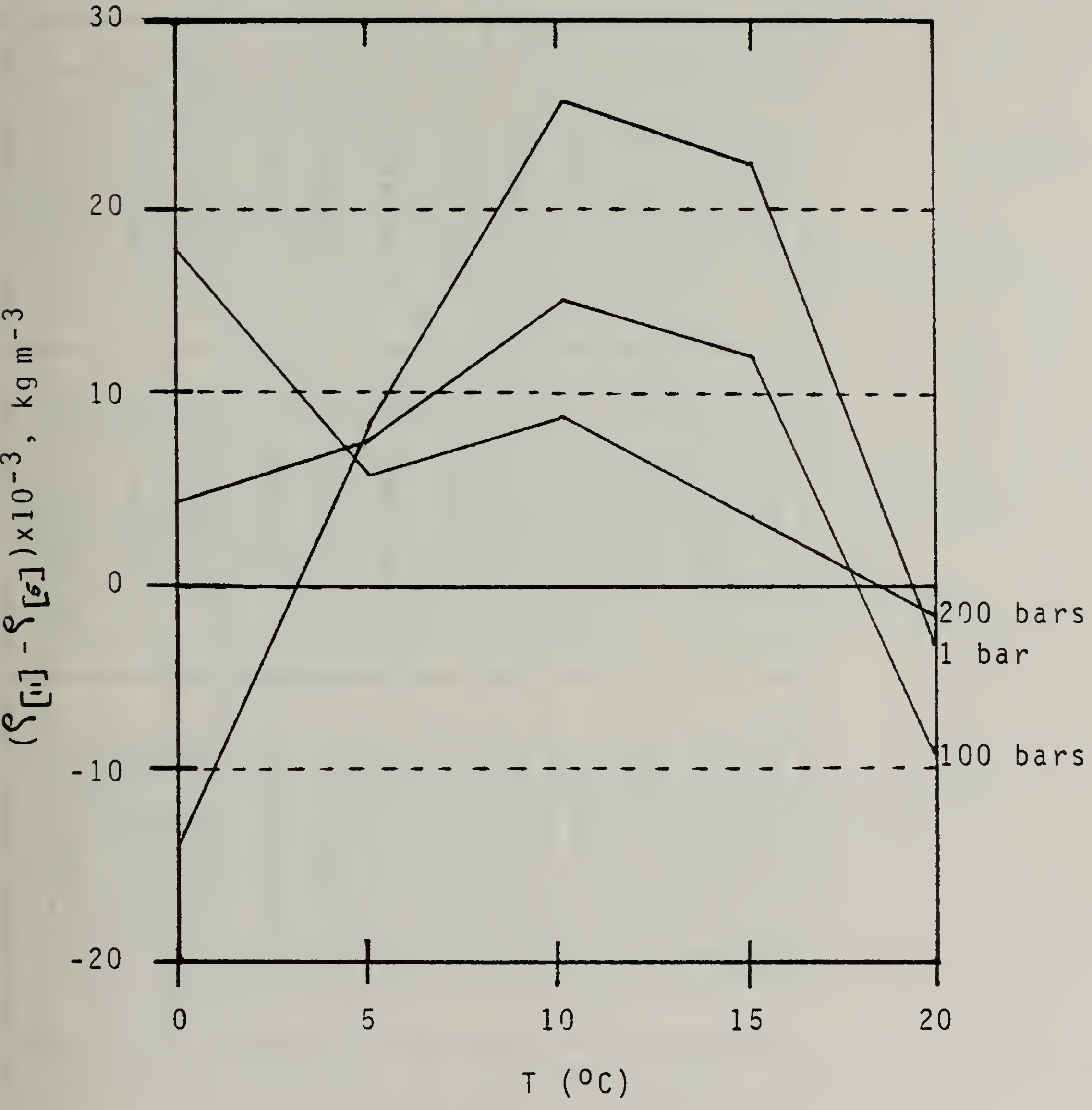

Figure C-1. Comparison of results of Gebhart and Mollendorf [11] with data of Chen and Millero [5]

Table C-1. Values of f_{ij}, g_{ij}, and h_{ij} in the Gebhart-Mollendorf Relation for Density of Water

	j			
	0	1	2	3
f_{1j}		4.960998E-05	-2.601973E-09	7.842619E-13
f_{2j}		1.377584E-04	1.497648E-06	2.903240E-10
f_{3j}		-5.430000E-03	7.720181E-07	-7.038846E-10
f_{4j}		-1.118758E-04	-1.238393E-07	5.857253E-11
g_{1j}	7.992252E-04	-5.194896E-08	1.031185E-10	-2.979653E-14
g_{2j}	1.623355E-02	1.129961E-05	-8.053248E-08	6.966452E-12
g_{3j}	-5.265509E-02	7.496781E-05	-2.792053E-07	1.411138E-10
g_{4j}	-3.136530E-03	2.983937E-06	4.453557E-09	-2.937601E-12
h_{1j}	1.918334E-07	1.347190E-09	-2.203133E-12	1.112440E-15
h_{2j}	-4.565866E-04	-4.352912E-07	1.978675E-09	-9.079379E-13
h_{3j}	0.000000	-3.683650E-06	7.694077E-09	-4.561113E-12
h_{4j}	7.599378E-05	-8.718915E-08	-4.166970E-11	5.870105E-14

LIST OF REFERENCES

1. Abraham, G., Transactions ASCE, J. Hydraulics Div., vol. 86, HY6, 1960, pp. 1-13.

2. Abraham, G., Proceedings ASCE, J. Hydraulics Div., vol. 91, HY4, 1965, pp. 139-154.

3. Albertson, M.L., Dai, Y.B., Jensen, R.A., and Rouse, H., Transactions ASCE, vol. 115, 1950, pp. 639-697.

4. Barstow, D., Gilbert, W., Park, K., Still, R., and Wyatt, "Hydrographic Data from Oregon Waters 1966", Dept. of Oceanography, Oregon State Univ., Corvallis, OR, 1966.

5. Chen, C.T., and Millero, F.J., Deep-Sea Research, vol. 23, 1976, pp. 595-612.

6. Davis, L.R., Shirazi, M.A., and Slegel, D.L., "Measurement of Buoyant Jet Entrainment from Single and Multiple Sources", Heat Transfer Division of ASME Paper 77-HT-43, Aug. 1977.

7. Fan, L.H., "Turbulent Buoyant Jets into Stratified and Flowing Ambient Fluids", California Institute of Technology, W.M. Keck Lab., Report KH-R-15, 1967.

8. Ibid., pp. 52-53.

9. Fan, L.H., and Brooks, N.H., "Numerical Solutions to Turbulent Buoyant Jet Problems", California Institute of Technology, W.M. Keck Lab., Report KH-R-18, 1969.

10. Fox, D.G., J. Geophysical Research, vol. 75(33), 1970, pp. 6818-6835.

11. Gebhart, B., and Mollendorf, J.C., Deep-Sea Research, vol. 24, 1977, pp. 831-848.

12. Ginsberg, T., and Ades, M., Transactions ANS, vol. 21, 1975, pp. 87-88.

13. Hirst, E.A., "Analysis of Buoyant Jets within the Zone of Flow Establishment", Oak Ridge National Laboratory, Report ORNL-TM-3470, 1971.

14. Hirst, E.A., J. Geophysical Research, vol. 76, 1971, pp. 7375-7384.

15. Hirst, E.A., "Analysis of Round, Turbulent, Buoyant Jets Discharged to Flowing Stratified Ambients", Oak Ridge National Laboratory, Report ORNL-4685, 1971.

16. Hoult, F.A., Fay, J.A., and Forney, C.J., J. of Air Pollution Control Association, vol. 19, 1969, pp. 585-590.

17. Johannessen, J.A., and others, "A CTD-Data Report from the Norsex Marginal Ice Zone Program North of Svalbard in September-October 1979", University of Bergen, Royal Norwegian Council of Scientific and INdustrial Research, Bergen, Norway, 1980.

18. List, E.J., and Imberger, J., Proceedings ASCE, J. Hydraulics Division, HY9, 1973, pp. 1461-1474.

19. Madni, I.D., and Pletcher, R.H., Transactions ASME, J. of Heat Transfer, vol. 99, 1977, pp. 99-104.

20. Morton, B.R., Taylor, A.G., and Turner, J.S., J. Royal Society of London, vol. A234, 1956, pp. 2-23.

21. Neumann, G., and Pierson, W.J., Principles of Physical Oceanography, Prentice-Hall Inc., 1966.

22. Pryputniewicz, R.J., and Bowley, W.W., Transactions ASME, J. of Heat Transfer, vol. 97, 1975, pp. 274-281.

23. Riester, J.B., Bajura, R.A., and Schwartz, S.H., Transactions ASME, J. of Heat Transfer, vol. 102, 1980, pp. 557-562.

24. Ibid., p. 23.

25. Schatzman, M., "A Mathematical Model for the Prediction of Plume Rise in Stratified Flows", Proceedings of the Penn State Symposium on Turbulent Shear Flows, 1977.

26. Shirazi, M.A., McQuivey, R.S., and Keefer, T.N., Proceedings ASCE, J. of the Hydraulics Division, vol. 100, HY7, 1974, pp. 919-934.

27. Taylor, G.I., Proceedings Royal Society of London, vol. 201A, 1950, p. 175.

INITIAL DISTRIBUTION LIST

No. Copies

1. Defense Technical Information Center 2
Cameron Station
Alexandria, Virginia 22314

2. Library, Code 0142 2
Naval Postgraduate School
Monterey, California 93940

3. Paul J. Marto 1
Department Chairman, Code 69
Department of Mechanical Engineering
Naval Postgraduate School
Monterey, California 93940

4. Dr. Benjamin Gebhart 1
Department of Mechanical Engineering
University of Pennsylvania
Philadelphia, Pennsylvania 19104

5. Dr. M. D. Kelleher, Code 69Kk 10
Department of Mechanical Engineering
Naval Postgraduate School
Monterey, California 93940

6. Dr. Gene Rudd 1
Naval Research Laboratory
Washington, D.C. 20375

7. Dr. Robert Whitehead 1
Office of Naval Research
800 Quincy Street
Arlington, Virginia 22217

8. Dr. Thomas Taylor 1
Applied Physics Laboratory
Johns Hopkins University
Columbia, Maryland 21045

9. LT David S. Hilder 1
R.R. #1, Box 192
Mullica Hill, New Jersey 08062

10. CAPT. Edward E. Henifin 1
(SEA 003)
Naval Sea Systems Command
Washington, D.C. 20362

11. Dr. Nat Kobitz 1
(SEA 03R)
Naval Sea Systems Command
Washington, D.C. 20362

12. Mr. Thomas E. Pierce 1
(SEA 63R3)
Naval Sea Systems Command
Washington, D.C. 20362

13. Mr. Robert G. Keane 1
(SEA 3213)
Naval Sea Systems Command
Washington, D.C. 20362